

2007

## Atrx deficiency in the murine forebrain leads to altered imprinted gene expression

Deanna Charlene Tremblay  
*Western University*

Follow this and additional works at: <https://ir.lib.uwo.ca/digitizedtheses>

---

### Recommended Citation

Tremblay, Deanna Charlene, "Atrx deficiency in the murine forebrain leads to altered imprinted gene expression" (2007). *Digitized Theses*. 4660.  
<https://ir.lib.uwo.ca/digitizedtheses/4660>

This Thesis is brought to you for free and open access by the Digitized Special Collections at Scholarship@Western. It has been accepted for inclusion in Digitized Theses by an authorized administrator of Scholarship@Western. For more information, please contact [wlsadmin@uwo.ca](mailto:wlsadmin@uwo.ca).

**Atrx deficiency in the murine forebrain leads to altered imprinted gene expression**

(Spine title: ATRX regulates expression of specific imprinted genes)

(Thesis format: Monograph)

by

**Deanna Charlene Tremblay**

**Graduate Program in Biochemistry**

**Submitted in partial fulfillment of the**

**Requirements for the degree of**

**Master of Science**

**Faculty of Graduate Studies**

**The University of Western Ontario**

**London, Ontario**

**© Deanna C. Tremblay 2007**

## Abstract

X-linked  $\alpha$ -thalassaemia mental retardation (ATR-X) syndrome is characterized by severe cognitive delay, broad developmental abnormalities and  $\alpha$ -thalassaemia. Disease-causing mutations in the *ATRX* gene give rise to a malfunctioning protein and result in aberrant DNA methylation at specific repeat sequences. ATRX is a SNF2 chromatin remodeling protein that targets  $\alpha$ -globin gene expression, but additional targets remain largely elusive. Using a mouse model in which *Atrx* is conditionally deleted in the developing forebrain, I show that DNA methylation at repeat sequences is comparable to that found in ATR-X patients. I further describe the identification of specific imprinted genes that are progressively regulated by *Atrx* throughout development. I show that aberrant imprinted gene expression in the *Atrx*<sup>null</sup> brain is not correlated with changes in DNA methylation at regulatory differentially methylated regions, but that *Atrx* co-localizes with MeCP2 at the *H19* ICR. Taken together, my findings establish for the first time a link between ATRX and the control of neuronal imprinted gene expression.

**Keywords:** ATR-X syndrome, X-linked mental retardation, forebrain, ATRX, chromatin remodeling, genomic imprinting, DNA methylation, *H19*, *Igf2*, MeCP2

## **Acknowledgements**

I would like to express my sincere thanks to all those who have supported and encouraged me throughout the duration of my academic life. Thank you to all my immediate and extended family members, especially my parents Audrey Tremblay and Larry Tremblay, for keeping me on track and ensuring that I am constantly surrounded by a positive and encouraging environment in which to grow and learn as an individual. A special thank-you to my friends, Kimberly Medaglia and Jennifer Chaytor, for understanding the uniqueness of graduate student life and continuously pushing me to succeed in the face of experimental failure. I am extremely grateful to my husband, Robert Rieveley, for making sure that life is always exciting and ensuring that I am genuinely happy.

I would like to acknowledge all the members of the Bérubé lab who have continuously provided an exciting and positive work environment. I would especially like to thank my supervisor, Dr. Nathalie Bérubé, for encouraging me to work and think as a scientist. You have provided invaluable support and insight regarding my own project as well as many other facets of life as a graduate student. Special thanks to Michael Levy, Kieran Ritchie, Sarah Francis, Alison Martens and Laurie Seifried for making me laugh and putting up with my quirks on a daily basis. Finally, I would like to acknowledge the members of my supervisory committee, Dr. Mellissa Mann and Dr. David Haniford, for numerous insightful suggestions and helping to keep me on track with a difficult project.

## Table of Contents

CERTIFICATE OF EXAMINATION.....	ii
ABSTRACT.....	iii
ACKNOWLEDGEMENTS.....	iv
TABLE OF CONTENTS.....	v
LIST OF TABLES.....	viii
LIST OF FIGURES.....	ix
LIST OF ABBREVIATIONS.....	xi

### CHAPTER 1 – Introduction

1.1 The Significance of ATRX.....	1
1.1.1 Early Discoveries.....	1
1.1.2 ATR-X and Related Mental Retardation Syndromes.....	2
1.1.3 ATRX and the Development of the Extra-Embryonic Trophoblast.....	4
1.1.4 ATRX and Neuronal Development.....	5
1.2 Cellular Functions of the ATRX Protein.....	8
1.2.1 The ATRX Gene.....	8
1.2.2 The ADD Domain.....	10
1.2.3 The SWI2/SNF2 Chromatin Remodelling Domain.....	11
1.2.4 Chromatin Remodelling and Regulation of Genomic Stability.....	12
1.2.5 Transcriptional Regulation of Gene Expression.....	14
1.2.6 Epigenetic Regulation of DNA Methylation.....	15

1.3	Epigenetic Regulation of Genomic Imprinting.....	17
1.3.1	Models of Genomic Imprinting.....	17
1.3.2	SNF2 Regulation of Genomic Imprinting.....	21
1.4	Hypothesis and Summary of Findings.....	23

## CHAPTER 2 – Materials and Methods

2.1	Animal Husbandry and Genotyping.....	26
2.2	Microarray.....	29
2.3	Semi-Quantitative RT-PCR.....	33
2.4	Quantitative Real Time RT-PCR.....	34
2.5	Methylation Sensitive Southern Blot.....	35
2.6	McrPCR Methylation Analysis.....	37
2.7	Bisulfite Mutagenesis.....	38
2.8	Chromatin Immunoprecipitation.....	39

## CHAPTER 3 – Results

3.1	Methylation of Repetitive DNA Elements in the <i>Atrx<sup>null</sup></i> Murine Forebrain.....	40
3.2	Transcription Profiling Reveals Increased Expression of Specific Imprinted Genes in the Newborn <i>Atrx<sup>null</sup></i> Forebrain.....	50
3.3	Loss of <i>Atrx</i> Induces a Progressive Deregulation of Imprinted Genes.....	65
3.4	Increased Imprinted Gene Expression May Correlate With Abnormal DNA Methylation at the <i>Dlk1 – Gtl2</i> Imprinted Domain.....	69

3.5	Increased Imprinted Gene Expression Does Not Correlate With Abnormal DNA Methylation at the <i>H19 – Igf2</i> Imprinted Domain.....	79
3.6	<i>Atrx</i> and MeCP2 Colocalize at the <i>H19</i> ICR.....	88

**CHAPTER 4 – Discussion and Conclusions**

4.1	Summary of Thesis Findings.....	92
4.2	Developmental Implications of Aberrantly Expressed Imprinted Genes.....	93
4.2.1	Conflict Theory and the Importance of Imprinted Genes in Placenta and Brain..	94
4.2.2	Expression and Role of Aberrantly Expressed Genes in the Brain.....	96
4.2.3	Expression and Role of Aberrantly Expressed Genes in the Placenta.....	99
4.3	Proposed Mechanism of <i>H19 – Igf2</i> Regulation in the Mouse Forebrain.....	102
4.3.1	Brain Specific Enhancers May Regulation <i>H19 – Igf2</i> Transcription.....	105
4.3.2	Transcriptional Regulation by Chromatin Looping and MARs.....	106
4.3.3	<i>Atrx</i> and MeCP2 May Repress the Paternal Allele.....	107
4.3.4	<i>Atrx</i> May Regulate Chromatin Looping of $\alpha$ -Globin and <i>Dlx5</i> .....	109
4.3.5	Concise Model of <i>Atrx</i> Regulate of <i>H19</i> and <i>Igf2</i> in the Mouse Forebrain.....	110
4.4	Future Directions.....	111
4.5	Conclusions.....	114

<b>CHAPTER 5 – References</b> .....	116
-------------------------------------	-----

APPENDIX I.....	134
-----------------	-----

CURRICULUM VITAE.....	135
-----------------------	-----

## **List of Tables**

Table 2.1 List of oligonucleotides used in genotyping, Southern blot, RT-PCR, McrPCR, cloning, bisulfite mutagenesis and ChIP assays.....	30
Table 3.1 Comprehensive list of imprinted genes extracted from RNA microarray.....	55

## List of Figures

Figure 1.1 Cre-LoxP mediated targeted deletion of <i>Atrx</i> exon 18.....	6
Figure 1.2 Models of genomic imprinting.....	18
Figure 2.1 Regions of the mouse brain used for experimental analyses.....	27
Figure 3.1 Southern blot analysis of DNA methylation at 18S and 28S rDNA repeats in the <i>Atrx<sup>null</sup></i> mouse forebrain.....	41
Figure 3.2 Southern blot analysis of DNA methylation at major satellite, minor satellite and IAP <i>gag</i> repeats in the <i>Atrx<sup>null</sup></i> mouse forebrain.....	45
Figure 3.3 <i>Mcr</i> PCR analysis of DNA methylation at major satellite, minor satellite and IAP <i>gag</i> repeats in the <i>Atrx<sup>null</sup></i> mouse forebrain.....	48
Figure 3.4 Semi-quantitative RT-PCR analyses of imprinted gene expression in the <i>Atrx<sup>null</sup></i> mouse forebrain.....	52
Figure 3.5 Quantitative real time RT-PCR analysis of imprinted gene expression in the <i>Atrx<sup>null</sup></i> mouse forebrain.....	58
Figure 3.6 Quantitative real time RT-PCR analysis of imprinted gene expression in multiple <i>Atrx<sup>null</sup></i> mouse forebrains.....	60
Figure 3.7 Quantitative real time RT-PCR analysis of <i>Dlx5</i> expression at E13.5 and P0.5 in the <i>Atrx<sup>null</sup></i> mouse forebrain.....	63
Figure 3.8 Developmental analysis of imprinted gene expression at E13.5, P0.5 and P17.....	66
Figure 3.9 Bisulfite mutagenesis of the <i>Dlk1 – Gtl2</i> IG DMR.....	71
Figure 3.10 Bisulfite mutagenesis of the <i>Dlk1</i> DMR.....	74

## List of Figures Continued

Figure 3.11 Bisulfite mutagenesis of the <i>Gtl2</i> DMR .....	77
Figure 3.12 Bisulfite mutagenesis of the <i>H19</i> ICR.....	81
Figure 3.13 Bisulfite mutagenesis of the <i>Igf2</i> DMR1.....	84
Figure 3.14 Bisulfite mutagenesis of the <i>Igf2</i> DMR2.....	86
Figure 3.15 ChIP analysis of CTCF, MeCP2 and Atrx across the <i>H19</i> ICR.....	89
Figure 4.1 Choroid plexus structure.....	103
Figure 4.2 Proposed mechanism of forebrain-specific Atrx-dependant regulation at the paternal <i>H19</i> – <i>Igf2</i> imprinted domain.....	112

## List of Abbreviations

ActB	$\beta$ -actin
ADD	ATRX, DNMT3A/B, DNMT3L
AS	Angelman Syndrome
Ascl2	Achaete-Scute complex homolog 2
ATR-X	$\alpha$ -thalassaemia mental retardation, X-linked syndrome
ATRX	$\alpha$ -thalassaemia mental retardation, X-linked
ATRXt	$\alpha$ -thalassaemia mental retardation, X-linked truncated
ATP	Adenosine triphosphate
C	Carboxy
CAST	<i>M. mus castaneus</i>
CCD	Centrally conserved domain
Cdh1	Cadherin 1
Cdkn1c	Cyclin dependant kinase 1C
cDNA	Complementary DNA
CHD8	<u>C</u> hromo domain, <u>S</u> NF2 <u>H</u> elicase domain, <u>D</u> NA binding domain
ChIP	Chromatin immunoprecipitation
CO <sub>2</sub>	Carbon dioxide
Cp	Cerruloplamin
Cre	Cre recombinase
C-terminus	Carboxy terminus
Cys	Cysteine
Daxx	Fas-death domain associated protein
Dcn	Decorin
DDM1	Decrease in DNA methylation 1
DEPC	Diethylpyrocarbonate
dH <sub>2</sub> O	Distilled water
Dlk1	Delta-like 1
Dlx5	Distal-less homeobox 5
DNA	Deoxyribonucleic acid
DNMT	DNA methyltransferase
dNTP	Deoxyribonucleotide triphosphate
DMEM	Dulbecco's modified eagle medium
DMR	Differentially methylation region
DTT	Diothiothreitol
E8.5	Embryonic day 8.5
E13.5	Embryonic day 13.5
EDTA	Ethylene diamine tetraacetic acid
ES	Embryonic stem cell
EtBr	Ethidium bromide
EtOH	Ethanol
EVT	Extravillous trophoblast
EZH2	Enhancer of Zeste homolog 2
FoxG1	Forkhead box G1
G1	Gap 1

G2	Gap2
GABA	Gamma-aminobutyric acid
GABRB3	Gamma-aminobutyric acid receptor beta 2
GATA1	GATA-binding protein 1
Gtl2	Gene-trap locus 2
HbH	Hemoglobin H
HCl	Sodium chloride
HDAC	Histone deacetylase
His	Histidine
H3K4	Histone 3 lysine 4
H3K9	Histone 3 lysine 9
H <sub>2</sub> O	Water
HP1 $\alpha$	Heterochromatin protein 1 alpha
IAP	Intracisternal A-particle
ICR	Imprinting control region
IG	Intergenic
Igf2	Insulin-like growth factor 2
Igf2r	Insulin-like growth factor 2 receptor
IgG	Immune globulin G
IPr	Isopropanol
Ipw	Imprinted in Prader-Willi syndrome
KCl	Potassium hydroxide
Kcnq1	Potassium channel voltage gated KQT-like subfamily member 1
Kcnq1ot1	Kcnq1 overlapping transcript 1
KO	Knockout
LB	Luria broth
LINE	Long interspersed nuclear element
LSH	Lymphoid specific helicase
MAR	Matrix attachment region
MEA	Medea
MeCP2	Methyl-CpG binding protein-2
MgCl <sub>2</sub>	Magnesium chloride
MHC	Major histocompatibility complex
Mkrn	Makorin
MNK	Menkes
mRNA	Messenger RNA
mUPD12	Uniparental disomy of maternal chromosome 12
N	Amino
NaCl	Sodium chloride
NaOH	Sodium hydroxide
NB	Nuclear body
ncRNA	Non-coding RNA
Neo	Neomycin
Ndn	Necdin
NMR	Nuclear magnetic resonance
N-terminus	Amino terminus

P0.5	Post-natal day 0.5
P17	Post-natal day 17
P18	Post-natal day 18
PASG	Proliferation associated SNF2-like gene
PBS	Phosphate buffered saline
PCR	Polymerase chain reaction
Peg1	Paternally expressed gene 1
PHD	Plant homeodomain
Phlda2	Pleckstrin homology like domain family A member 2
Pigt	Phosphatidylinositol glycan class T
Pgk1	Phosphoglycerate kinase 1
PML	Promyelocytic leukaemia
Ptgds	Prostaglandin D2 synthase
pUPD12	Uniparental disomy of paternal chromosome 12
Rad54	<i>S. Cerevisiae</i> homolog of radiation sensitive gene 54
rDNA	Ribosomal DNA
RNA	Ribonucleic acid
RNAi	RNA interference
RNase A	Ribonucleotide reductase A
RT-PCR	Reverse transcriptase polymerase chain reaction
RTT	Rett Syndrome
S	Synthesis
SATB1	Special AT-rich sequence-binding protein 1
SDS	Sodium dodecyl sulfate
SINE	Short interspersed nuclear element
siRNA	Short interfering RNA
Slc2211	Solute carrier family member 2211
Slc38a4	Solute carrier family member 38a4
SNc	Substantia nigra pars compacta
SNF2	Sucrose non-fermenting 2
SSC	Sodium chloride – Sodium citrate
Suv39h1	Suppressor of variegation 39 homolog 1
SWI2	Yeast mating type switching
TAE	Tris-Acetate-EDTA
TE	Tris EDTA solution
TGF-beta	Transforming growth factor beta
Trpc4	Transient receptor potential cation channel, subfamily C
Ube3a	Ubiquitin protein ligase E3A
UV	Ultraviolet
VTA	Ventral tegmental area
WT	Wild type
XH2	X-linked helicase 2
Xist	X-inactivation specific transcript
XLMR	X-linked mental retardation
XNP	X-linked nuclear protein
Zim1	Imprinted zinc-finger gene 1

## CHAPTER 1 – Introduction

### 1.1 The Significance of ATRX

Over a decade ago, mutations in the *ATRX* gene were identified in young males with a rare syndrome known as X-linked  $\alpha$ -thalassaemia mental retardation (ATR-X) (1). Since that time, *ATRX* mutations have been implicated in a number of additional X-linked mental retardation (XLMR) disorders (2-7), many of which share similarities with the ATR-X syndrome. Using a mouse model system, null mutations in the murine *Atrx* gene were found to be lethal early in embryonic development due to defective formation of the extra-embryonic trophoblast (8). Furthermore, conditional deletion of *Atrx* in the mouse forebrain led to the discovery that *Atrx* is critical for development of the murine cortex and hippocampus (9). Despite the known requirement for ATRX in the developing trophoblast and forebrain, the mechanisms by which ATRX functions and how this relates to development remain elusive.

#### 1.1.1 Early Discoveries

The discovery of a relationship between mental retardation and the blood disorder  $\alpha$ -thalassaemia was first described in three families of Northern European descent (10). Initial cases involved patients who had deletions mapping to the  $\alpha$ -globin locus on chromosome band 16p13.3, with unexplained mild mental retardation (10-12). However, the medical community was soon perplexed by the finding of new patients with severe mental retardation in which no disease-causing mutations existed in the 16p chromosomal region (13). After almost a decade, it was determined that patients could be classified as

having one of two distinct syndromes (13, 14). In the latter syndrome, where  $\alpha$ -globin mutations are not present, it was speculated that an unknown *trans*-acting factor that is normally involved in  $\alpha$ -globin regulation was mutated (13). Following the description of six unrelated patients who were all cytogenetically male, it was postulated that the mutated gene causing the non-deletion type of  $\alpha$ -thalassaemia/mental retardation was X-linked (15-17). Within one year, the non-deletion type of  $\alpha$ -thalassaemia/mental retardation was formally named X-linked  $\alpha$ -thalassaemia mental retardation (ATR-X) syndrome (18) and the disease-causing gene was preliminarily localized to the Xq12-21.31 chromosomal region by X-inactivation and linkage analysis (19).

### **1.1.2 ATR-X and Related Mental Retardation Syndromes**

X-linked  $\alpha$ -thalassaemia mental retardation syndrome is characterized by severe to profound cognitive delay (95% of cases) in association with characteristic diagnostic features including facial anomalies (>90% of cases) and moderate levels of  $\alpha$ -thalassaemia (90% of cases) (20). A wide range of additional phenotypes are present and include genital abnormalities, skeletal abnormalities, microcephaly, short stature, seizures, heart problems and renal/urinary defects (20, 21). In addition, ATR-X patients exhibit hypomethylation at ribosomal DNA (rDNA) arrays, while hypermethylation occurs at repetitive sequences encompassing the Y-specific satellite DYZ2 and the TelBam3.4 sub-telomeric repeat family (22). Epidemiological analysis indicates that the prevalence of ATR-X syndrome in the global population is quite low, affecting <1-9/1,000,000 individuals (20). Although a number of documented cases cited death at a

young age due to pneumonia or gastro-oesophageal reflux, it is not uncommon for ATR-X patients to thrive well into adulthood (20).

Diagnosis of the ATR-X syndrome previously relied on the haematological presence of  $\alpha$ -thalassaemia as a defining characteristic of the disease, however, a number of ATR-X families showing no signs of  $\alpha$ -thalassaemia have since been identified (23, 24). It is now thought that a variety of mutations occurring throughout the *ATRX* gene may have differential effects on  $\alpha$ -globin expression (20). Past diagnoses relied on the presence of excess  $\beta$ -globin chains, more commonly referred to as HbH inclusions, however these aggregates may not appear until there is 30-40% decrease in  $\alpha$ -globin synthesis (25). Therefore, although some ATR-X patients do not exhibit HbH inclusions (2, 23, 24), it does not rule out the possibility that  $\alpha$ -globin is downregulated.

Since the *ATRX* gene is found exclusively on the X chromosome (1), inherited point mutations or partial duplications will affect male children. Until recently, no female ATR-X patients had been identified due to extremely skewed patterns of X-inactivation found in carrier females (19, 26). This extreme skewing, which is observed in other XLMR disorders (27), is proposed to be caused by selection favouring cells that express the wild-type *ATRX* allele (28). Recently, a carrier female patient was identified in which skewed X-inactivation resulted in an unexpected silencing of the wild type *ATRX* allele (29). Although this observation remains unexplained, the female patient did have a *de novo* *ATRX* mutation and was the product of artificial reproductive technology (29), which has been associated with increased instances of epigenetic disorders (30-32).

Mutations in the *ATRX* gene have been linked to a number of additional XLMR disorders such as Juberg-Marsidi (2), X-linked mental retardation with spastic paraplegia

(3), Carpenter-Waziri (5), Holmes-Gang (4), Smith-Fineman-Myers (7) and Chudley-Lowry (6) syndromes. Due to phenotypic overlap, ATR-X syndrome may be improperly diagnosed as one of Coffin-Lowry, Angelman or Smith-Lemli-Opitz syndromes, however mutational analysis should differentiate between these diseases (20).

### 1.1.3 ATRX and the Development of the Extra-Embryonic Trophoblast

Until recently, very little information was known regarding the role ATRX plays during mammalian development. In order to address this question, a mouse model system was engineered in which the major isoform of *Atrx* was deleted in mouse embryonic stem (ES) cells and embryos (8). Using different vectors that remove exon 18 from the *Atrx* gene in an ES cell culture system, homologous recombination resulted in failure to recover target clones, suggesting that *Atrx* is likely important for normal ES cell growth and expansion (8). After adopting a Cre-mediated conditional deletion strategy, clones were obtained in which both *Atrx* transcript and protein were abolished, indicating that deletion of exon 18 has a highly destabilizing effect on the *Atrx* transcript (8, 9).

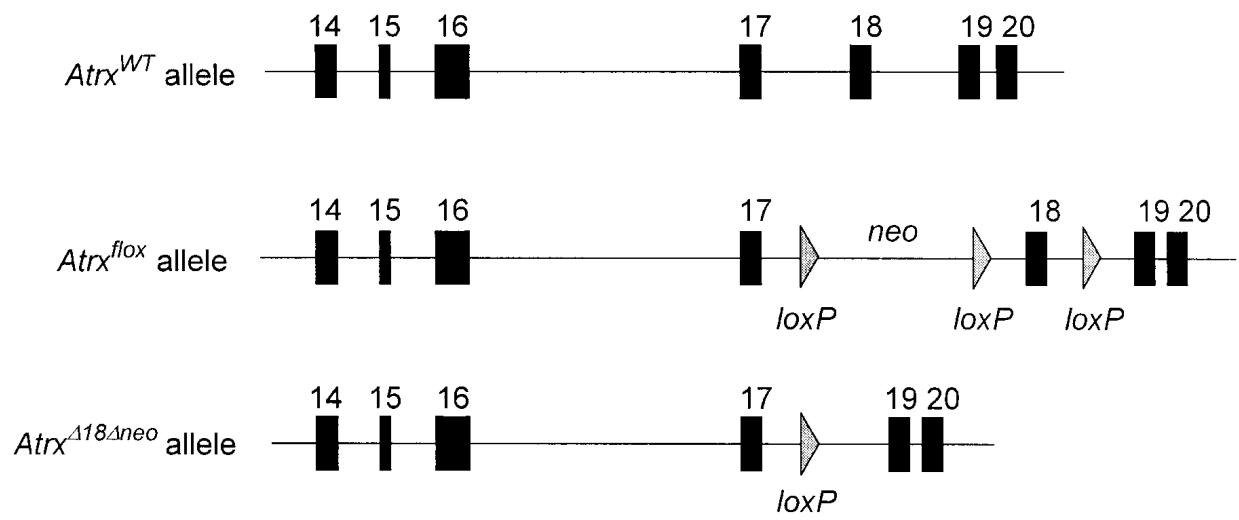
To generate *Atrx*<sup>null</sup> embryos, a Cre-mediated recombination system was used under control of the mouse *GATA-Binding protein-1* (*GATA-1*) regulatory elements, and resulted in active Cre recombinase (Cre) expression at the 16-cell morula stage (8, 33). Zero recovery of *Atrx*<sup>null</sup> male mice at birth indicated that *Atrx* plays a role in embryonic development, which was supported by the finding that embryonic lethality occurred before 9.5 days postcoitus (dpc) (8). Prior to lethality, *Atrx*<sup>null</sup> embryos were smaller in size due to defects in cell proliferation (8). The most striking observation was the highly disorganized appearance of the extra-embryonic tissue caused by defective formation of

the secondary giant cell compartment in the developing trophoderm (8). It is now proposed that the essential role *Atrx* plays in the developing mouse trophoblast may explain the lack of null mutations identified in patients with ATR-X syndrome (8).

#### 1.1.4 ATRX and Neuronal Development

Considering that the major diagnostic feature of ATR-X syndrome is severe mental retardation (20, 21), it is not surprising that ATRX plays a role in neuronal development. To address the function of ATRX in central nervous system development, a mouse model was established whereby Cre-mediated conditional deletion of exon 18 from the *Atrx* gene occurs specifically in the forebrain (9). Recombination of the floxed *Atrx* allele, which was the same strategy used for deletion of *Atrx* in ES cells, is outlined in Figure 1.1. Under control of the *Forkhead box G1 (FoxG1)* promoter, Cre expression is confined to the forebrain commencing at embryonic day 8.5 (E8.5) (34). All *Atrx*<sup>FoxG1Cre</sup> males were smaller at birth and most did not survive past the first 48 hours (9). Furthermore, a profound size reduction in the frontal cortex and hippocampus was observed in combination with a replacement of the entire dentate gyrus by a small mass of disorganized cells (9). Cortical hypocellularity was found to be caused by a drastic increase in neuronal apoptosis during early corticogenesis, ultimately resulting in fewer neurons migrating to the cortex and dentate gyrus (9). The results of this study demonstrated that *Atrx* is critical for neuronal survival during corticogenesis, and this may be a contributing factor to the severe mental retardation found in ATR-X patients.

Figure 1.1 Cre-LoxP mediated targeted deletion of *Atrx* exon 18. The upper line is the wild type (*Atrx*<sup>WT</sup>) allele. The middle line is the floxed (*Atrx*<sup>lox</sup>) allele showing insertion of LoxP Cre target sites with a *neo* marker. The bottom line is the recombined (*Atrx*<sup>Δ18Δneo</sup> or *Atrx*<sup>null</sup>) allele from which exon 18 and the *neo* cassette have been deleted.



## 1.2 Cellular Functions of the ATRX Protein

Since the identification of disease-causing *ATRX* mutations, there has been a great deal of research focused both on determining how the *ATRX* gene is regulated and elucidating the complex functions of the ATRX protein throughout the cell cycle. Important features of the *ATRX* gene and protein are outlined below, with subsequent explanation of the known cellular functions of ATRX. Briefly, the ATRX protein has been implicated in numerous cellular activities including, but not limited to, chromatin remodelling and regulation of genomic stability, transcriptional control of  $\alpha$ -globin gene expression, and epigenetic regulation of DNA methylation. Although many important discoveries have been made regarding ATRX function, numerous questions remain unanswered such as determining what additional genes ATRX targets and how transcriptional regulation is mediated.

### 1.2.1 The ATRX Gene

Following the description of ATR-X syndrome as a disease, linkage analysis was used to localize the ATR-X locus to a proximal region encompassing the chromosomal bands Xq12-q21.31 (19), with a minor refinement of the candidate region to Xq12-q21.1 within one year (35). Subsequent linkage analysis narrowed the chromosomal region to Xq13.1-q21.1 (1), however deletion analysis demonstrated that missing genomic regions in ATR-X patients corresponded to the previously described protein and cDNA sequences encoded by *X-linked nuclear protein (XNP)* (36) or *X-linked helicase 2 (XH2)* (37). This analysis precisely identified the location of *ATRX* at Xq13.3, between the gene for Menkes disease (*MNK*) and the X-chromosome region DXS56 (37). The murine *Atrx*

homolog was shown to map to the homologous region between the *Phosphoglycerate kinase-1 (Pgk1)* and *X-inactivation specific transcript (Xist)* genes (36).

The *ATRX* gene encompasses approximately 300kb of genomic DNA (38) and has an intron-exon boundary that codes for 36 exons (38, 39). This gene encodes a primary transcript of approximately 280 kDa and gives rise to a protein of 2492 amino acid residues (39). The human gene codes at least two transcripts that are the result of alternative splicing of exon 6 and these give rise to proteins of size 278 or 283 kDa (39). Similar splicing of the mouse gene gives predicted proteins of size 274 or 279 kDa (40). A second alternative splice site has been reported for the *ATRX* gene in exon 7 (38), however it has been proposed that this is a rare human-specific transcript that introduces a premature in-frame stop codon to the splice variant (40). Reported failure to splice intron 34 results in partial truncation of the C-terminal region giving rise to a protein of size 267 and 265 kDa in human and mouse, respectively (40). The functional significance of the alternate splice variants has not been determined.

The primary *ATRX* transcript is translated into a novel member of the sucrose non-fermenting 2 (SNF2) family of chromatin remodelling proteins (38), which are a class of enzymes that use the energy of adenosine tri-phosphate (ATP) hydrolysis to disrupt nucleosome stability and are often involved in transcriptional regulation (41). The amino (N)-terminal encodes a nuclear localization signal and a zinc finger region commonly referred to as the ADD (ATRX, DNMT3, DNMT3L) domain (42, 43), while the carboxy (C)-terminal encodes the SNF2 helicase and ATPase domains (38, 44). A truncated *ATRX* protein (*ATRXt*) has been identified in human HeLa, 293 and lymphocyte cell lines (45, 46) as well as mouse embryonic fibroblasts (47). *ATRXt* is

missing the entire C-terminal SNF2 domain due to a failure to splice intron 11 from the primary transcript, however no functional significance has been established for this protein isoform (47). ATRX contains several additional protein motifs, however documented ATR-X mutations most commonly map to either the SNF2 or ADD domains, indicating that both are functionally significant (21).

### 1.2.2 The ADD Domain

Following establishment of the full-length complementary DNA (cDNA) sequence of *ATRX* (38), three zinc finger motifs were located in the five-prime region of the gene (39). Analysis of the N-terminal protein region identified a cysteine-rich motif (cys4-his-cys3) similar to a putative zinc-finger called the plant homeodomain (PHD) (48). Accumulating evidence suggests that PHD fingers regulate gene expression by interacting with the activating histone modification trimethylated lysine 4 on histone H3 (H3K4) (49). The ATRX protein is unique in that the PHD finger is flanked by an additional C<sub>2</sub>-C<sub>2</sub> zinc finger motif, which is a feature shared only with the *de novo* DNA methyltransferases DNMT3A, DNMT3B and DNMT3L (50). Taken together, the zinc finger arrangement has been named the ATRX-DNMT3-DNMT3L (ADD) domain (42).

Recent nuclear magnetic resonance (NMR) structure determination of the ATRX ADD domain has determined that three distinguishable regions including a GATA-like zinc finger, an imperfect PHD-like zinc finger and a C-terminal helix pack together through hydrophobic interactions to form the ADD domain (51). Due to sequence similarity (52), it is likely that the DNMT3 ADD domains fold in a similar manner. Known missense mutations in the ADD domain were originally proposed to disrupt zinc

finger structure (50), and recent evidence shows that the majority of disease-causing mutations affect buried residues in the hydrophobic core while a few affect exposed surface residues (51). While buried mutations are proposed to affect the structural integrity of the ADD domain, surface mutations may affect protein interaction sites (51).

To date, no studies have identified exact protein interaction residues and the function of the ATRX ADD domain ultimately remains unresolved. However, a recent study has shown that the ADD domain of DNMT3L recognizes unmethylated lysine 4 on the amino tail of histone H3 and induces *de novo* DNA methylation by recruitment or activation of DNMT3A2 (53). In addition, the ADD domains of DNMT3L and DNMT3A have been implicated in the recruitment of repressive histone deacetylases (HDAC) to silent chromatin domains (54, 55). These studies suggest that the ATRX ADD domain is involved in recruitment of DNA methyltransferases and/or recruitment of repressive histone modifying enzymes.

### 1.2.3 The SWI2/SNF2 Chromatin Remodelling Domain

Initial characterization of the *ATRX* gene, originally called *XH2* or *XNP*, described a putative member of the helicase II superfamily that shared six conserved domains with other helicases, most notably the switching-2 (SWI2)/SNF2 chromatin remodelling protein RAD54 (*S. Cerevisiae* homolog of *Radiation sensitive gene 54*) (37). Comparative analysis then determined that ATRX is a unique member of the RAD54-like grouping of the SNF2 superfamily of chromatin remodelling proteins with similar catalytic ATPase domains and seven collinear helicase motifs (38, 40). Homologous members of the ATRX subfamily have been predicted or identified in a variety of

eukaryotic species such as the fruitfly *Drosophila melanogaster* (56). SNF2 family members are involved in a broad range of cellular activities, including transcriptional regulation, DNA repair and chromosome segregation (57), however a few RAD54-like SNF2 proteins have been specifically implicated in mitotic repair and meiotic crossover (58). A number of mutations in the C-terminal domain of ATRX result in truncation of the protein and are often associated with urogenital abnormalities in ATR-X patients, however no additional genotype-phenotype correlations have been observed (20).

#### **1.2.4 Chromatin Remodelling and Regulation of Genomic Stability**

The identification of a nuclear localization signal in the N-terminal of ATRX (38) soon led to the discovery that ATRX is associated with the core nuclear matrix during interphase (45, 46), which is a hub for actively transcribed genes. At the same time, the N-terminal was also shown to contain sufficient information to mediate an interaction with Heterochromatin protein 1 $\alpha$  (HP1 $\alpha$ ), resulting in protein localization to pericentric heterochromatin during all stages of the cell cycle (46). It was subsequently demonstrated that ATRX is phosphorylated in a cell cycle dependant manner, leading to the hypothesis that a dual role exists for ATRX in the cell: During mitosis ATRX is involved in chromosome segregation and during interphase ATRX is associated with the nuclear matrix where it regulates gene expression (45).

Upon mitotic entry the ATRX protein becomes phosphorylated predominantly at serine residues, which is proposed to be necessary for release of ATRX from the nuclear matrix and progression into mitosis (45). Targeted short interfering RNA (siRNA) depletion of ATRX in immortal HeLa cells (cervical carcinoma line) results in a variety

of mitotic abnormalities including misalignment at the mitotic plate, cohesion and segregation defects (59). Furthermore, it has also been shown that ATRX is required for meiotic chromosome alignment and spindle organization in murine oocytes (60). These studies suggest that ATRX is required for both the maintenance of genomic stability and the segregation of chromosomes during mitosis and meiosis.

Dephosphorylation of ATRX coincides with exit from mitosis (45). Throughout the Gap 1 (G1) to early Synthesis (S) phases of the cell cycle, ATRX is localized both to pericentric heterochromatin where it interacts with HP1 $\alpha$  (46), as well as promyelocytic leukaemia nuclear bodies (PML-NB) where it interacts with the Fas death domain associated protein (DAXX) (61, 62). At the middle to late S-phase, a site-specific phosphorylation event on ATRX is proposed to result in accumulation of DAXX at condensed heterochromatin (61). Here it is hypothesized that the ATRX-DAXX complex is involved in transcriptional repression via interaction with chromatin-associated proteins such as histone deacetylases and core histones (61). *In vitro* studies have shown that ATRX forms a chromatin remodelling complex with DAXX, thereby supporting a role in transcriptional regulation. In particular, the ATP-dependant ATRX-DAXX complex has translocase activity and is capable of disrupting the DNaseI digestion of a nucleosome (62), both of which are common *in vitro* activities for other members of the SWI2/SNF2 family (63). This finding is clinically significant because the level of ATRX-DAXX complex is decreased in a patient cell line for ATR-X syndrome (62).

At the Gap2 (G2) phase of the cell cycle ATRX is once again dephosphorylated (45) and localizes both to pericentric heterochromatin (46) and the PML-NB (61, 62). At this time, juxta-centromeric satellite DNA localizes with the PML-NB and a series of

proteins layer around the satellite DNA in the order of HP1 $\alpha$ /HP1 $\beta$  - ATRX - DAXX - PML (64). It is now proposed that the PML-NB is tethered to the nuclear matrix where its function is to re-establish the condensed heterochromatic state on late-replicated satellite DNA (64). Additional evidence suggests that the PML is also involved in the regulation of chromatin loop formation at the major histocompatibility complex (MHC) class 1 genes (65). In particular, PML physically interacts with the matrix attachment region (MAR) binding protein, special AT-rich binding protein 1 (SATB1), in an effort to organize the MHC into higher order chromatin loops with restricted expression profiles at individual genes (65). Through the PML, ATRX may therefore be involved in regulation of gene transcription via chromatin looping. Following the G2-phase, ATRX is once again phosphorylated and restarts its functional program within the cell cycle.

### 1.2.5 Transcriptional Regulation of Gene Expression

Downregulation of  $\alpha$ -globin expression in patients with ATR-X syndrome is an additional indication that ATRX may be involved in the regulation of gene transcription. ATR-X patients show changes in  $\alpha$ -globin, but not  $\beta$ -globin expression (38), suggesting that ATRX regulates specific genes depending on their chromatin environment. Studies on the epigenetic status of  $\alpha$ -globin in ATR-X patient cell lines show that *cis*-acting regulatory sequences and patterns of DNA methylation are unchanged (13). However, recent evidence indicated that in erythroid cells, distant regulatory elements come in close proximity with the  $\alpha$ -globin genes in a chromatin-looping mediated transcription factory (66). Conversely, silenced  $\alpha$ -globin genes in other cell types formed a different chromatin

loop resulting in segregation from the transcription factory (66). The  $\alpha$ -globin loop may therefore target ATRX because it is in a different chromatin environment than  $\beta$ -globin.

Additional lines of evidence support a role for ATRX in transcriptional regulation. Although SNF2 chromatin remodelling proteins have been implicated in the control of gene expression and DNA repair, studies on fibroblasts from ATR-X patients show no defects in the DNA repair pathway (37), suggesting that ATRX is likely a transcriptional regulator. A yeast two-hybrid screen later identified an interaction between ATRX and the polycomb-group heterochromatin-associated protein Enhancer of Zeste homolog-2 (EZH2) that is involved in chromatin repression (67). It was suggested that ATRX interacts with EZH2 to counteract chromatin repression, ultimately facilitating transcriptional activation at the  $\alpha$ -globin locus (67).

### **1.2.6 Epigenetic Regulation of DNA Methylation**

Concurrent with the discovery that ATRX localizes to heterochromatin, a striking observation was made that during metaphase ATRX also localizes to the short arms of acrocentric chromosomes where the rDNA arrays are located (46). This prompted researchers to determine whether ATRX plays a role in transcriptional regulation via an epigenetic effect on chromatin. In normal individuals, approximately 20% of rDNA repeats are methylated, whereas patients with ATR-X syndrome show a substantial reduction in DNA methylation at the transcribed 18S and 28S rDNA regions (22). Since ATRX is also associated with heterochromatin, where a variety of repetitive elements reside, a large panel of repeat sequences were screened for ATRX-dependant changes in DNA methylation. Hypermethylation was found at the Y-specific satellite DYZ2, while

subtle changes were observed at the TelBam3.4 repeat family (22). Other repeat families such as the satellites and retroviral-like intracisternal A-particles (IAP) were unaffected in ATR-X patients (22). In the *Atrx*<sup>null</sup> ES cell model, hypomethylation was confirmed at 18S and 28S rDNA sequences, while no change was observed at major satellites, minor satellites and IAP repeats (8).

Although it is not known how ATRX regulates DNA methylation at rDNA, a new clue has emerged which sheds light on one possible mechanism of epigenetic control. Recently, it was discovered that ATRX interacts with Methyl CpG-Binding Protein-2 (MeCP2) specifically at heterochromatin of mature neurons (68). MeCP2 binds methylated CpG sites throughout the genome where it recruits corepressors such as histone deacetylase-1 (HDAC1) (69-71). More importantly, MeCP2 activity is essential for proper brain function, and females heterozygous for mutations in MeCP2 develop the severe X-linked neurological disorder Rett Syndrome within the first two years of life (72). It was determined that the N-terminal of ATRX is sufficient to target the protein to heterochromatin in the absence of MeCP2 in both methylated and non-methylated cells, however, MeCP2 specifically targets the C-terminal of ATRX only at methylated heterochromatin of mature neurons (68). In the post-natal brain, loss of MeCP2 results in a major decrease of ATRX at heterochromatin, despite both normal levels of ATRX protein and normal targeting to heterochromatin in non-brain tissues where MeCP2 is less abundant (68). It is now proposed that disruption of the ATRX-MeCP2 interaction alters the normal epigenetic environment of neuronal heterochromatin and ultimately leads to pathologic changes that contribute to mental retardation (68).

### 1.3 Epigenetic Regulation of Genomic Imprinting

A few members of the SNF2 chromatin remodelling family play roles in the transcriptional control of imprinted genes, wherein epigenetic marks such as DNA methylation, histone acetylation and histone methylation have been touted as the major modifications regulating changes in gene expression. Genomic imprinting is a heritable process in which genes exhibit monoallelic expression from one of the parental alleles by regulating the accessibility of chromatin via epigenetic chromatin modifications. Examining changes in imprinted gene expression patterns can therefore be used as a tool to determine whether a particular protein is involved in epigenetic transcriptional control.

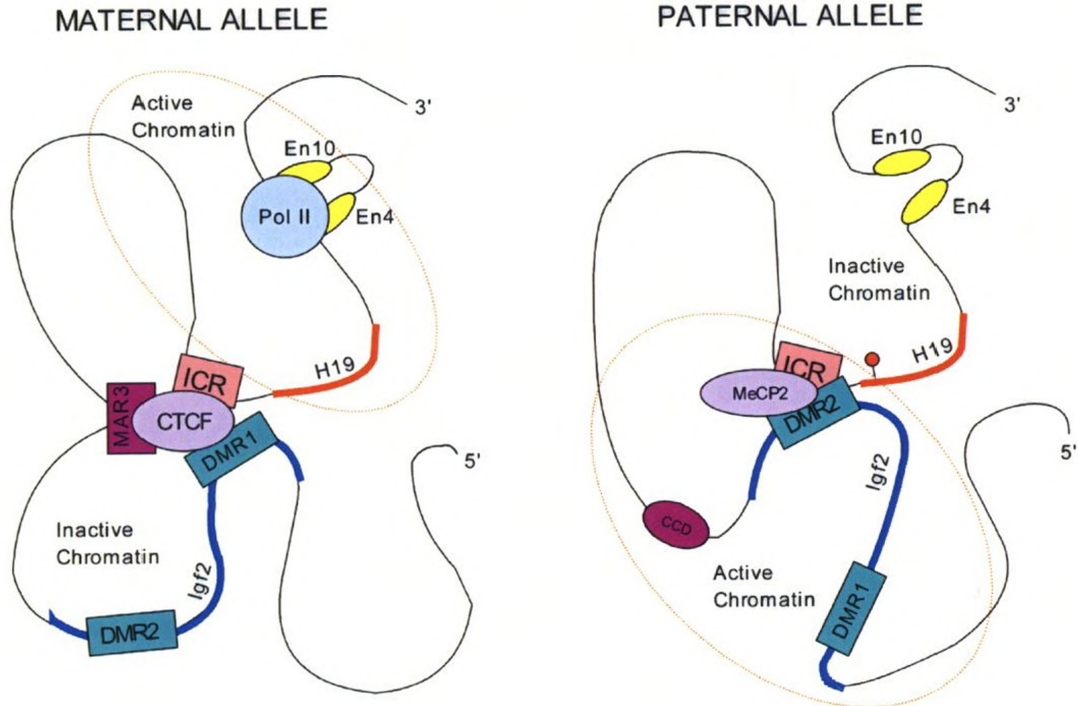
#### 1.3.1 Models of Genomic Imprinting

Over two decades ago it was shown that both parental genomes are required for normal embryogenesis, indicating that there is a parent of origin effect on gene function (73, 74). It was subsequently determined that specific chromosomal regions are hot-spots for this parental effect, wherein certain maternally and paternally derived loci showed differential gene expression patterns (75). These unique chromosomal regions contain clusters of imprinted genes that are differentially marked by a variety of epigenetic modifications depending on whether the active allele is maternally or paternally inherited. Two mechanisms have now been proposed to explain the regulation of imprinted loci: Long range chromatin looping and chromatin spreading by non-coding RNAs.

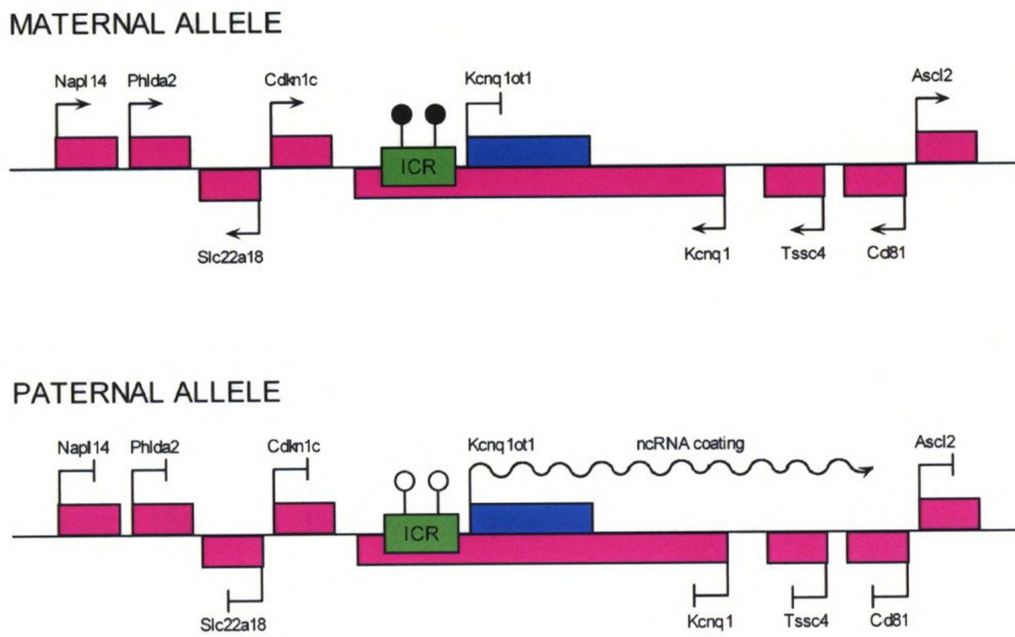
The non-coding RNA gene *H19* and its reciprocal imprint *Insulin-like growth factor 2 (Igf2)* are the most studied of the imprinted genes (Figure 1.2A). Just upstream of the *H19* promoter is an imprinting control region (ICR) that is differentially methylated

Figure 1.2 Models of genomic imprinting. (A) Chromatin looping model of imprinting at the *H19 – Igf2* domain. The unmethylated maternal *H19* ICR and *Igf2* DMR1 form a CTCF-mediated loop in which only *H19* is actively transcribed. The methylated paternal *H19* ICR and *Igf2* DMR2 form a chromatin loop involving MeCP2 in which only *Igf2* is actively transcribed. This model is based on results from neonatal liver and may not apply to other tissues. (B) Non-coding RNA model of imprinting at the *Kcnq1* domain. Methylation (black dots) of the maternal *Kcnq1* ICR prevents *Kcnq1ot1* transcription and all other genes are transcribed. Lack of methylation (white dots) at the paternal *Kcnq1* ICR results in *Kcnq1ot1* transcription and all genes centromeric to the ICR are silenced by the *Kcnq1ot1* ncRNA (squiggly line). Genes that are telomeric to the ICR are silenced by an unknown mechanism. Maternally expressed genes are shown in pink and paternally expressed genes are shown in blue.

A. H19 - Igf2 Chromatin Looping



B. Kcnq1ot1 ncRNA Coating



(76). The unmethylated maternal ICR recruits the insulator CCCTC-binding factor (CTCF), which in turn forms a chromatin loop via interaction with a downstream matrix attachment region (MAR3) and the unmethylated *Igf2* DMR1 (Differentially methylated region 1) (77). This results in the formation of a transcriptionally silent chromatin loop surrounding the maternal *Igf2* gene. Alternatively, CTCF does not bind to the methylated paternal allele and an interaction between the methylated ICR and methylated *Igf2* DMR2 (Differentially methylated region 2) occurs via undetermined protein factors (77). One candidate protein is MeCP2, which has a known association with the ICR (78), but has not been shown to interact with the *Igf2* DMR2. Regardless, this chromatin environment shuttles *Igf2* to a transcriptionally active region, whereas *H19* is no longer expressed.

The long-range chromatin looping model of imprinted gene regulation also takes boundary elements into account. For example, two MARs at the paternal *H19/Igf2* locus associate with the nuclear matrix (79), while the maternal MAR3 site is in complex with the ICR and CTCF (77). The nuclear matrix is therefore likely important for chromatin organization. Nuclear matrix interactions with MAR regions may act as boundary elements to prevent the spreading of chromatin modifications or to separate specific chromatin loops or domains.

The second model of imprinted gene regulation involves chromatin spreading by non-coding RNAs. While the majority of genes in an imprinted cluster are imprinted protein-coding mRNA genes, at least one non-coding ncRNA is present in every imprinted cluster identified thus far. Imprinted mRNAs and ncRNAs are always reciprocally expressed, suggesting that ncRNAs may be involved in the repression of mRNA genes in an imprinted cluster. Perhaps the best-defined locus showing non-coding

RNA control is the large *Potassium channel Q1 (Kcnq1)* domain (Figure 1.2B). Nine imprinted mRNA genes are maternally expressed (80, 81), while the ncRNA *Potassium channel Q1 overlapping transcript-1 (Kcnq1ot1)* is paternally expressed from a promoter presiding within the *Kcnq1* ICR (82). Maternal methylation of the *Kcnq1* ICR ensures that the ncRNA *Kcnq1ot1* is transcribed only from the paternal allele, after which it has the potential to silence the paternal mRNA genes on the centromeric side of the locus by overlapping with their coding regions in an antisense orientation (83). Genes on the telomeric side of the locus are not coated by *Kcnq1ot1*, and their regulation is believed to be via CTCF-dependant chromatin looping interactions.

Both mechanisms of imprinted gene regulation rely initially on differential CpG methylation of an imprinting control center. Although allele-specific epigenetic marks are the basic regulators of genomic imprinting, there is little understanding regarding the relationship between primary and secondary establishment of DMR methylation, implications for the various histone modifications, and how different epigenetic marks are translated into tissue-specific patterns of genomic imprinting.

### 1.3.2 SNF2 Regulation of Genomic Imprinting

Besides ATRX, three additional members of the SWI2/SNF2 chromatin remodelling superfamily have demonstrated involvement in the regulation of genomic imprinting. In the flowering plant, *Arabidopsis thaliana*, mutations in the protein DECREASE IN DNA METHYLATION-1 (DDM1) cause a 70% decrease in global DNA methylation (84-86). Mutations in the imprinted MEDEA (MEA) locus result in defective cell proliferation in the plant embryo and endosperm, however, concurrent

DDM1 mutations rescue the *mea* phenotype by reactivating paternally inherited MEA alleles during seed development (87). Maintenance of the genomic imprint at the MEA locus therefore requires the chromatin remodelling activity of the SNF2 protein DDM1.

Closely related in sequence and function to DDM1 is the human and murine SWI2/SNF2 protein Proliferation Associated SNF2-like Gene (PASG; also known as LSH or lymphoid specific helicase). Depletion of PASG during embryonic development results in global hypomethylation and re-expression of normally repressed genes such as IAP repeats (88-90). Loss of murine PASG results in altered expression specifically of the imprinted gene *Cyclin dependant kinase inhibitor 1c* (*Cdkn1c*), whereas other imprinted genes are unaffected (91). Reactivation of the paternal *Cdkn1c* allele was caused by loss of DNA methylation at the DMR in the *Cdkn1c* promoter, where chromatin immunoprecipitation (ChIP) analysis showed direct binding of PASG (91). This research showed that the SNF2 chromatin remodelling protein PASG is not required for the maintenance of CpG methylation at all imprinted loci, but rather PASG is required at specific genomic imprints such as *Cdkn1c*.

In humans, a third SNF2 protein called CHD8 (Chromo domain, SNF2 Helicase domain, DNA binding domain) has been shown to interact with CTCF at the unmethylated maternal *H19* ICR (92). Using an RNA interference (RNAi) strategy to target CHD8 depletion, insulator activity of the *H19* ICR was significantly reduced and resulted in activation of maternal IGF2 expression (92). Although methylation analysis at non-imprinted CTCF target sites revealed hypermethylation of CpGs and hypoacetylation of histone H3, the methylation status of the *H19* ICR did not change in the absence of CHD8 (92). Taken together, this research showed that the human SNF2 protein CHD8 is

involved in DNA methylation, however that function may be distinct from the role CHD8 plays in the regulation of imprinting at the *H19 – Igf2* locus.

#### 1.4 Hypothesis and Summary of Findings

To assess a potential role for ATRX in the epigenetic regulation of chromatin structure, determining the effect of ATRX deletion at a variety of imprinted domains is essential. **I hypothesize that ATRX regulates imprinted gene expression in the murine forebrain via the maintenance of epigenetic DNA methylation marks.** This hypothesis was addressed using the previously described mouse model system in which *Atrx* is conditionally deleted from the cortex and hippocampus beginning at E8.5 (34).

In chapter 3.1, I compare forebrain DNA methylation patterns at rDNA, major satellite, minor satellite and intracisternal A-particle (IAP) repeats to findings from ATR-X patients and *Atrx*<sup>null</sup> murine ES cells. I demonstrate that there is a change in DNA methylation at 18S rDNA repeats, while DNA methylation patterns at major satellite, minor satellite and IAP repeats are unchanged. These results indicate that the *Atrx*<sup>null</sup> forebrain model is comparable with ATR-X patients and the *Atrx*<sup>null</sup> ES cell model, although not completely since 28S methylation seems unaffected.

Chapter 3.2 focuses on investigating the effect of *Atrx* nulligosity on imprinted gene expression at post-natal day 0.5 (P0.5). I show that deletion of *Atrx* causes upregulation of specific imprinted genes, including the micro-RNA *H19*, *Insulin-like growth factor 2 (Igf2)*, *Delta-like 1 (Dlk1)*, *Solute carrier family member 38a4 (Slc38a4)* and *Decorin (Dcn)*, while other imprinted genes are unchanged. I also show that the partially imprinted gene *Distal-less homeobox gene 5 (Dlx5)* is upregulated at P0.5. In

chapter 3.3, I demonstrate that not all stages of development display aberrant gene expression, whereby increased gene expression was only observed at post-natal time points. This result suggests that there is a gradual effect on imprinted gene expression, which supports a role for ATRX in the maintenance of epigenetic imprinting marks.

In chapters 3.4-3.5, I present results from DNA methylation analysis at the regulatory differentially methylated regions (DMR) of the *Gene-trap locus 2 (Gtl2) – Dlk1* and the *H19 – Igf2* imprinted domains. With respect to the *Gtl2 – Dlk1* locus, I show that there is a change in DNA methylation at the *Gtl2* DMR, but this does not occur for all *Atrx*-null forebrains analysed. Conversely, at the *H19 – Igf2* locus I demonstrate that DNA methylation patterns are unchanged and do not correlate with changes in gene transcription. These experiments demonstrate that ATRX plays a minor role in the regulation of DNA methylation at the *Gtl2 – Dlk1* imprinting domain, however the transcriptional control of the *Gtl2 – Dlk1* and *H19 – Igf2* imprinted loci is likely by an alternate means of epigenetic modification.

In chapter 3.6, I present results from chromatin immunoprecipitation analysis of *Atrx* and MeCP2 at the *H19* ICR. I demonstrate that *Atrx* specifically targets the *H19* ICR in the same location as MeCP2. This experiment strongly suggests that *Atrx* is involved in regulation of *H19 – Igf2* imprinting and supports the observed upregulation of *H19* and *Igf2* from transcriptional profiling of the *Atrx<sup>null</sup>* forebrain. Furthermore, this is the first evidence that *Atrx* and MeCP2 co-localize at a target genomic site besides pericentric heterochromatin in order to regulate gene expression in brain tissue.

The results presented in this thesis show that *Atrx* plays a role in DNA methylation at rDNA repeats in the mouse forebrain, confirming that the *Atrx<sup>null</sup>* forebrain

model is comparable to ATR-X patients and *Atrx*<sup>null</sup> ES cells. I have shown that *Atrx* regulates gene transcription by targeting specific imprinted genes during post-natal stages of development, which is the first evidence of a link between ATRX and the control of imprinted gene expression. I also determined that upregulation of target imprinted genes is not due to changes in DNA methylation at regulatory DMRs, making this report one of few that demonstrate a change in imprinted gene expression without a change in DNA methylation (92-94). In addition, I have identified the first known gene target site for *Atrx* at the *H19* ICR and provide evidence that *Atrx* and MeCP2 can co-localize at target sites other than pericentric heterochromatin. Taken together, I have shown that *Atrx* is essential for the proper genomic regulation of *H19*, *Igf2*, *Dlk1*, *Slc38a4* and *Dcn*.

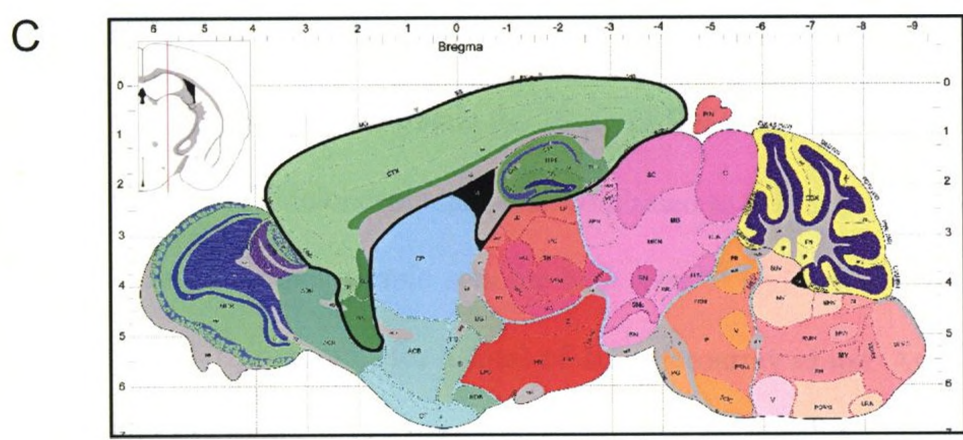
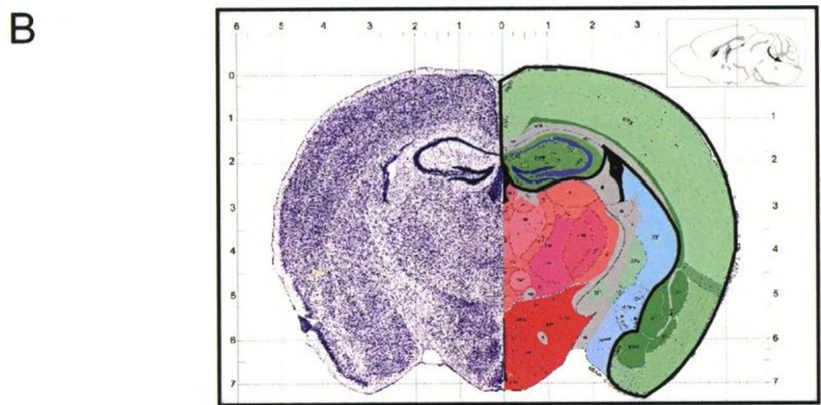
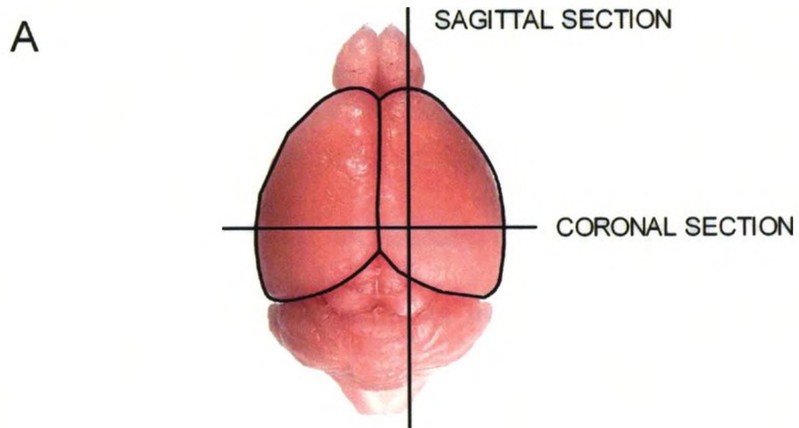
## CHAPTER 2 – Materials and Methods

### 2.1 Animal Husbandry and Genotyping

Conditional deletion of *Atrx* in the murine forebrain was achieved by crossing *Atrx<sup>loxP</sup>* females (129Sv background) with heterozygous *Foxg1Cre* knock-in males (129Sv/FVBN mixed background) (9), as outlined in Figure 1.1. The *Atrx<sup>loxP</sup>* line was kindly provided by D. Higgs (Weatherall Institute of Molecular Medicine, John Radcliffe Hospital, Oxford, United Kingdom). *Foxg1Cre* males (34) were provided by R. Slack (Ottawa Health Research Institute, Ottawa, Ontario, Canada) from a line originally obtained from S. McConnell (Stanford University, Stanford, California, USA). *Atrx<sup>loxP</sup>* females were generated by recombinant cloning of a *loxP* site into the middle of *Atrx* intron 18, in addition to insertion of a neomycin (neo)-selectable marker flanked by *loxP* sites midway between *Atrx* exons 17 and 18 (9). The *Foxg1* promoter specifically targets *Cre* expression to the forebrain beginning at the E8.5 stage of development (34), as outlined in Figure 2.1. The genotype of control animals was *Atrx<sup>lox/y</sup> Cre<sup>-</sup>* and the genotype of *Atrx<sup>null</sup>* animals was *Atrx<sup>lox/y</sup> Cre<sup>+</sup>*.

Wild type mice with polymorphic alleles were generated by crossing *Mus musculus domesticus* females (129Sv background) with *Mus musculus castaneus* males (CAST). To generate polymorphic *Atrx<sup>null</sup>* males, attempts were made to cross heterozygous *Atrx<sup>lox/wt</sup> Cre<sup>+</sup>* females with CAST males, however these crosses were unsuccessful to date. CAST males were kindly provided by M. Mann (Child Health Research Institute, London, Ontario, Canada).

Figure 2.1 Regions of the mouse brain used for experimental analyses. (A) Outline of the cortical lobes encompassing the mouse forebrain. (B) Coronal view of the mouse brain. Areas outlined in black and coloured in green encompass the forebrain and include the cerebral cortex and hippocampus. Other areas coloured in blue, orange or peach comprise the cerebral nuclei and regions of the interbrain such as the hypothalamus and thalamus, which are areas where Atrx is not depleted. (C) Sagittal view of the mouse brain. Areas outlined in black and coloured in green encompass the forebrain region used for experimentation. The black triangular structure is the region containing the cortical choroid plexus. The remaining green and blue area is the olfactory bulb and the cerebral nuclei, and this region was excluded from experimentation. The orange and peach areas comprise the interbrain, the pink area is the midbrain, the yellow and purple area is the cerebellum and the remaining lighter orange and pink areas comprise the hindbrain. Images were adapted from the Allen Brain Atlas available online at [www.brain-map.org](http://www.brain-map.org).



DNA from tail or ear biopsies was genotyped by PCR using primer sets for Cre (Cre3b and Cre5b) and *Atrx* (17F, 18R and *neo<sup>R</sup>*) or Sry (SryF and SryR), as listed in Table 2.1. For the developmental study at E13.5, midday of the day of vaginal plug discovery was considered E0.5. For post-natal time-points, midday of the day of birth was considered P0.5 and morning of the seventeenth day of life was considered P17. At scheduled time-points, pregnant females were anesthetized by CO<sub>2</sub> and sacrificed by cervical dislocation. Newborn animals were sacrificed by decapitation. P17 males were anesthetized by CO<sub>2</sub> and sacrificed by cervical dislocation. All animal studies were conducted in compliance with the regulations of The Animals for Research Act of the province of Ontario, the guidelines of the Canadian Council on Animal Care and the policies and procedures approved by the University of Western Ontario Council on Animal Care.

## 2.2 Microarray

Forebrain tissue was collected at E13.5 and P0.5 from *Atrx<sup>null</sup>* mice and control littermates. Total RNA was extracted using an RNeasy Mini Kit (QIAGEN) according to the manufacturer's instructions. To obtain the 10 µg of RNA required for each microarray chip, RNA from two E13.5 telencephelons was combined to achieve the required amount for one sample. Three unique sample sets for both *Atrx<sup>null</sup>* and control littermates were processed at the E13.5 timepoint, for a total of six microarray chips. At the P0.5 time-point, one forebrain gave sufficient RNA for microarray analysis. Four *Atrx<sup>null</sup>* and three control littermates were processed at the P0.5 time-point, of which two of the *Atrx<sup>null</sup>* samples were from the same litter and therefore normalized to the same control littermate

**Table 2.1 List of oligonucleotides used in genotyping, Southern blot, RT-PCR, McrPCR, cloning, bisulfite mutagenesis and ChIP assays**

**Primers used to genotype progeny of *Atrx<sup>ff</sup>* x *BflCre<sup>+</sup>* matings**

17F: 5'-AGAACCGTTAGTTGCAGGTTCA-3'

18R: 5'-TGAACCTGGGGACTTCTTTG-3'

NeoR: 5'-CCACCATGATATTCGGCAAG-3'

SryF: 5'-GCAGGTGGAAAAGCCTTACA-3'

SryR: 5'-AAGCTTTGCTGGTTTTTGGGA-3'

Cre3b: 5'-TGACCAGAGTCATCCTTAGCG-3'

Cre5b: 5'-AATGCTTCTGTCCGTTTGCC-3'

**Primers used to amplify cDNA by RT-PCR or quantitative RT-PCR**

bactinF: 5'-ATGGAGAAGATCTGGCAC-3'

bactinR: 5'-CGTCACACTTCATGATGG-3'

H19F: 5'-TGATGGAGAGGACAGAAGGG-3'

H19R: 5'-TTGATTCAGAACGAGACGGAC-3'

Igf2F: 5'-AGCGGCCTCCTTACCCAACTTCAG-3'

Igf2R: 5'-AAGGCCTGCTGAAGTAGAAGCCG-3'

Dlk1 4/5 F: 5'-CACCTGGGTTCTCTGGAAAG-3'

Dlk1 4/5 R: 5'-AGGGGTACAGCTGTTGGTTG-3'

Gtl2 2/3 F: 5'-TTGCTGTTGTGCTCAGGTTC-3'

Gtl2 2/3 R: 5'-ATCCTGGGGTCCTCAGTCTT-3'

Slc38a4F: 5'-TGCATGGTGTTCGTCAG-3'

Slc38a4R: 5'-CTGTTCCCGATCCGTAATTC-3'

DcnF1: 5'-AGCTTCAACAGCATCACCGTT-3'

DcnR1: 5'-GCAGTCTGGCCAATGTTTCCT-3'

Zim1F: 5'-AGTCAAGCATCCAAAGGC-3'

Zim1R: 5'-AGGCAAGGGAGTCTGTTTAG-3'

**Primers used to amplify rDNA probes for Southern blot analysis**

RIB3F: 5'-AAGAAGACCCTGTTGAGCTTGACTC-3'

RIB3R: 5'-GCTTCACAATGATAGGAAGAGCCG-3'

RIB4F: 5'-GACCAGAGCGAAAGCATTTC-3'

RIB4R: 5'-GGACATCTAAGGGCATCACAGACC-3'

**Primers used to amplify mutagenized DNA for bisulfite sequencing analysis**

H19 ICR OF: 5'-GAGTATTTAGGAGGTATAAGAATT-3'

H19 ICR OR: 5'-ATCAAAAATAACATAAACCCCT-3'

H19 ICR IF: 5'-GTAAGGAGATTATGTTTATTTTTGG-3'

H19 ICR IR: 5'-CCTCATTAATCCCATAACTAT-3'

Igf2 DMR1 OF: 5'-GGTTAGGTGAAGGTTTTGTGGGTAGTTATA-3'

Igf2 DMR1 OR: 5'-ATATCCCCTTTCAAATCCAATCTACATC-3'

Igf2 DMR1 IF: 5'-GGTGGTTTTTTAATGGATATTTAAGGTGA-3'

Igf2 DMR1 IR: 5'-CCAACCTCTATCCCTAACTTTTCTAACCTC-3'

Igf2 DMR2 OF: 5'-AACTAAAATTATCTATCCTATAAAAC-3'

Igf2 DMR2 OR: 5'-TTGATGGTATTATATTGTAGAATTAT-3'

Igf2 DMR2 IF: 5'-TATCTATCCTATAAACTTCCAAACAAACCTTCAAA-3'

Igf2 DMR2 IR: 5'-AATTTGATTTATTGATGGTTGTTGGATATTTT-3'

Dlk1 DMR OF: 5'-GATTAGTGATTTATAATTTGTGTTTTGGTT-3'

Dlk1 DMR OR: 5'-AAACTCACCTAAATATACTAAAAACAAATA-3'

Dlk1 DMR IF: 5'-GAGATTAAGTAAGAGGTGGGAAAGGGT-3'

IG DMR OF: 5'-TTAAGGTATTTTTTATTGATAAAATAATGTAGTTT-3'

IG DMR OR: 5'-CCTACTCTATAATACCCTATATAATTATACCATAA-3'

IG DMR IF: 5'-TTAGGAGTTAAGGAAAAGAAAGAAATAGTATAG-3'

Gtl2 DMR OF: 5'-TGGTTTGGGGGTAGTTTTTTATTGTAG-3'

Gtl2 DMR OR: 5'-AAAAAATACAAATAAATTAATTAACAAATCACAAA-3'

Gtl2 DMR IF: 5'-ATTTTTAAATGATGGTTGATGTGGGTTT-3'

**Primers used to amplify DNA for McrPCR methylation analysis**

MajSatF: 5'-GACGACTTGAAAAATGACGAAATC-5'

MajSatR: 5'-CATATTCCAGGTCCTTCAGTGTGC-3'

MinSatF: 5'-CATGGAAAATGATAAAAACC-3'

MinSatR: 5'-CATCTAATATGTTCTACAGTGTGG-3'

IAPgagF: 5'-AGCAGGTGAAGCCACTG-3'

IAPgagR: 5'-CTTGCCACACTTAGAGC-3'

28SF: 5'-CCTGTGAATTCTCTGAACTC-3'

28SR: 5'-CCTAAACTGCTGACAGGGTG-3'

18SF: 5'-CGGTACAGTGAAACTGCGAAT-3'

18SR: 5'-GGATGCGTGCATTTATCAGA-3'

**Primers used to amplify inserts from cloning vectors**

M13F: 5'-GTAAAACGACGGCCAG-3'

M13R: 5'-CAGGAAACAGCTATGAC-3'

pCC1F: 5'-GGATGTGCTGCAAGGCGATTAAGTTGG-3'

pCC1R: 5'-CTCGTATGTTGTGTGGAATTGTGAGC-3'

**Primers used to amplify regions of the *H19* ICR for ChIP**

ICRAF: 5'-CCTGGAGCCTGAGTTAAAACC-3'

ICRAR: 5'-AAGCCGACCTTGTTGATTTG-3'

ICRBF: 5'-TTTCTAGGCTGGTACCTCGTG-3'

ICRBR: 5'- ACCATGCTTAGTGGGGTCTG-3'

ICRCF: 5'-TGTGGTGATCATGGAATGTATTG-3'

ICRCR: 5'- CCACATGCACTGGTTTATGG-3'

ICRDF: 5'-AACCGCCAACAAGAAAGTCTGG-3'

ICRDR: 5'- GCTTCGGACATTGCTGTGGG-3'

ICREF: 5'-ATGGCAGGAGGGGCATAG-3'

ICRER: 5'- CTGTCACCTTGTGGTGGTTG-3'

sample. Collection and processing of E13.5 tissue was performed by Michael Levy, who is a PhD student in the Bérubé laboratory.

Microarray services were performed by the London Regional Genomics Centre Microarray Facility at the Robarts Research Institute. Qualitative assessment of RNA was conducted using an Agilent Bioanalyzer 2100. RNA from each sample was analyzed on an Affymetrix GeneChip Mouse Genome 430 2.0 Array and scanned with an Affymetrix GeneChip Scanner 3000 7G. The Affymetrix GeneChip Mouse Genome 430 2.0 Array detects 45,101 transcripts that represent approximately 34,000 genes.

Using Agilent GeneSpring software, gene expression profiles were subsequently analyzed with the assistance of Michael Levy. Three steps for data normalization were used. First, all values lower than 0.01 were set to 0.01. Second, each measurement was divided by the 50<sup>th</sup> percentile of all measurements in the sample. Last, all control and *Atrx*<sup>null</sup> samples were normalized against the median of the control samples. Each measurement for each gene was divided by the median of the gene's measurements in the corresponding control samples. To generate expression lists, samples were first filtered using normalized data from *Atrx*<sup>null</sup> samples with values greater than or less than a factor of 1.5 fold. Probes were then filtered with a t-test p-value of 0.05 using a cross-gene error model. A secondary multiple testing correction was performed using the Benjamini and Hochberg false discovery rate test.

### 2.3 Semi-Quantitative RT-PCR

Three micrograms of total RNA obtained from *Atrx*<sup>null</sup> and littermate control forebrains were reverse-transcribed into cDNA. The conditions for reverse transcription

were as follows: RNA (3 µg) in DEPC-H<sub>2</sub>O was mixed with random primers, heated for ten minutes at 65°C and incubated on ice for two minutes. The 5X first strand buffer, 100 mM DTT, 25 mM dNTPs, Superscript Reverse Transcriptase, RNA guard and DEPC-H<sub>2</sub>O were added and the reaction mixture was incubated for ten minutes at 30°C and then forty-five minutes at 42°C. cDNA was stored at -20°C. Control reactions without reverse transcriptase were prepared in parallel.

Reverse-transcribed cDNA was used for RT-PCR amplification with the primers listed in Table 2.1. Conditions for amplification were as follows: 35 cycles of 95 °C for 30 seconds, 55 °C for 30 seconds, and 72 °C for 1 minute. Depending on the linear range of amplification, after 25-33 cycles PCR reactions were paused and 15 µL of PCR product was resolved on a 1.2% agarose gel. PCR reactions were then resumed through to 35 cycles. Initial screening was performed on one *Atrx*<sup>null</sup> and litter-matched control pair. For genes showing aberrant expression, changes were confirmed in two additional *Atrx*<sup>null</sup> and litter-matched control pairs.

## 2.4 Quantitative Real Time RT-PCR

Reverse-transcribed cDNA was used for quantitative real time PCR amplification with the same primers used for semi-quantitative RT-PCR (Table 2.1). cDNA was amplified with iQ<sup>TM</sup> SYBR<sup>®</sup> Green mastermix (BioRad) using the standard curve Ct method of quantification. Experiments were performed on a Chromo-4 thermocycler and analyzed with Opticon Monitor 3 and GeneX (BioRad) software. Gene expression analysis was repeated in triplicate for each sample. Conditions for amplification were as follows: 25-35 cycles of 95 °C for 10 seconds, 55 °C for 20 seconds, 72 °C for 30

seconds, and a final melting curve generated in increments of 0.5 °C per plate read. In some cases where primer-dimers were generated, experiments were repeated with the addition of a pre-plate-read melt just below the melting temperature of the desired amplicon. This approach ensured that primer-dimers were not quantified. Standard curves were generated for each primer pair using three-fold serial dilutions of control cDNA. Primer efficiency was calculated as  $E = [10^{(-1/\text{slope})} - 1] * 100\%$ , where a desirable slope is  $-3.32$  and  $r^2 > 0.990$ . All data was corrected against *β-actin* or *Gapdh* as an internal control. To confirm amplification of the desired product, PCR amplicons were size-separated on 1.2% agarose gel by electrophoresis. Quantitative RT-PCR was performed on the four *Atrx<sup>null</sup>* and control litter-matched pairs used for RNA microarray, with subsequent analysis of seven additional pairs.

## 2.5 Methylation Sensitive Southern Blot

P0.5 forebrain tissue was collected and then digested with Proteinase K over a period of approximately 24 hours. DNA was purified using the standard phenol:chloroform extraction method. For the IAPgag and minor satellite analyses, DNA from three *Atrx<sup>null</sup>* and littermate control pairs was digested with the methylation-sensitive restriction enzyme *HpaII* and its methylation insensitive isoschizomer *MspI*. DNA for the major satellite blot was digested with methylation-sensitive *HpyCH41V*. DNA for the 18S rDNA blot was digested with *BamHI* and methylation-sensitive *SmaI*, while DNA for the 28S rDNA blot was digested with *EcoRI* and methylation-sensitive *PvuI*. For each restriction digest, reaction components were size-separated on a 1% agarose gel by electrophoresis to ensure complete digestion of sample DNA. Following complete

digestion, agarose gels were bathed in acid (0.25M HCl) to depurinate DNA fragments. An alkali bath (88g NaCl, 20g NaOH, 1L dH<sub>2</sub>O) was then used to denature the double-stranded DNA, which was followed by neutralization (60.5g Tris, 87.6g NaCl, 37.5 mL HCl, 1L dH<sub>2</sub>O). For the major satellite, minor satellite and IAP blots, 1 µg of DNA was transferred to Hybond-N membrane (Amersham) using a PosiBlot<sup>®</sup> 30-30 Pressure Blotter (Stratagene) in 10X SSC buffer. For the rDNA blots, 5 µg of DNA was transferred using the same approach. Following transfer, DNA was crosslinked to the Hybond-N membrane using a Stratalinker<sup>®</sup> UV Crosslinker (Stratagene).

For IAP, major satellite and minor satellite blots, pIAP, pMR150 and pSAT probes were obtained from F. Dick (Cancer Research Institute; University of Western Ontario, London, Canada) and have been previously published (95). Primer sequences used to amplify 18S and 28S probes are outlined in Table 2.1 and were obtained from R. Gibbons (Weatherall Institute of Molecular Medicine; University of Oxford, Oxford, United Kingdom) (8). All probes were labelled with RediVue [ $\alpha^{32}\text{P}$ ]-dCTP (Amersham) using the Prime-It II Random Primer Labelling Kit (Stratagene) according to the manufacturer's instructions. Labelled probes were purified on a Sephadex G50 spin column and levels of [ $\alpha^{32}\text{P}$ ] incorporation were measured using an LKB Wallac 1211 Rock Beta liquid scintillation counter. Membranes were pre-soaked in hybridization buffer and then hybridized overnight with  $2.0 \times 10^6$  cpm [ $\alpha^{32}\text{P}$ ]-labelled probe per 1 mL of hybridization buffer at 65 °C. Following hybridization, excess probe was washed from the membrane using two low stringency washes (40mL 20X SSC, 2mL 20% SDS, 358 mL dH<sub>2</sub>O) and one high stringency wash (4mL 20X SSC, 2mL 20% SDS, 394mL dH<sub>2</sub>O)

for 15 minutes each at 65 °C. Membranes were exposed to X-ray film (Kodak BioMAX) at -80 °C and patterns of hybridization were visualized by autoradiography. Films were developed in a Kodak M35A X-OMAT Processor.

## 2.6 McrPCR Methylation Analysis

Genomic DNA was digested with the restriction enzyme *McrBC* (New England Biolabs), which only cleaves methylcytosine of the form (G/A)<sup>m</sup>C in the recognition sequence 5'...Pu<sup>m</sup>C(N<sub>40-30000</sub>)Pu<sup>m</sup>C...3'. Quantitative real time PCR was used to determine the relative levels of unmethylated DNA at *IAPgag*, major satellite, minor satellite and ribosomal DNA repeats, following a previously published protocol (95). Conditions for amplification were as follows: 25-35 cycles of 95 °C for 10 seconds, 55 °C for 20 seconds, 72 °C for 30 seconds, and a final melting curve generated in increments of 0.5 °C per plate read. Major satellite and minor satellite samples were diluted 100-fold due to high copy number in the mouse genome (95). Standard curves were generated for each pair using three-fold serial dilutions of control littermate cDNA. Primer efficiency was calculated as  $E = [10^{(-1/\text{slope})} - 1] * 100\%$ , where a desirable slope is  $-3.32$  and  $r^2 > 0.99$ . All data was corrected against equal input levels of internal control undigested DNA. Samples with lower levels of methylation showed increased amounts of PCR product.

## 2.7 Bisulfite Mutagenesis

Genomic DNA isolated from the forebrain of two *Atrx*<sup>null</sup> and littermate control pairs was mutagenized with sodium bisulfite using an EpiTect Bisulfite Conversion Kit (QIAGEN) according to the manufacturer's instructions. Sodium bisulfite deaminates unmethylated cytosine resulting in the conversion to uracil, which is further converted to thymine in a PCR reaction. Methylated cytosines remain unconverted. PCR amplification was carried out with primers specific for bisulfite-treated DNA as outlined in Table 2.1. All DMRs were amplified by the nested or semi-nested PCR approach using previously described conditions (96-99). In general, the initial PCR reactions used amplification conditions as follows: 2-4 cycles of 94 °C for 1-4 minutes, 50-55 °C for 2 minutes, 68-72 °C for 2-3 minutes, followed by 25-35 cycles of 94 °C for 30 seconds – 1 minute, 50-55 °C for 1.5-2 minutes, 68-72 °C for 1-2 minutes, and a final hold at 68-72 °C for 2-6 minutes. The nested PCR reactions used amplification conditions equivalent to the outside PCR with the omission of the initial 2-4 cycles. The resulting nested PCR products were cut from agarose gel on an Alpha Innotec Ultra Violet Box and purified using a QIAquick gel extraction kit (Qiagen) according to the manufacturer's instruction. All PCR products were ligated into the pCR2.1 vector using a TOPO-TA cloning kit (Invitrogen) with the exception of the *Dlk1-Gtl2* IG DMR that was ligated into the pCC1 vector using a Copy Control cloning kit (Epicentre Biotechnologies), both according to the manufacturer's instructions. Cloning vectors were transformed into chemically competent *E. coli* bacteria TOP10 (TOPO clones) or TransforMax EPI300 (Copy Control clones) and grown at 37 °C overnight. Colonies were picked by blue/white selection and screened for positive inserts by PCR using either M13 or pCC1 primers (Table 2.1).

Positive clones were sequenced at the Robarts Research Institute using an ABI GeneAmp Thermocycler and an Applied Biosystems 3730 Analyzer. Clones were accepted at  $\geq 95\%$  cytosine conversion. Non-converted cytosine residues and mismatched base pairs were used to ensure that accepted clones originated from a unique template DNA.

## 2.8 Chromatin Immunoprecipitation

Three wild type forebrains at P18 were rinsed in cold 1X PBS, cut and homogenized. Mashed tissue was diluted with DMEM and passed through a 70  $\mu\text{m}$  cell strainer (Falcon) to ensure single cell suspension. An EZ-ChIP (Upstate) kit protocol was followed according to the manufacturer's instructions. Briefly, cells were crosslinked in 37% formaldehyde and lysed in SDS buffer supplemented with protease inhibitors. A sonicator was used to shear DNA. Immunoprecipitation was performed using the following antibodies: anti-Mecp2 (Upstate, 07-013), anti-ATRAX (FxnP5 was a gift obtained from R. Gibbons) and anti-CTCF (Santa Cruz, sc-15914). Negative control antibodies for rabbit IgG, sheep IgG and goat IgG were used alongside MeCP2, ATRAX and CTCF antibodies, respectively. Protein-DNA complexes underwent reverse crosslinking by treatment with 5M NaCl. Free DNA was purified using the standard phenol:chloroform method. PCR was used to amplify regions spanning the *H19* ICR using primers outlined in Table 2.1. Conditions for amplification were as follows: 95 °C for 5 minutes followed by 30 cycles of 95 °C for 30 seconds, 53.5 °C for 30 seconds, and 72 °C for 30 seconds. A final extension was performed at 72 °C for 10 minutes. Note that mouse husbandry and primer design was performed by D. Tremblay, while tissue processing and ChIP were performed by Yan Jiang, who is a technician in the Bérubé lab.

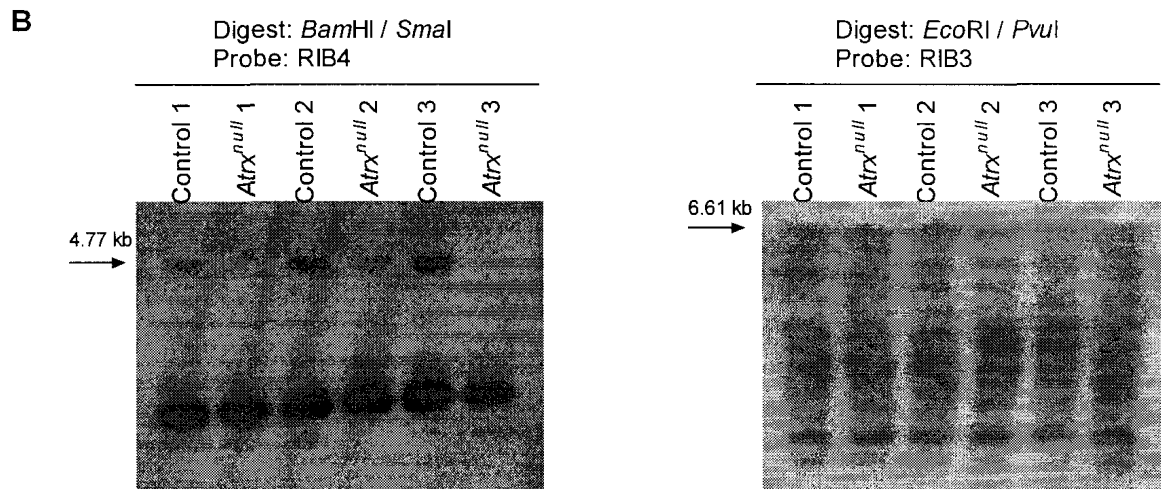
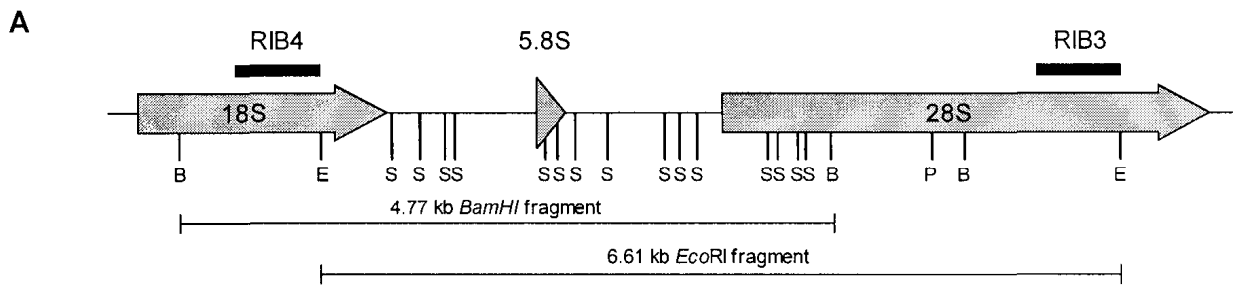
## CHAPTER 3 – Results

### 3.1 Methylation of Repetitive DNA Elements in the *Atrx*<sup>null</sup> Murine Forebrain

Loss of ATRX in patient lymphocytes and *Atrx*<sup>null</sup> ES cells results in hypomethylation of the 18S and 28S genes in the transcribed portion of the rDNA repeat (8, 22). Hypermethylation of the Y-specific satellite DYZ2 and subtle changes at the TelBam3.4 subtelomeric repeat families have also been reported in human lymphocytes and peripheral blood tissue, while other regions including a variety of satellites, *Alu* and LINE1 repeats were unchanged (22). In the mouse, analysis of major satellite, minor satellite, IAP, Line1 and SineB1 repeats revealed that methylation patterns were not detectably altered in *Atrx*<sup>null</sup> ES cells (8).

To determine if similar effects occur in the developing mouse brain, I used the previously described model system in which *Atrx* is conditionally deleted from the cortex and hippocampus beginning at E8.5 (9). I assessed patterns of DNA methylation at the 18S and 28S rRNA genes by Southern blot analysis (Figure 3.1A). Digestion of DNA with the restriction enzyme *Bam*HI gives rise to a predicted fragment of size 4.8 kilobases (kb) and contains the 18S CpG island. Subsequent digestion with the methylation-sensitive restriction enzyme *Sma*I cleaves unmethylated regions of the 4.8 kb fragment into a variety of sizes ranging from only 16 to 1400 base pairs (bp). If the 4.8 kb fragment is fully methylated at all CpG sites then *Sma*I does not cleave and the full-length 4.8 kb fragment will be observed by Southern blot. Since moderate levels of total methylation have been detected at rDNA arrays in wild type mouse cells (95), it was expected that the full length and cleaved 18S fragments could be observed by Southern blot analysis of

Figure 3.1 Southern blot analysis of DNA methylation at 18S and 28S rDNA repeats in the *Atrx<sup>null</sup>* mouse forebrain. (A) Restriction map of the transcribed portion of the rDNA gene. The limit-digesting probes are *Bam*HI (B) and *Eco*RI (E). The methylation sensitive probes are *Sma*I (S) and *Pvu*I (P). Probe RIB4 is specific for the 18S gene and probe RIB3 is specific for the 28S gene. (B) 18S rDNA methylation was analyzed by double digestion of DNA from control or *Atrx<sup>null</sup>* forebrain tissue with *Bam*HI / *Sma*I and probed with RIB4. 28S rDNA methylation was analyzed by double digestion of DNA from control or *Atrx<sup>null</sup>* forebrain tissue with *Eco*RI / *Pvu*I and probed with RIB3. Arrows indicate the fully methylated copies that were only cut by the limit-digesting enzyme; the expected 18S band is 4.77 kb and the expected 28S band is 6.61 kb.



*Atrx<sup>null</sup>* and littermate control DNA. As shown in Figure 3.1B, the full length *Bam*HI fragment is strongly detected in lanes containing control DNA, however the signal is drastically decreased in lanes containing *Atrx<sup>null</sup>* DNA. This result indicated that loss of *Atrx* in the mouse forebrain is associated with hypomethylation of the 18S rDNA repeats.

To assess DNA methylation at the 28S rDNA repeat, I digested DNA with the restriction enzyme *Eco*RI. This gives rise to a predicted DNA fragment of 6.6 kb that contains the 28S CpG island. Subsequent digestion with the methylation-sensitive restriction enzyme *Pvu*I only cleaves the *Eco*RI fragment once, resulting in a smaller product of size 1.9 kb that can be detected by the 28S probe. As with the 18S experiment, it was expected that Southern blot analysis should detect the full length and cleaved 28S fragments. As shown in Figure 3.1B, the full length *Eco*RI fragment is equally detected in lanes containing control and *Atrx<sup>null</sup>* DNA. It is suspected that the additional bands are non-specific cross-hybridization of the 28S probe with other repeat sequences. Although this result indicated that loss of *Atrx* in the mouse forebrain does not change the pattern of methylation at the 28S rDNA repeat, it is still possible that DNA methylation patterns at other CpG sites presiding in the 28S locus are affected.

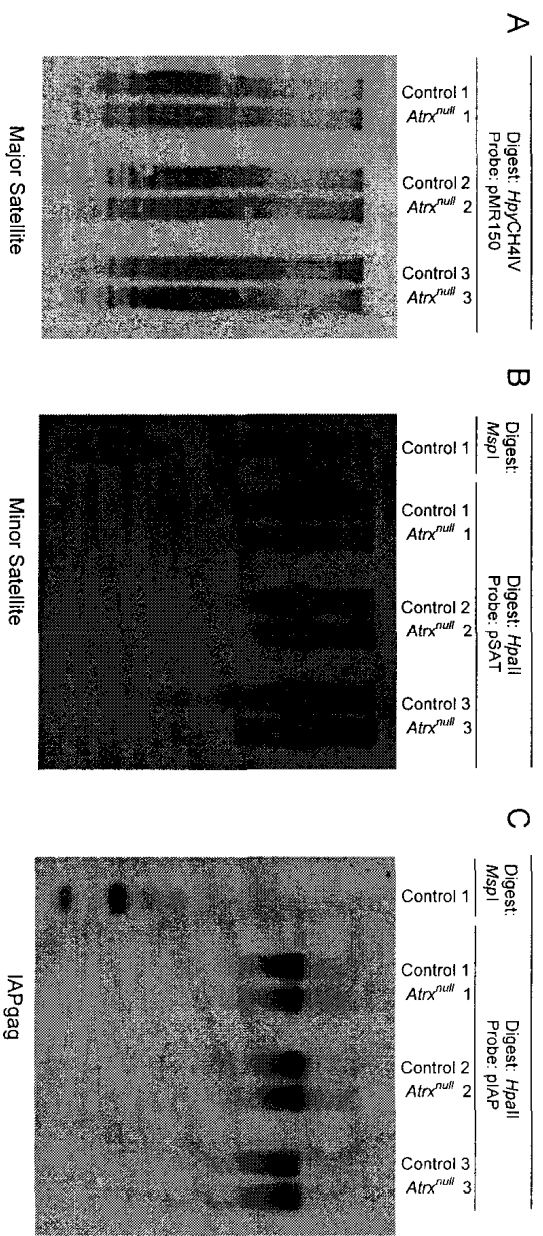
Although the main cellular localization of ATRX is at pericentric heterochromatin, where the major satellites are located, previous studies on *Atrx<sup>null</sup>* ES cells and ATR-X patient cell lines have reported no change in DNA methylation at this family of repetitive elements (8, 22). To assess DNA methylation of major satellite repeats in the *Atrx<sup>null</sup>* forebrain, I digested DNA with the methylation-sensitive restriction enzyme *Hpy*CH4IV, which is an isoschizomer of the more commonly used *Mae*II enzyme. This digest was expected to yield a specific banding pattern in which changes in

methylation are denoted as differences in the intensity of radioactive decay at individual bands. For example, hypermethylated DNA would appear as darkened hybridization signals at the larger molecular weights due to lack of *Hpy*CH41V cleavage. Since there is no methylation-insensitive isoschizomer of *Hpy*CH41V, I was unable to perform a control reaction showing complete sample digestion regardless of methylation status. As shown in Figure 3.2A, there is no difference in the banding patterns upon comparison of lanes containing control and *Atrx*<sup>null</sup> DNA. This result indicated that loss of *Atrx* in the mouse forebrain does not change the pattern of DNA methylation at major satellite repeats.

Levels of DNA methylation were also assessed at minor satellite and IAP*gag* repeats. For both experiments, DNA was digested with the restriction enzyme *Msp*I and its methylation-sensitive isoschizomer *Hpa*II. In this case, it was expected that *Msp*I would fully digest DNA samples, yielding a predicted banding pattern. *Hpa*II on the other hand would give multiple bands only if DNA was in the unmethylated state. As shown in the first lane of the blots in Figure 3.2B-C, control DNA digested with *Msp*I gives the same banding pattern expected from a *Hpa*II digest if the DNA was entirely unmethylated. Alternatively, the remaining lanes in Figure 3.2B-C show that all DNA samples were heavily methylated and there were consequently no observed differences between *Atrx*<sup>null</sup> and control forebrains in three different litter-matched pairs.

A positive control showing loss of methylation is often included in methylation-sensitive Southern blot analyses. For example, digestion of DNA from ES cells deficient for DNMT3A or DNMT3B is expected to result in a methylation-sensitive *Hpa*II digestion pattern very similar to the methylation-insensitive *Msp*I pattern. This is caused by lack of establishment of the DNA methylation marks by the *de novo* DNMT3A or

Figure 3.2 Southern blot analysis of DNA methylation at major satellite, minor satellite and IAP *gag* repeats in the *Atrx<sup>null</sup>* mouse forebrain. (A) Major satellite methylation was analyzed by digestion with *Hpy*CH41V and probed with pMR150. (B) Minor satellite methylation was analyzed by digestion with *Hpa*II and probed with pSAT. Control DNA was also digested with *Msp*I, which is the methylation insensitive isoschizomer of *Hpa*II. The control *Msp*I digest shows the predicted hypomethylated digestion pattern. (C) IAP *gag* methylation was analyzed by digestion with *Hpa*II and probed with pIAP. Control DNA was digested with *Msp*I to show the hypomethylated digestion pattern.

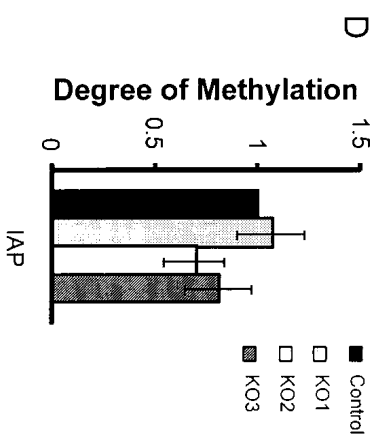
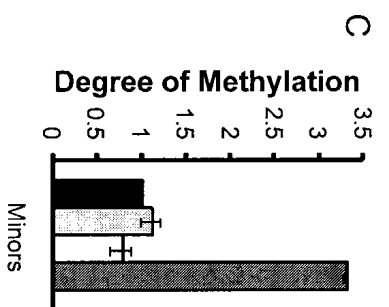
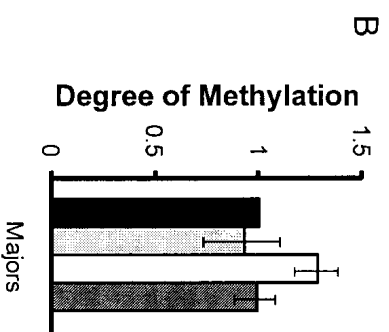
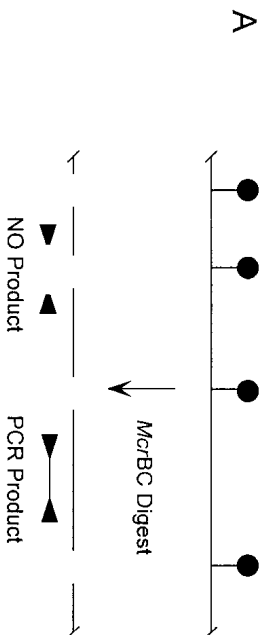


DNMT3B methyltransferases. Including this additional digest on a methylation-sensitive Southern blot would act as a positive control both showing loss of methylation as well as verifying that the assay worked. Since a DNMT-deficient cell line was not available at the time of Southern blot analysis, I used the methylation-sensitive *Mcr*PCR approach to verify Southern blot results at major satellite, minor satellite and IAP*gag* repeats.

Briefly, the *Mcr*PCR methylation analysis involved digestion of genomic DNA with the restriction enzyme *Mcr*BC, which only cleaves (G/A)<sup>m</sup>C methyl-cytosines on one or both strands. The *Mcr*BC recognition sequence is quite intricate, cleaving DNA only in the pattern of 5'...Pu<sup>m</sup>C(N<sub>40-30000</sub>)Pu<sup>m</sup>C...3'. Following digestion, quantitative real time PCR was used to determine the relative levels of unmethylated DNA. Samples with lower levels of methylation showed increased amounts of PCR product due to lack of digestion by *Mcr*BC (Figure 3.3A) (95, 100, 101). At each repeat element, three *Atrx*<sup>mut</sup> and littermate control pairs were compared and corrected against equal levels of internal control undigested DNA. Figure 3.3 panels B and D show that *Mcr*PCR analysis of major satellite and IAP*gag* repeats verified the methylation-sensitive Southern blot results in that the level of DNA methylation was not changed upon *Atrx* deletion. At minor satellite repeats, however, one out of three pairs showed a 3.2-fold increase in methylation, which does not agree with the Southern blot data (Figure 3.3C).

Attempts were made to verify rDNA methylation using the *Mcr*PCR approach, however this technique is not sensitive enough to detect methylation changes at genes with lower copy number. The rDNA genes have approximately 200 copies in the genome, while IAP repeats code >100,000 copies, minor satellites code >50,000 copies and major satellites code >200,000 copies (95). In addition, the total methylation of wild type mouse

Figure 3.3 *Mcr*PCR analysis of DNA methylation at major satellite, minor satellite and IAP *gag* repeats in the *Atrx*<sup>null</sup> mouse forebrain. (A) Outline of the *Mcr*PCR technique. Following digestion of genomic DNA with the restriction enzyme *Mcr*BC, only methylated CpG sites will be cleaved. PCR amplification therefore only generates products in regions with hypomethylated DNA sequences. Black circles represent methylated CpG sites. (B) DNA methylation at major satellites, minor satellites and IAP *gag* repeats was measured by the inverse ability of unmethylated DNA fragments to amplify PCR products with primer sets specific to each repeat class. Samples were normalized against equal input levels of internal control undigested DNA.



ES cell rDNA is only moderate in comparison to satellite and IAP genes (95). If moderate levels of methylation are present, and the region of PCR amplification is small (eg. 100-300 bp), then the *McrBC* enzyme has limited recognition sites to cleave, ultimately resulting in fewer cleavage products and a decreased ability to resolve differences in overall methylation levels.

Taken together, establishing whether *Atrx* nulligosity in the mouse forebrain leads to aberrant methylation of repetitive elements was important for determining how comparable the *Atrx*<sup>null</sup> forebrain model is with ATR-X patients and the *Atrx*<sup>null</sup> ES cell model. Methylation-sensitive Southern blot and *McrPCR* analysis of major satellite, minor satellite and IAPgag repeats revealed normal methylation levels in the *Atrx*<sup>null</sup> forebrain, which corresponds with findings from ATR-X patients and *Atrx*<sup>null</sup> ES cells (8, 22). More importantly, I established that loss of *Atrx* in the newborn mouse forebrain induces hypomethylation of the 18S rDNA locus, suggesting that *Atrx* plays a role in the epigenetic regulation of DNA methylation in ATR-X patients, *Atrx*<sup>null</sup> ES cells and the developing *Atrx*<sup>null</sup> forebrain.

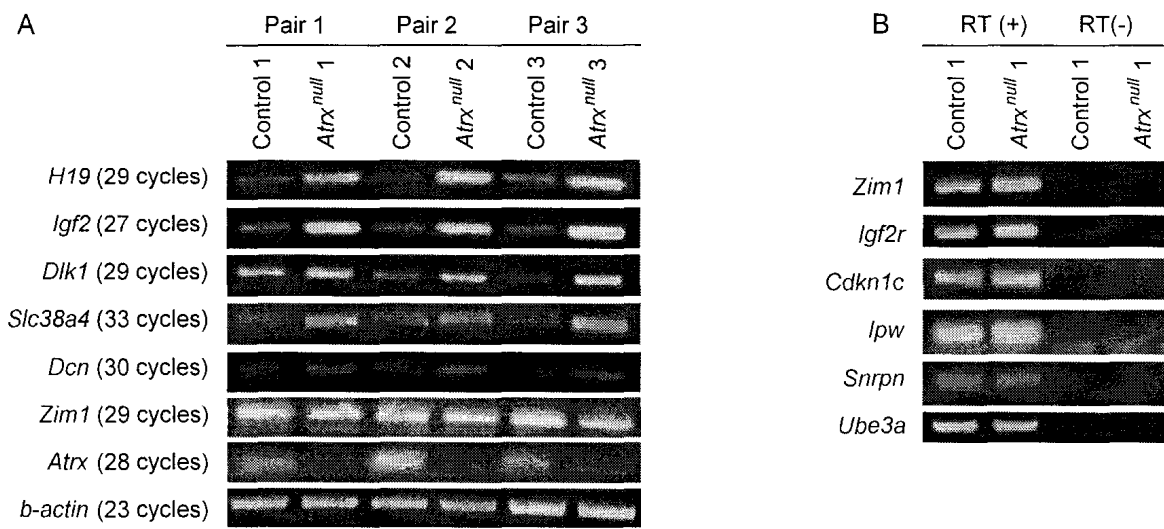
### **3.2 Transcriptional profiling reveals increased expression of specific imprinted genes in the newborn *Atrx*<sup>null</sup> forebrain**

ATR-X has been reported to have chromatin remodelling activity in an *in vitro* system (62) and has been described as a transcriptional regulator based on reduced expression of the  $\alpha$ -globin gene often observed in patients with *ATR-X* mutations (21, 102). Since no other target genes for ATR-X have yet been reported, I wanted to determine the transcriptional profile of the *Atrx*<sup>null</sup> brain on a genome-wide scale.

Initially, I screened a panel of imprinted genes using semi-quantitative RT-PCR analysis. Gene expression levels were qualitatively assessed after 23-33 RT-PCR cycles via ethidium bromide (EtBr) staining and agarose gel electrophoresis. As shown in Figure 3.4A, a subset of imprinted genes, including *H19*, *Igf2*, *Dlk1*, *Slc38a4* and *Dcn* were identified as displaying aberrant expression. This observed upregulation was confirmed in three *Atrx<sup>null</sup>* animals that were compared to litter-matched control mice. Additional imprinted genes, including *Zim1*, *Igf2r*, *Cdkn1c*, *Ipw*, *Gtl2*, *Snrpn* and *Ube3a* were unaffected by *Atrx* nulligosity in one *Atrx<sup>null</sup>* animal (Figure 3.4B). To confirm that unaltered genes show the same expression profile in multiple *Atrx<sup>null</sup>* animals, the third panel from the bottom in Figure 3.4A shows semi-quantitative RT-PCR analysis of the unaffected gene *Zim1* in three of three animals. These results suggest that loss of *Atrx* in the murine forebrain affects the expression of a limited subset of imprinted genes.

In a parallel study, I used RNA microarray technology to determine the outcome of *Atrx* loss-of-function on global gene expression by comparing the transcriptional profile of four newborn *Atrx<sup>null</sup>* and litter-matched control forebrain samples. Surprisingly, I found that very few genes exhibited changes in expression, indicating that *Atrx* unlikely acts as a global transcriptional regulator. The Affymetrix GeneChip Mouse Genome 430 2.0 array contained 45,101 sequences that represent approximately 34,000 genes. Only 51 transcripts were affected using a threshold of 2.0-fold change and a t-test ( $p \leq 0.05$ ) (Appendix I), and 307 transcripts displayed a threshold difference of 1.5-fold or more using a t-test ( $p \leq 0.05$ ).

Figure 3.4 Semi-quantitative RT-PCR analyses of imprinted gene expression in the *Atrx*<sup>null</sup> mouse forebrain. (A) The imprinted genes *H19*, *Igf2*, *Dlk1*, *Slc38a4* and *Dcn* are upregulated in three of three *Atrx*<sup>null</sup> forebrains, while the internal control housekeeping gene *β-actin* is not changed. PCR amplifications were analyzed during the linear range of amplification which occurred between 23-33 cycles depending on the gene. (B) Not all genes are affected by *Atrx* nulligosity as shown by normal expression of *Zim1*, *Igf2r*, *Cdkn1c*, *Ipw*, *Snrpn* and *Ube3a*. Reactions were also run using RT-negative samples to show that primer pairs were specific to the desired cDNA transcript.



Not surprisingly, 9 of the aberrantly expressed genes were related to neuronal development and represented 17% of altered transcripts with a change of 2.0-fold or more. In support of the abnormal bone development phenotype of ATR-X patients, 6 of the aberrantly expressed genes were related to bone development and represented 12% of altered transcripts with a change of 2.0-fold or more. Another highly represented group of genes were the ion or solute carriers, of which 9 (17%) showed changes of 2.0-fold or more. Finally, 5 imprinted genes were altered by 1.5-fold or more. Interestingly, the transcript showing the second highest change in expression was *Pigt*, which is an 18S rDNA probe. Upregulation of *Pigt* by 3.914-fold ( $p=0.00022$ ) correlates with the hypomethylation of 18S rDNA and suggests that *Atrx* is involved in epigenetic silencing of rDNA. It is also possible that additional unnamed genes implicated in neuronal development, bone development or DNA methylation will be identified in the future since 13 of the altered transcripts (25%) showing 2-fold change or more were uncharacterized IMAGE or RIKEN clones.

Table 3.1 outlines a comprehensive analysis of all imprinted genes on the Affymetrix GeneChip Mouse Genome 430 2.0 array. Genes are separated based on chromosomal location and position within respective imprinted domains. *Atrx*<sup>null</sup> samples are highlighted based on expression level, where purple represents upregulation  $\geq 1.5$  fold ( $p \leq 0.07$ ), light blue represents minor upregulation between 1.2-1.5 fold ( $p \leq 0.07$ ), pink represents minor downregulation between 1.2-1.5 fold ( $p \leq 0.07$ ) and olive green represents upregulation or downregulation between 1.2-1.5 fold ( $p \geq 0.1$ ). From this analysis it is apparent that a few domains, such as the imprinted chromosome 6 region

**Table 3.1 Comprehensive list of imprinted genes extracted from RNA microarray analysis of four *Atrx<sup>null</sup>* forebrain samples**

Gene Symbol	Chromosome Location	Status	Expressed Allele	Fold Change	p-value
Gatm	2 E5 2 69.0 cM	Imprinted	Maternal	1.03	0.959
Nnat	2 H1 2 88.0 cM	Imprinted	Paternal	1.06	0.397
Gnas	2 E1-H3 2 104.0 cM	Imprinted	Maternal	1.14	0.181
Nespas	2 H4 2 104.0 cM	Imprinted	Maternal	1.00	1.000
Calcr	6 A1 6 3.8 cM	Imprinted	Maternal	1.15	0.310
Sgce	6 A1 6 1.0 cM	Imprinted	Paternal	1.09	0.256
Peg10	6 A1 6 0.5 cM	Imprinted	Paternal	1.36	0.051
Ppp1r9a	6 A1 6 0.5 cM	Imprinted	Maternal	1.01	0.748
Pon3	6 A1 6 0.5 cM	Provisional	Maternal	1.15	0.137
Pon2	6 A1	Provisional	Maternal	1.31	0.060
Asb4	6 A1 6 0.6 cM	Imprinted	Maternal	1.41	0.052
Dlx5	6 A1 6 2.0 cM	Conflicting Data	Maternal	0.90	0.762
Mest	6 B1 6 7.5 cM	Imprinted	Paternal	1.30	0.036
Copg2	6 A3.3	Imprinted	Maternal	1.06	0.913
Copg2as2	6 A3.3	Imprinted	Paternal	1.36	0.067
Nap1l5	6 C1	Imprinted	Maternal	1.05	0.993
Zim3	7 7 7.0 cM	Imprinted	Maternal	1.04	0.974
Zfp264	7 A1 7 7.0 cM	Imprinted	Paternal	0.89	0.975
Zim2	7 A1	Imprinted	Maternal	1.04	0.775
Zim1	7 A1 7 6.5 cM	Imprinted	Maternal	0.95	0.997
Peg3	7 A2-B1 7 6.5 cM	Imprinted	Paternal	1.20	0.396
Usp29	7 A1 7 6.5 cM	Imprinted	Paternal	1.01	0.725
Atp10a	7 B5	Conflicting Data	Maternal	1.06	0.889
Ube3a	7 B5 7 28.65 cM	Imprinted	Maternal	0.89	0.402
Pwcr1	7 B5 7 29.0 cM	Imprinted	Paternal	1.01	0.966
Snrpn	7 B5 7 29.0 cM	Imprinted	Paternal	1.07	0.908
Snurf	7 B5	Imprinted	Paternal	0.83	0.067
Ndn	7 C 7 28.0 cM	Imprinted	Paternal	1.09	0.241
Magel2	7 C 7 28.0 cM	Imprinted	Paternal	1.02	0.691
Mkrn3	7 C 7 29.0 cM	Imprinted	Paternal	0.88	0.207
Ipw	7 7 28.0 cM	Imprinted	Paternal	0.94	0.483
Peg12	7 C 7 28.0 cM	Imprinted	Paternal	1.11	0.474
H19	7 F5 7 69.03 cM	Imprinted	Maternal	2.25	0.004
Igf2	7 F5 7 69.09 cM	Imprinted	Paternal	1.97	0.006
Igf2as	7 F5 7 69.09 cM	Imprinted	Paternal	1.14	0.319
Ins2	7 F5 7 69.1 cM	Imprinted	Paternal	1.11	0.884

Table 3.1 Continued

Gene Symbol	Chromosome Location	Status	Expressed Allele	Fold Change	p-value
Ascl2	7 F5 7 69.3 cM	Imprinted	Maternal	1.00	0.849
Tspan32	7 F5 7 69.0 cM	Imprinted	Maternal	1.02	0.900
Cd81	7 F5 7 69.3 cM	Imprinted	Maternal	1.11	0.130
Tssc4	7 F5 7 69.3 cM	Imprinted	Maternal	0.93	0.637
Kcnq1	7 F5 7 69.3 cM	Imprinted	Maternal	0.89	0.944
Kcnq1ot1	7 F5 7 69.3 cM	Imprinted	Paternal	1.15	0.189
Cdkn1c	7 F5 7 69.49 cM	Imprinted	Maternal	1.27	0.270
Slc22a18	7 F5 7 69.5 cM	Imprinted	Maternal	1.02	0.801
Phlda2	7 F5 7 69.5 cM	Imprinted	Maternal	1.08	0.880
Nap114	7 F5 7 69.55 cM	Imprinted	Maternal	0.96	0.994
Tnfrsf23	7 F5 7 69.56 cM	Imprinted	Maternal	1.00	0.895
Osbpl5	7 F5 7 69.59 cM	Imprinted	Maternal	0.95	0.901
Rasgrf1	9 E3.1 9 50.0 cM	Imprinted	Paternal	1.16	0.276
Plagl1	10 A2 10 15.0 cM	Imprinted	Paternal	1.26	0.044
Dcn	10 C3 10 55.0 cM	Imprinted	Maternal	2.04	0.029
Grb10	11 A1 11 8.0 cM	Imprinted	Isoform Dependant	1.30	0.050
Commd1	11 A3.2 11 12.0 cM	Imprinted	Maternal	1.11	0.568
U2af1-rs1	11 A3.2 11 12.0 cM	Imprinted	Paternal	0.83	0.240
Mirg	12 F1	Imprinted	Maternal	0.86	0.131
Dlk1	12 E-F1 12 54.0 cM	Imprinted	Paternal	1.24	0.049
Gtl2	12 F1 12 54.0 cM	Imprinted	Maternal	0.72	0.051
Rian	12 F1 12 54.5 cM	Imprinted	Maternal	1.07	0.555
Peg13	15 D3	Imprinted	Paternal	0.98	0.681
Slc38a4	15 F1	Imprinted	Paternal	1.68	0.070
Slc22a3	17 A1 17 7.31 cM	Imprinted	Maternal	0.95	0.531
Slc22a2	17 A1 17 7.32 cM	Imprinted	Maternal	1.51	0.016
Igf2r	17 A-C 17 7.35 cM	Imprinted	Maternal	1.09	0.177
Impact	18 A2-B2	Imprinted	Paternal	1.01	0.946
Xlr4c	X A7.3	Imprinted	Maternal	1.07	0.370
Xlr4b/Xlr4a	X A7.3 X 29.0 cM	Imprinted	Maternal	0.90	0.062
Xist	X D	Imprinted	Paternal	1.11	0.176
Tsix	X D X 42.0 cM	Imprinted	Maternal	1.01	0.844

containing the *Dlx5* locus may also be regulated by *Atrx* to a lesser degree than genes such as *H19*, *Igf2*, *Slc38a4*, *Slc22a2* and *Dcn*.

Importantly, the microarray results validated the initial screen of imprinted genes by RT-PCR analysis: the imprinted genes *H19*, *Igf2*, *Dcn*, and *Slc38a4* all showed upregulation of approximately 2-fold in four out of four *Atrx*<sup>null</sup> forebrain samples compared to controls. Although the microarray did not detect aberrant expression of *Dlk1* greater than 1.5-fold, mild upregulation of 1.24-fold (p=0.05) was observed. All other imprinted genes showed no *Atrx*-dependent changes in expression, indicating that *Atrx* may be targeted to specific regulatory elements that are unique to *H19*, *Igf2*, *Dcn*, *Slc22a2*, *Slc38a4* and possibly *Dlk1*.

The next step in the transcriptional profiling of the *Atrx*<sup>null</sup> forebrain was to validate the semi-quantitative RT-PCR and microarray results using quantitative real time RT-PCR. As outlined in Figure 3.5, I performed quantitative expression analysis of the *H19*, *Igf2*, *Dlk1*, *Slc38a4* and *Dcn* genes on three *Atrx*<sup>null</sup> and litter-matched control forebrains. For each gene analyzed, the RNA expression level was approximately 2.5-fold increased when normalized to control samples and corrected with one of the internal control housekeeping genes *β-actin* or *Gapdh*. Analysis of additional samples revealed that the extent of transcript upregulation varied between litters, but that an increase of approximately 1.5-2 fold is observed on average (Figure 3.6). I also chose to analyze the imprinted gene *Gtl2* since it is the known reciprocal imprint of *Dlk1* (103-105), however aberrant expression of this gene  $\geq 1.5$ -fold was only detected in four of eleven samples, of which one was an extreme outlier (Figure 3.6). In addition, a control analysis of the *Zim1* locus was included. Using semi-quantitative and quantitative RT-PCR in combination

Figure 3.5 Quantitative real time RT-PCR analysis of imprinted gene expression in the *Atrx<sup>null</sup>* mouse forebrain. The imprinted genes *H19*, *Igf2*, *Dlk1*, *Slc38a4* and *Dcn* are upregulated by at least 1.5-fold in three of three *Atrx<sup>null</sup>* forebrains after correction against the internal control housekeeping gene  $\beta$ -*actin*. Gene expression analysis was repeated in triplicate for each sample. Standard error of the mean is shown for the average expression level of *Atrx<sup>null</sup>* samples at each gene, but not for controls as these were all pooled and normalized to one.

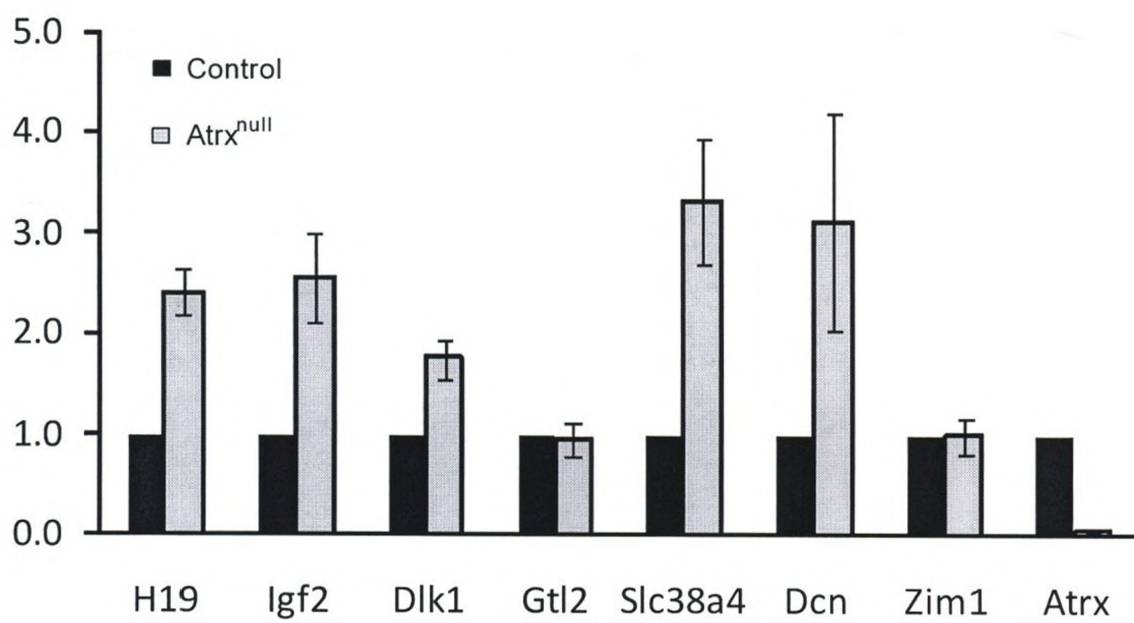
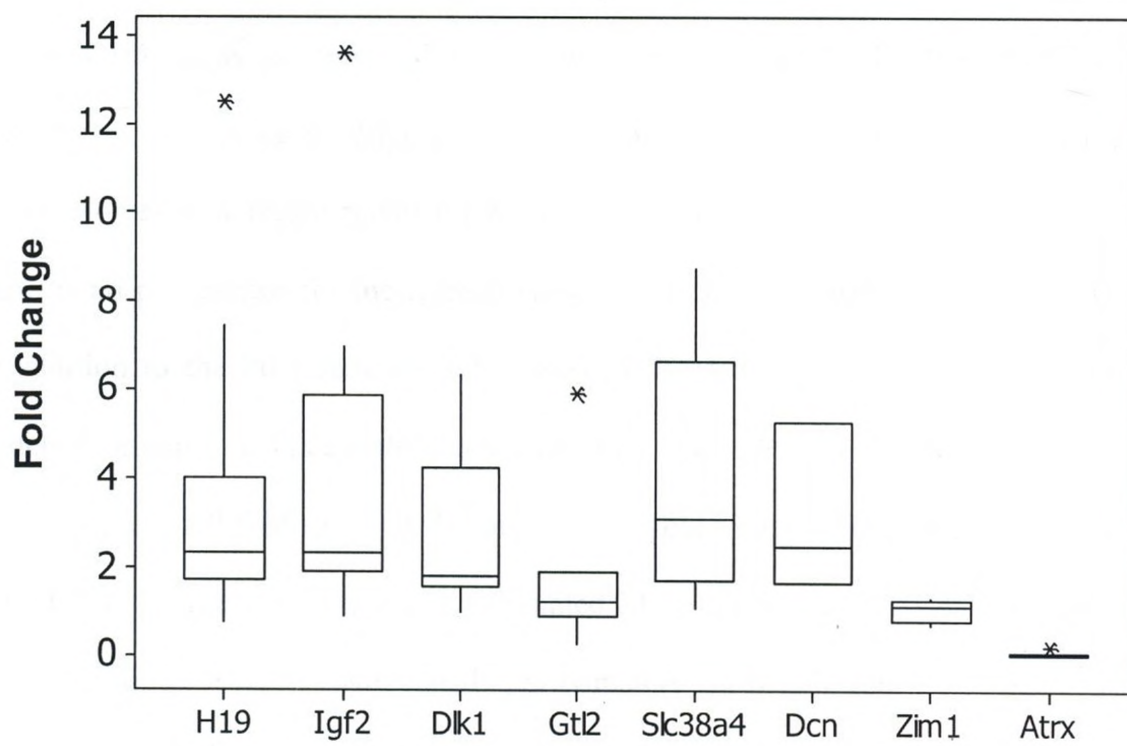


Figure 3.6 Quantitative real time RT-PCR analysis of imprinted gene expression in multiple *Atrx<sup>null</sup>* mouse forebrains. Boxplot analysis of gene expression in up to eleven *Atrx<sup>null</sup>* forebrains shows variation between samples but highlights that the median expression for *H19*, *Igf2*, *Dlk1*, *Slc38a4* and *Dcn* shows at least 2.0-fold upregulation. For this data set, \* represents outliers, the bottom whisker is the lowest non-outlier, the top whisker is the largest non-outlier, the box is the interquartile range (IQR = Q3 – Q1, where Q3 is the upper quartile top horizontal line  $x_{0.75}$  and Q1 is the lower quartile bottom horizontal line  $x_{0.25}$ ) and the midline is the median (Q2,  $x_{0.5}$ ). Three times the IQR marks the boundary between mild outlier and extreme outlier, therefore *H19*, *Igf2* and *Gtl2* each contain an extreme outlier.

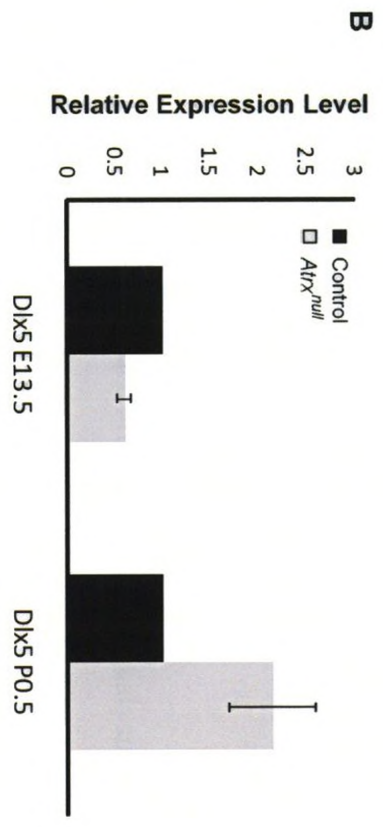
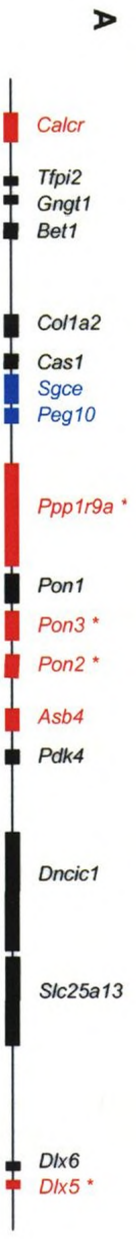


with RNA microarray, *Zim1* is not affected by *Atrx* nulligosity, demonstrating that aberrant expression changes are restricted to a subset of imprinted genes.

Since the P0.5 microarray analysis alluded to possible aberrant regulation within the chromosome 6 imprinted domain, I chose to investigate this region further. In mouse, the *Dlx5* gene may be partially imprinted and it has been suggested that there is preferential expression from the maternal allele (Figure 3.7A) (106). Interestingly, the mouse *Dlx5* locus is proposed to be regulated by MeCP2 binding that results in recruitment of histone modifying enzymes and formation of an 11-kb chromatin loop (106). However, a recent report refutes the imprinting status of *Dlx5* and suggests that there is no precedence for the formation of an MeCp2-dependant chromatin loop (107). In addition to the P0.5 analysis, microarray analysis on three E13.5 *Atrx*<sup>null</sup> and litter-matched control telencephalon revealed that the *Dlx5* gene was downregulated approximately 2.0-fold ( $p \leq 0.0247$ ) at this embryonic stage. Using quantitative real time RT-PCR I verified that *Dlx5* is downregulated 2.0-fold in three E13.5 *Atrx*<sup>null</sup> samples and I also found that *Dlx5* is upregulated approximately 2.0-fold in four P0.5 *Atrx*<sup>null</sup> samples (Figure 3.7B). These data suggest that although the imprinting status of *Dlx5* is unresolved, this locus is likely regulated in a similar fashion as the *H19*, *Igf2*, *Dlk1*, *Slc38a4* and *Dcn* imprinted domains, ultimately resulting in *Atrx*-dependant targeting and regulation of gene expression.

Taken together, data from the transcriptional analysis of the newborn *Atrx*<sup>null</sup> forebrain indicate that the *Atrx* chromatin remodelling enzyme is involved in the regulation of specific imprinted genes, including *H19*, *Igf2*, *Dlk1*, *Slc38a4*, *Dcn* and *Dlx5*,

Figure 3.7 Quantitative real time RT-PCR analysis of *Dlx5* expression at E13.5 and P0.5 in the *Atrx<sup>null</sup>* mouse forebrain. (A) Physical map of the proximal mouse chromosome 6 imprinted domain. Maternally expressed genes are shown in red, paternally expressed genes are shown in blue and biallelically expressed genes are shown in black. \* Denotes genes where there is controversy regarding imprinting status. (B) *Dlx5* is downregulated in three of three *Atrx<sup>null</sup>* telencephalons at E13.5 and is upregulated in 4 of 4 *Atrx<sup>null</sup>* forebrains at P0.5. All samples were corrected against the internal control housekeeping gene *β-actin* and gene expression analysis was repeated in triplicate. Standard error of the mean is shown for each *Atrx<sup>null</sup>* sample but not for controls as these were all pooled and normalized to one.



and it is possible that *Atrx* is targeted to similar regulatory elements involved in the transcription of these genes.

### 3.3 Loss of *Atrx* induces a progressive deregulation of imprinted genes

Under the control of the *FoxG1* forebrain-specific promoter, Cre-recombinase does not conditionally delete *Atrx* in the mouse cortex and hippocampus until E8.5 (34). By this timepoint, imprinted methylation marks have been permanently established throughout the genome (108). Therefore, it is conceivable that *Atrx* participates in the maintenance or reading of imprinting marks, wherein *Atrx* deletion gives rise to increased gene expression at the *H19*, *Igf2*, *Dlk1*, *Slc38a4* and *Dcn* loci. To assess whether aberrant expression of imprinted genes fluctuates throughout development, I investigated the expression of these genes at different developmental time points, with inclusion of *Zim1* as a control.

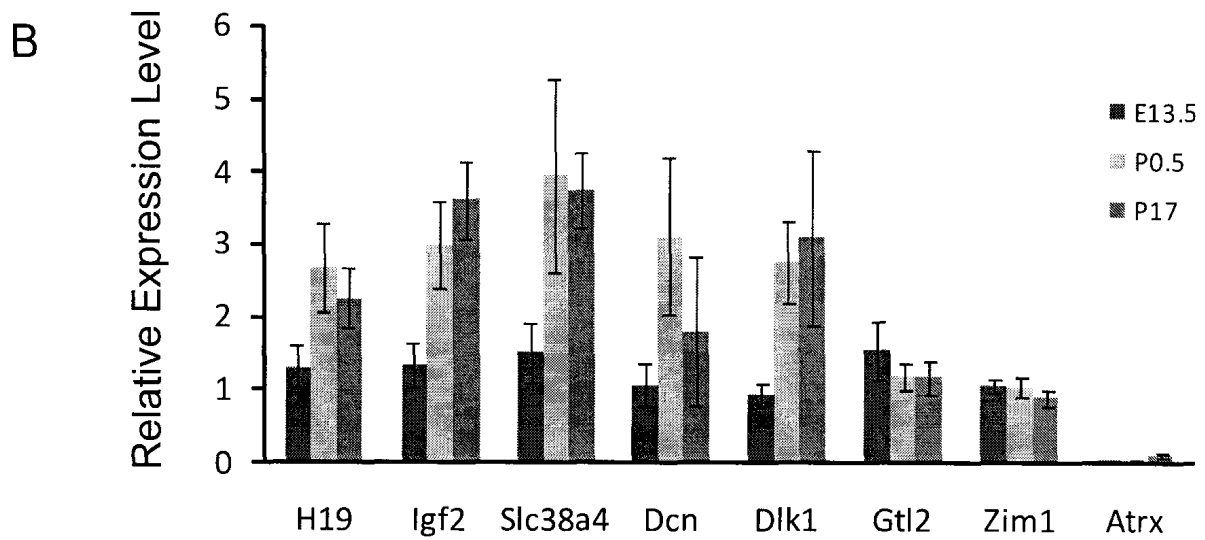
As outlined in Figure 3.8A, microarray analysis on three E13.5 *Atrx*<sup>null</sup> and litter-matched control telencephalon revealed that the expression of *H19*, *Igf2*, *Dlk1*, *Slc38a4* and *Dcn* was not altered in the absence of *Atrx* during a large portion of post-implantation embryogenesis. The previously described P0.5 microarray showed that deletion of *Atrx* at the newborn stage of development resulted in upregulation of *H19*, *Igf2*, *Slc38a4* and *Dcn*. For both microarray analyses, all *Atrx*<sup>null</sup> samples were normalized to litter-matched control samples, with the assumption that control samples were displaying normal transcription patterns.

As shown in Figure 3.8B, microarray results were verified by quantitative expression analysis using real time RT-PCR. I confirmed that expression is normal in

Figure 3.8 Developmental analysis of imprinted gene expression at E13.5, P0.5 and P17. (A) Comparison of imprinted gene expression levels from RNA microarray of *Atrx*<sup>null</sup> mouse forebrain tissue at E13.5 and P0.5. (B) Quantitative real time RT-PCR analysis of imprinted gene expression in the *Atrx*<sup>null</sup> mouse forebrain at E13.5, P0.5 and P17. At E13.5 there is no change in imprinted gene expression in three of three *Atrx*<sup>null</sup> telencephalons. At postnatal timepoints, the imprinted genes *H19*, *Igf2*, *Dlk1* and *Slc38a4* are upregulated by at least 1.5-fold in up to eleven P0.5 and three P17 *Atrx*<sup>null</sup> forebrains. All genes were corrected against the internal control housekeeping genes  $\beta$ -actin and gene expression analyses were repeated in triplicate for each sample. Standard error of the mean is shown for the average expression level of *Atrx*<sup>null</sup> samples at each gene for each developmental time point.

**A**

Gene	E13.5 Fold Change	P-value	P0.5 Fold Change	P-value
<i>H19</i>	1.08	0.478	2.25	0.004
<i>Igf2</i>	1.13	0.063	1.97	0.006
<i>Slc38a4</i>	1.19	0.158	1.68	0.070
<i>Dcn</i>	1.39	0.011	2.04	0.029
<i>Dlk1</i>	1.15	0.496	1.24	0.049
<i>Gtl2</i>	1.15	0.138	0.72	0.051
<i>Zim1</i>	1.01	0.963	0.95	0.997
<i>Atrx</i>	0.29	0.003	0.31	0.022
<i>Actb</i>	0.90	0.190	0.96	0.701



three *Atrx*<sup>null</sup> and litter-matched control pairs at E13.5, but is increased by birth. Overall comparison of expression levels at E13.5 and P0.5 suggests that at some developmental time-point between E13.5 and P0.5, *Atrx* is normally targeted to regulatory elements at *H19*, *Igf2*, *Dlk1*, *Slc38a4* and *Dcn*. In the *Atrx*<sup>null</sup> forebrain, this targeting is interrupted and maintenance of chromatin compaction is likely altered.

One in every ten *Atrx*<sup>null</sup> males survived beyond the newborn period, up to 27 post-natal days in one case (our unpublished results). This allowed extension of the developmental analysis to the P17 time-point using forebrain tissue obtained from three *Atrx*<sup>null</sup> and litter-matched control pairs. Figure 3.8 shows that an approximately two-fold increase in expression persisted in the P17 *Atrx*<sup>null</sup> forebrain by quantitative real time RT-PCR, except for *Dcn* which showed no change in expression. This may be related to the varying results found at P0.5, and collection of more P17 tissue could still verify upregulation of *Dcn*. Alternatively, it is possible that the few surviving *Atrx*<sup>null</sup> males have unique neuronal environments, which could explain both variability in gene expression at P0.5 and unchanged *Dcn* expression at P17. Ultimately, findings from the analysis of *Atrx*-nulligosity on the developing forebrain demonstrate that there is an *Atrx*-dependant effect on imprinted gene expression in the brain, with increased expression appearing sometime between E13.5 and P0.5 and persisting through the post-natal stages of brain development.

Restriction of upregulated imprinted gene expression to the post-natal stages of development suggests that loss of *Atrx* alters some aspect of the primary imprint such as DNA methylation, or secondary features of the imprint such as recruitment of regulatory enzymes. Considering that *ATRX* is involved in the regulation of DNA methylation at

rDNA repeats, it is possible that Atrx is targeted to methylated imprinted loci in order to maintain chromatin repression. DNA methylation is the major epigenetic modification known to regulate genomic imprinting at the *Gtl2-Dlk1* and *H19-Igf2* loci. Methylation is also believed to be important for *Slc38a4* and *Dcn* regulation, although distinct regions of differential methylation have not been identified (109, 110). Examining the status of methylation marks at the well-defined regulatory DMRs of the *Gtl2-Dlk1* and *H19-Igf2* loci was therefore the first logical step in elucidating the mechanism by which ATRX regulates imprinted gene expression.

### **3.4 Increased imprinted gene expression may correlate with abnormal DNA methylation at the *Gtl2-Dlk1* imprinted domain**

*Gtl2* and *Dlk1* are reciprocally imprinted neighbours located within a 1 Megabase (Mb) imprinted domain on distal mouse chromosome 12 and human chromosome 14q32 (103-105). *Dlk1* is one of three protein-coding genes in the imprinted domain (104), while *Gtl2* is a non-coding RNA (111). Three DMRs have been identified at the *Gtl2-Dlk1* locus (Figure 3.9A), of which the germ-line derived intergenic DMR (IG-DMR) located 13 kb upstream of *Gtl2* represents the major control site for proper imprinting specifically on the maternal chromosome (96). A second DMR, called the *Gtl2* DMR, is located within the promoter and first exon of the *Gtl2* gene (104). The third *Dlk1* DMR is located within the three-prime region of the *Dlk1* gene and has an undefined regulatory function (105).

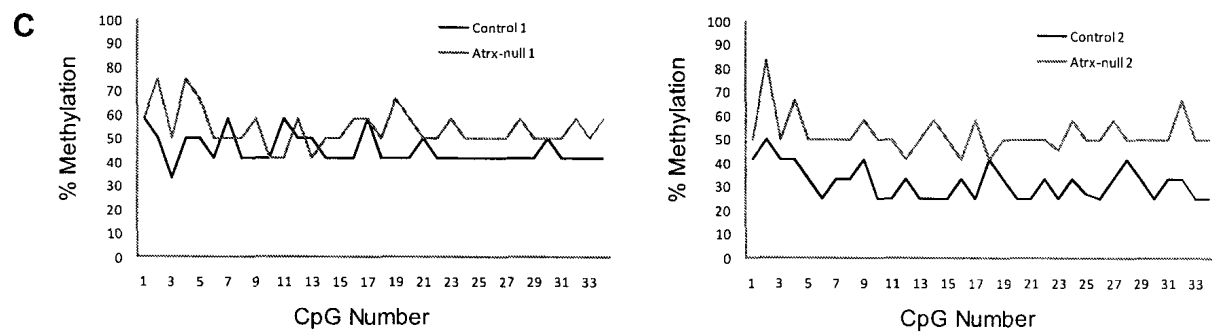
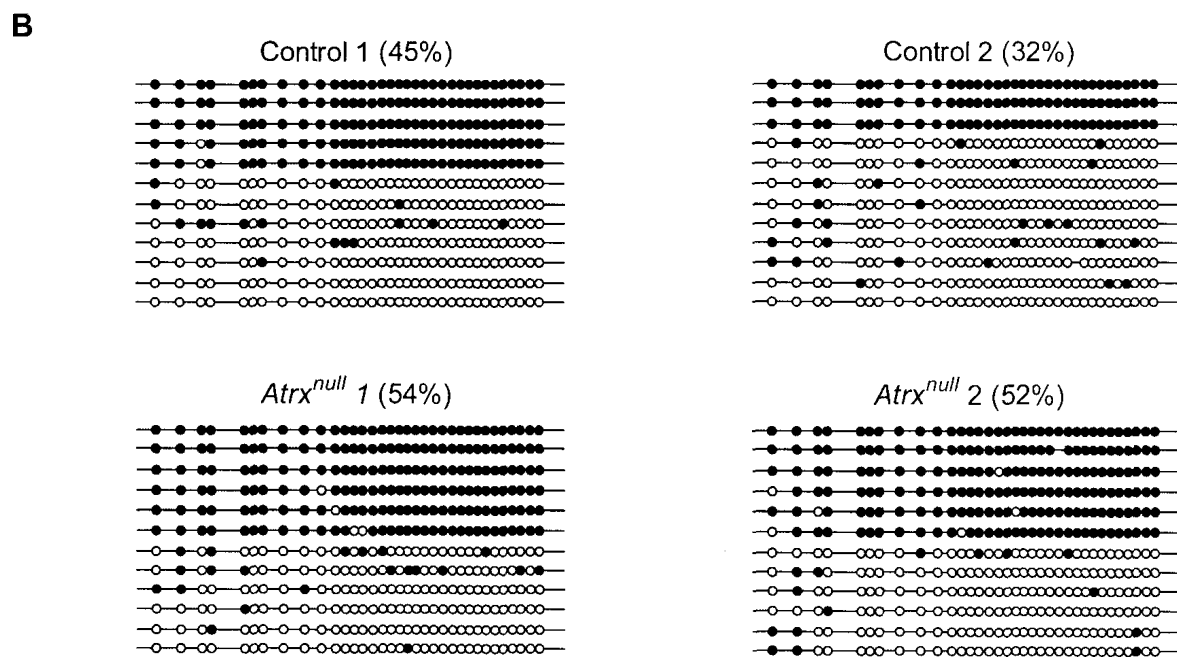
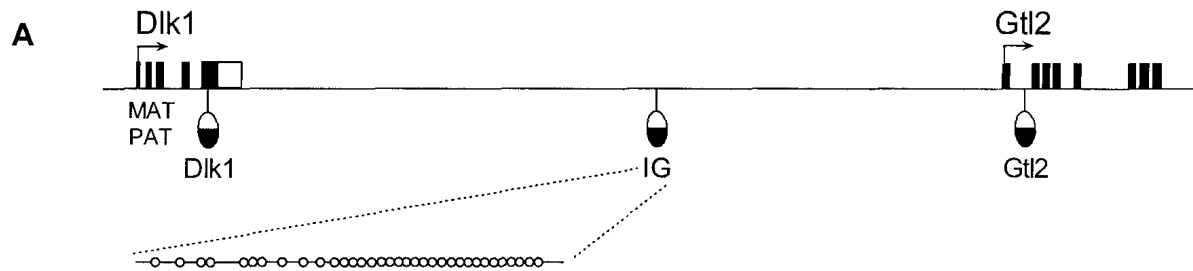
A non-allelic bisulfite mutagenesis approach was undertaken to analyze the *Dlk1* – *Gtl2* imprinted domain in two pairs of newborn *Atrx*<sup>null</sup> and litter-matched control

animals. Although allelic analysis would be ideal, this was not possible at the time of experimentation due to the lack of *Atrx*<sup>null</sup> males with polymorphic alleles. In order to generate such mice, I have established a colony of heterozygous *Atrx*<sup>flox/wt</sup> *Cre*<sup>+</sup> females (129 Sv background) and attempted to cross with wild type *Mus castaneus* males (CAST background) in hopes of obtaining *Atrx*<sup>flox/y</sup> *Cre*<sup>+</sup> males with polymorphic 129Sv and CAST alleles. Several months were spent establishing this colony, however matings proved difficult because the heterozygous *Atrx*<sup>flox/wt</sup> *Cre*<sup>+</sup> females do not express normal levels of *Atrx* and consequently show phenotypic signs of mental retardation. As a result, there were no successful matings.

Initial analysis of the IG-DMR determined that the 4.5 kb region is unmethylated on the maternal allele and methylated on the paternal allele (96). Furthermore, the region is methylated in sperm and unmethylated in unfertilized eggs, suggesting that the IG-DMR bears a germline imprint on the paternal allele (96). Deletion of the maternally inherited IG-DMR causes bidirectional loss of imprinting at the *Gtl2-Dlk1* locus, whereas paternal deletion does not alter imprinted gene expression, thereby indicating that the IG-DMR only controls imprinted genes on the maternal chromosome (112).

Nested PCR primer pairs were used to specifically amplify the bisulfite-mutagenized IG DMR within the *Dlk1-Gtl2* imprinted domain and sequencing of at least twelve unique individual clones showing greater than 95% overall conversion enabled identification of methylated CpG dinucleotides. Analysis of IG-DMR methylation is outlined in Figure 3.9B-C and demonstrates that there may be allelic methylation bias with no change in the pattern of methylation in the *Atrx*<sup>null</sup> forebrain, although Control 2 displayed lower overall methylation (32%) in comparison to all other samples. This may

Figure 3.9 Bisulfite mutagenesis of the *Dlk1* – *Gtl2* IG DMR. (A) Schematic of the *Dlk1* – *Gtl2* imprinted domain. Black squares represent exons and white squares represent 3' untranslated regions. Black semi-ovals represent methylated DMRs and white semi-ovals represent unmethylated DMRs. The string with white circles represents the 34 CpG sites analyzed within the IG DMR. (B) Twelve alleles from each sample were analysed and individual alleles are represented as a string with 34 CpG circles. Black circles are methylated and white circles are unmethylated. The total percent methylation for each sample is indicated beside the sample name. (C) Analysis of total methylation levels at individual CpG sites. Control samples are black and *Atrx*<sup>null</sup> samples are grey.

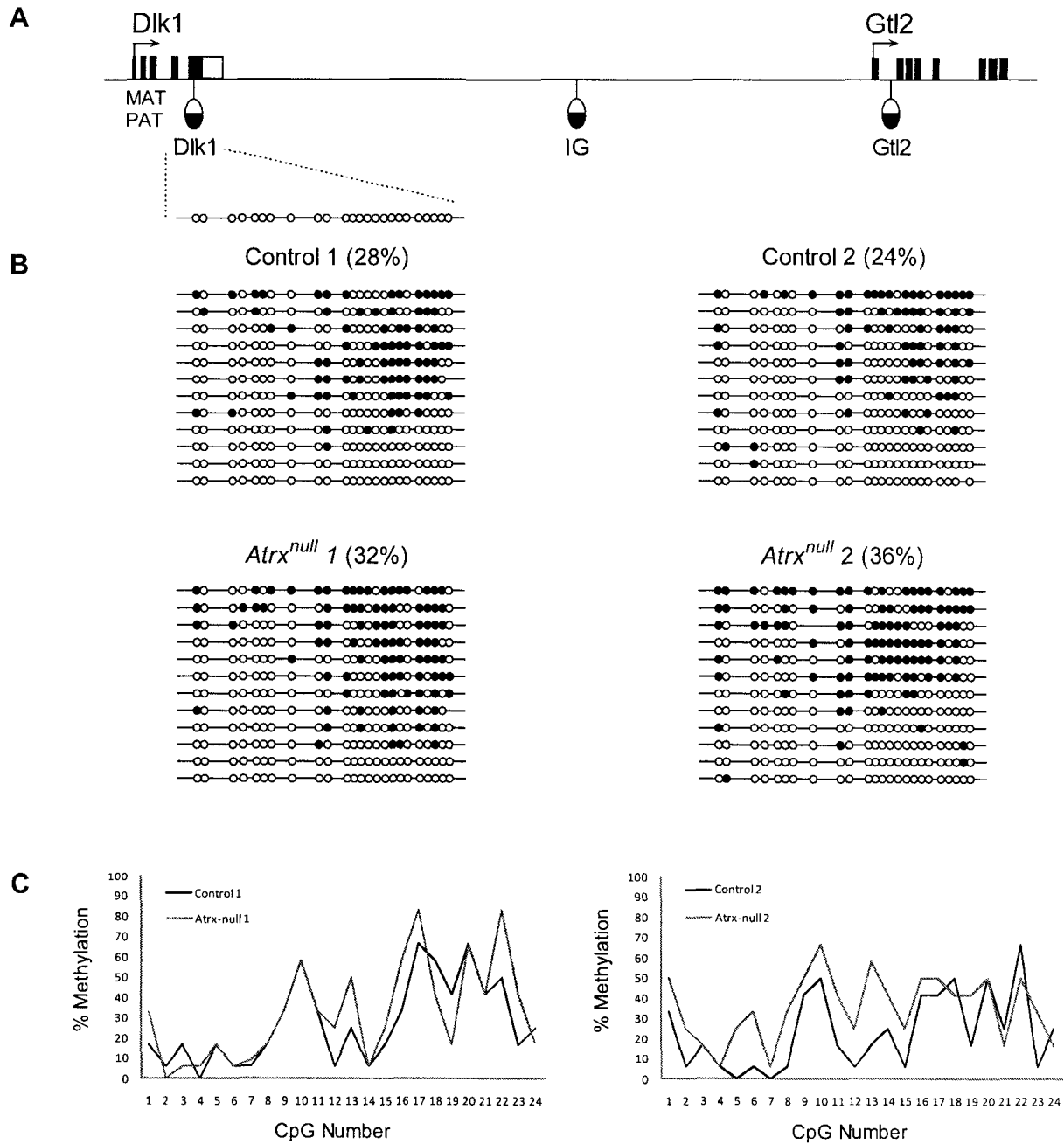


be reflective of increased contribution from the maternal unmethylated allele. Conversely, it is possible that the *Atrx*<sup>null</sup> 2 sample is hypermethylated, which would suggest that *Atrx* is involved in the regulation of DNA methylation at the IG DMR. In order to resolve this question, allelic methylation analysis is required, and is dependant on successful generation of *Atrx*<sup>null</sup> mice with polymorphic alleles.

Although the *Dlk1* DMR has an undefined regulatory function, it is nevertheless a region of differential methylation and should not be discounted. The small CpG island in the fifth exon of *Dlk1* was previously established as being unmethylated on the inactive maternal allele and partially methylated on the active paternal allele (96). Tissue-specific analysis of *Dlk1* DMR methylation revealed that the paternal allele in the E18.5 brain is more methylated than the maternal allele, however no obvious correlation between the level of methylation and the level of expression was found (96). As shown in Figure 3.10B, current analysis of the *Dlk1* DMR in the newborn forebrain showed that the region is relatively unmethylated, and there is no obvious *Atrx*-dependant change in DNA methylation in *Atrx*<sup>null</sup> samples. Analysis of individual CpG sites confirmed that *Atrx* deletion does not alter DNA methylation patterns at the *Dlk1* DMR (Figure 3.10C).

In contrast, the *Gtl2* DMR plays an important role in the regulation of imprinting at the *Gtl2-Dlk1* domain. As outlined in Figure 3.11A, the *Gtl2* DMR is unmethylated on the maternal allele and methylated on the paternal allele (111). Paternal inheritance of an insertional mutation in the five-prime region of *Gtl2* caused loss of *Gtl2* DMR methylation on the paternal allele, and suggested methylation is involved in maintenance of the paternal imprint (113). Reciprocal loss of *Dlk1* imprinting upon maternal inheritance indicated that the unmethylated *Gtl2* DMR is important for imprinting of the

Figure 3.10 Bisulfite mutagenesis of the *Dlk1* DMR. (A) Schematic of the *Dlk1* – *Gtl2* imprinted domain. Black squares represent exons and white squares represent 3' untranslated regions. Black semi-ovals represent methylated DMRs and white semi-ovals represent unmethylated DMRs. The string with white circles represents the 24 CpG sites analyzed within the *Dlk1* DMR. (B) Twelve alleles from each sample were analysed and individual alleles are represented as a string with 24 CpG circles. Black circles are methylated and white circles are unmethylated. The total percent methylation for each sample is indicated beside the sample name. (C) Analysis of total methylation levels at individual CpG sites. Control samples are black and *Atrx*<sup>null</sup> samples are grey.

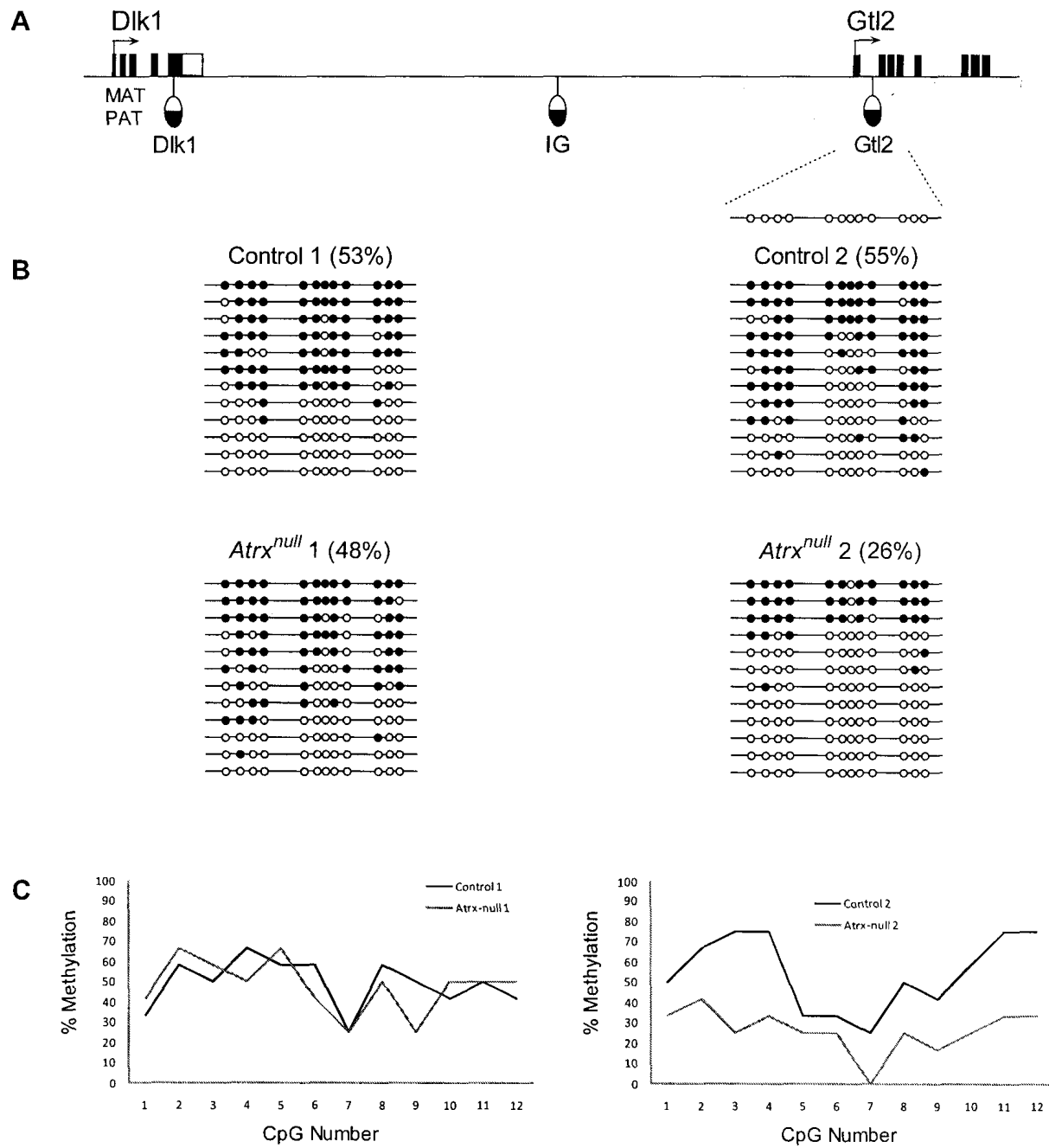


maternal chromosome (113). While the exact role of the *Gtl2* DMR remains undefined, proper methylation of this site is still crucial for normal expression of both *Dlk1* and *Gtl2*.

As shown in Figure 3.11B, analysis of the *Gtl2* DMR in the newborn forebrain gave variable results. The first *Atrx*<sup>null</sup> animal showed no overall change in methylation as well as no change at individual CpG sites, suggesting that *Atrx* does not regulate *Dlk1* expression by an effect on the *Gtl2* DMR. However, analysis of the second *Atrx*<sup>null</sup> animal showed strikingly different results. In this case, the *Gtl2* DMR was grossly hypomethylated, with consistent decreases of approximately 25% occurring at most individual CpG sites (Figure 3.11C). Interestingly, Figure 3.11C highlights that the pattern of methylation is very similar when comparing CpGs from control and *Atrx*<sup>null</sup> samples. Since the methylation pattern is similar, but the level of methylation is different, this suggests that changes may be attributed to over-representation from the maternal allele. As with the IG DMR, the possibility that *Atrx* is involved in maintenance of DNA methylation at the *Gtl2* DMR can not be ruled out and allelic analysis is the only way to resolve this question.

An effort was made to correlate transcriptional profiling with methylation analysis of the *Gtl2-Dlk1* imprinted domain. For the second *Atrx*<sup>null</sup> and control pair (marked as #2 in Figures 3.9-3.11), half of the forebrain was treated with sodium bisulfite while the second half was processed for transcriptional analysis. Using real time RT-PCR, it was found that *Dlk1* was upregulated 3.5-fold while *Gtl2* was unchanged. Upon comparison of methylation patterns to expression levels, no obvious mechanism emerged, therefore allelic analysis must be performed in order to correlate changes in methylation at the *Gtl2-Dlk1* locus with the observed upregulation of *Dlk1* in the *Atrx*<sup>null</sup> forebrain.

Figure 3.11 Bisulfite mutagenesis of the *Gtl2* DMR. (A) Schematic of the *Dlk1 – Gtl2* imprinted domain. Black squares represent exons and white squares represent 3' untranslated regions. Black semi-ovals represent methylated DMRs and white semi-ovals represent unmethylated DMRs. The string with white circles represents the 12 CpG sites analyzed within the *Gtl2* DMR. (B) Twelve alleles from each sample were analysed and individual alleles are represented as a string with 12 CpG circles. Black circles are methylated and white circles are unmethylated. The total percent methylation for each sample is indicated beside the sample name. (C) Analysis of total methylation levels at individual CpG sites. Control samples are black and *Atrx<sup>null</sup>* samples are grey.



### **3.5 Increased imprinted gene expression does not correlate with abnormal DNA methylation at the *H19-Igf2* imprinted domain**

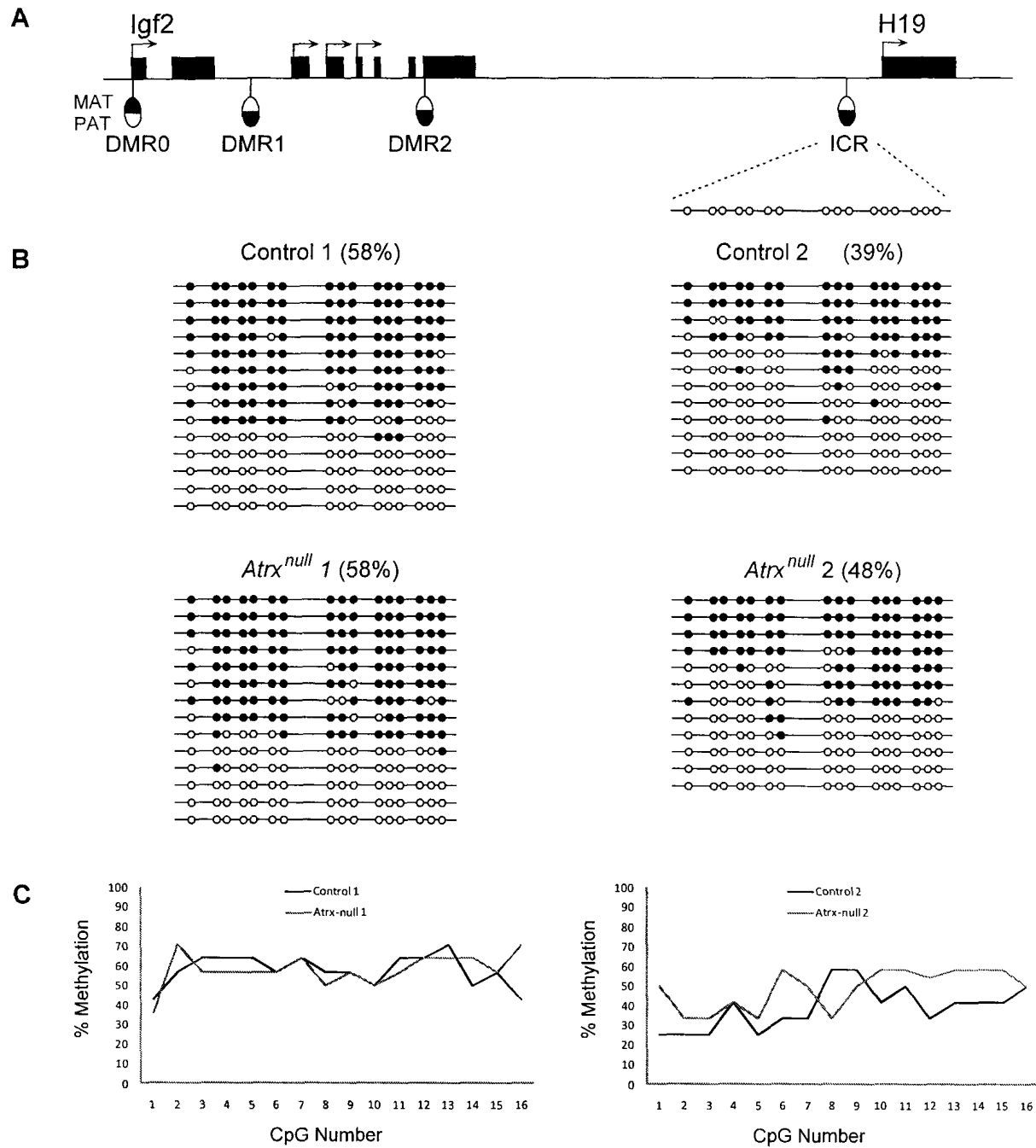
Regulation of genomic imprinting at the *H19-Igf2* locus has been characterized with much greater detail in comparison to the *Gtl2-Dlk1* locus. In most tissues, differential methylation occurs at three specific regions throughout the *H19-Igf2* locus, including the *H19* imprinting control region (ICR), the *Igf2* DMR1 and the *Igf2* DMR2. In addition, a placental-specific *Igf2* DMR0 is located upstream of the first *Igf2* promoter (76, 114-116). With the exception of the *Igf2* DMR0, the three major regulatory DMRs are paternally methylated. As previously described in Figure 1.3A, paternal methylation of the *H19-Igf2* DMRs gives rise to a chromatin loop in which only *Igf2* is actively transcribed, while maternal loss of methylation results in CTCF-dependant chromatin loop formation in which only *H19* is actively transcribed (77, 117, 118). It is important to note, however, that the chromatin looping model of *H19-Igf2* regulation has only been demonstrated in the murine liver and that the regulation of this chromosomal region has not been resolved in the mouse forebrain.

In the murine brain, *Igf2* is readily expressed throughout mesenchymal structures and the neural crest during embryonic development (119). Expression is restricted to the choroid plexus and leptomeninges in the postnatal brain, with transient expression in the granule cells of cerebellar parenchyma during the first week of postnatal development (120). At the choroid plexus epithelium and leptomeninges, loss of imprinting and biallelic expression of *Igf2* has been reported (119, 121), with recent suggestions that in non-imprinted tissue a brain-specific enhancer domain in the intergenic region supports imprinting control distinct from differentially methylated domains (122, 123). The brain-

specific enhancer functions independent of the previously identified mesoderm (124, 125) and endoderm-specific enhancers (126). At the same time, H19 is not expressed in the choroid plexus epithelium and is imprinted throughout the remainder of the choroid plexus and leptomeninges (122, 127). Taken together, data from previous studies indicated that regulation of *H19-Igf2* imprinting in the brain is complex and should not be interpreted in the same context as other tissues. With this caveat in mind, I assessed the effect of *Atrx* deletion in the mouse forebrain on *H19-Igf2* DMR methylation patterns using the same bisulfite mutagenesis approach as outlined for the *Gtl2-Dlk1* analysis.

The *H19* ICR is the main control centre for methylation-dependant regulation of the *H19-Igf2* imprinted domain. On the unmethylated maternal allele, post-fertilization binding of four CTCF proteins at the *H19* ICR acts as a protective shield against *de novo* methylation of the maternal *H19* ICR and *Igf2* DMRs (77, 128). The *H19* ICR also contains regulatory sequences that repress *H19* transcription from the paternal allele (129). The *H19* ICR therefore plays multiple roles in imprinting regulation, and disruption of DNA methylation would likely influence gene expression. As shown in Figure 3.12B, analysis of the *H19* ICR in the newborn mouse forebrain showed allelic methylation bias, but there was no change in methylation patterns upon *Atrx* loss-of-function. Further analysis of individual CpG sites confirmed that *Atrx* deletion in the forebrain does not alter DNA methylation patterns at the *H19* ICR (Figure 3.12C). From analysis of the wild-type forebrain, it is also important to note that the presence of approximately 50% methylated paternal alleles and 50% unmethylated maternal alleles supports previous findings that *H19* is imprinted in regions of the mouse brain outside of the choroid plexus epithelium (130).

Figure 3.12 Bisulfite mutagenesis of the *H19* ICR. (A) Schematic of the *H19* - *Igf2* imprinted domain. Black squares represent exons. Black semi-ovals represent methylated DMRs and white semi-ovals represent unmethylated DMRs. The string with white circles represents the 16 CpG sites analyzed within the *H19* ICR. (B) At least twelve alleles from each sample were analysed and individual alleles are represented as a string with 16 CpG circles. Black circles are methylated and white circles are unmethylated. The total percent methylation for each sample is indicated beside the sample name. (C) Analysis of total methylation levels at individual CpG sites. Control samples are black and *Atrx*<sup>null</sup> samples are grey.



In the liver, regulation of DNA methylation at the *Igf2* DMR1 and *Igf2* DMR2 is dependant on CTCF insulation at the *H19* ICR. In general, when the *H19* ICR is unmethylated, CTCF will block *de novo* methylation of the *Igf2* DMRs (77). Alternatively, when the *H19* ICR is methylated, CTCF can not bind and the *Igf2* DMRs are methylated (97). Since the unmethylated maternal *Igf2* DMR1 interacts with the maternal *H19* ICR, but the methylated paternal *Igf2* DMR2 interacts with the paternal *H19* ICR, it has been deduced that the function of the *Igf2* DMRs is to loop the *H19-Igf2* locus such that *Igf2* is paternally transcribed and *H19* is maternally transcribed (77). At the same time, tissue-specific patterns showing only partial methylation have not been accounted for (114).

Bisulfite analysis of the *Igf2* DMR1 and DMR2 regions in the newborn forebrain revealed that these areas are largely unmethylated for both wild type and *Atrx*<sup>null</sup> mice (Figures 3.13B and 3.14B). As with the *H19* ICR, methylation levels were calculated at individual CpG sites (Figures 3.13C and 3.14C), however only a slight increase in methylation was found at a few specific CpG sites for both DMRs. These differences are mild and not striking enough to definitively correlate changes in methylation patterns with the upregulation of *H19* and *Igf2* observed in the *Atrx*<sup>null</sup> forebrain. Perhaps the more relevant finding was that neither of the *Igf2* DMRs showed differential methylation, suggesting that *Igf2* is not imprinted in the mouse forebrain.

Similar to the *Gtl2-Dlk1* analysis, I attempted to correlate transcriptional profiling with methylation analysis of the *H19-Igf2* imprinted domain. Using the same *Atrx*<sup>null</sup> and control litter-matched pair as described previously, quantitative RT-PCR revealed that *H19* was upregulated 12.5-fold while *Igf2* was upregulated 13.6-fold, however Figure 3.6

Figure 3.13 Bisulfite mutagenesis of the *Igf2* DMR1. (A) Schematic of the *H19 - Igf2* imprinted domain. Black squares represent exons. Black semi-ovals represent methylated DMRs and white semi-ovals represent unmethylated DMRs. The string with white circles represents the 7 CpG sites analyzed within the *Igf2* DMR1. (B) Twelve alleles from each sample were analysed and individual alleles are represented as a string with 7 CpG circles. Black circles are methylated and white circles are unmethylated. The total percent methylation for each sample is indicated beside the sample name. (C) Analysis of total methylation levels at individual CpG sites. Control samples are black and *Atrx<sup>null</sup>* samples are grey.

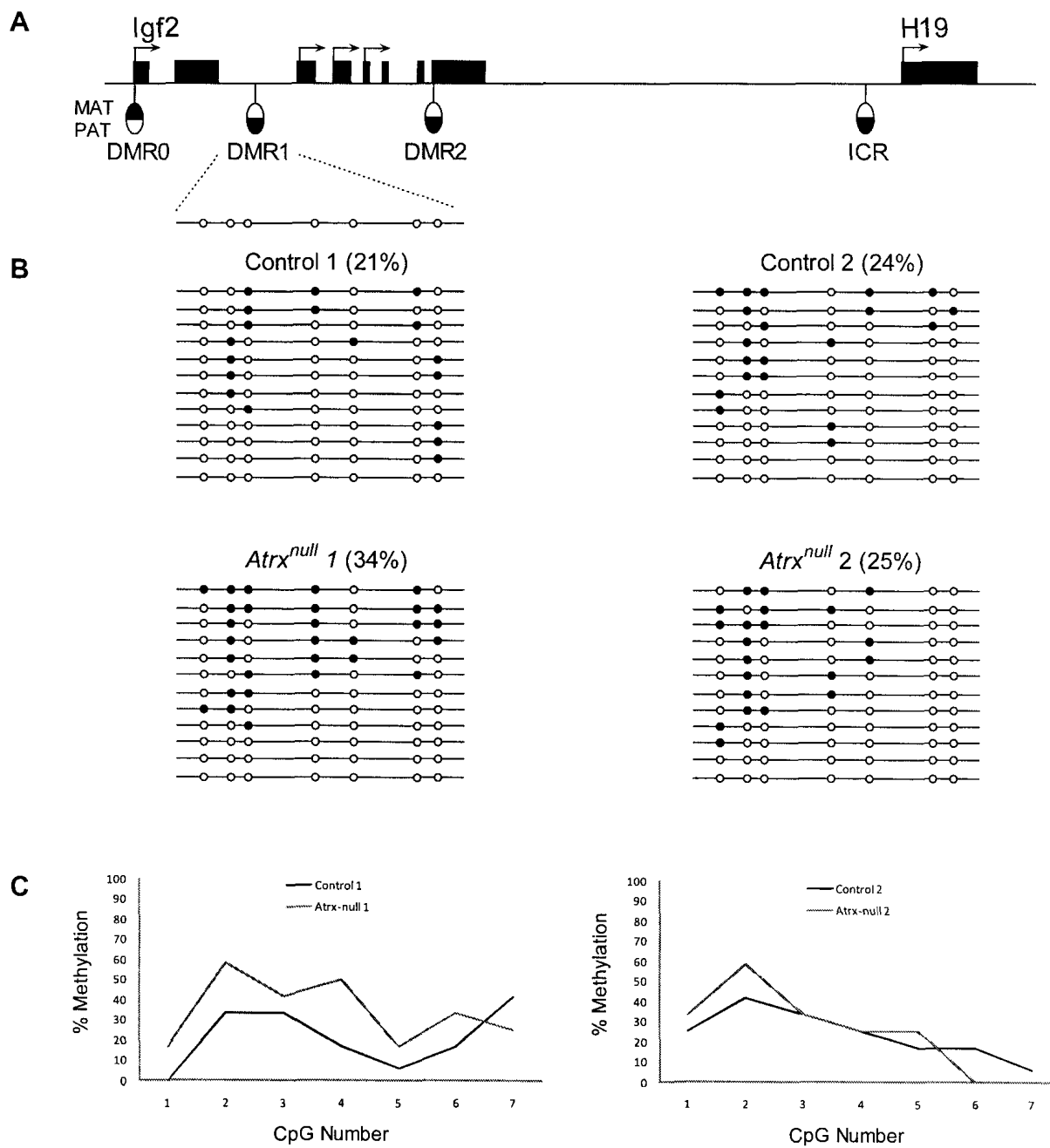
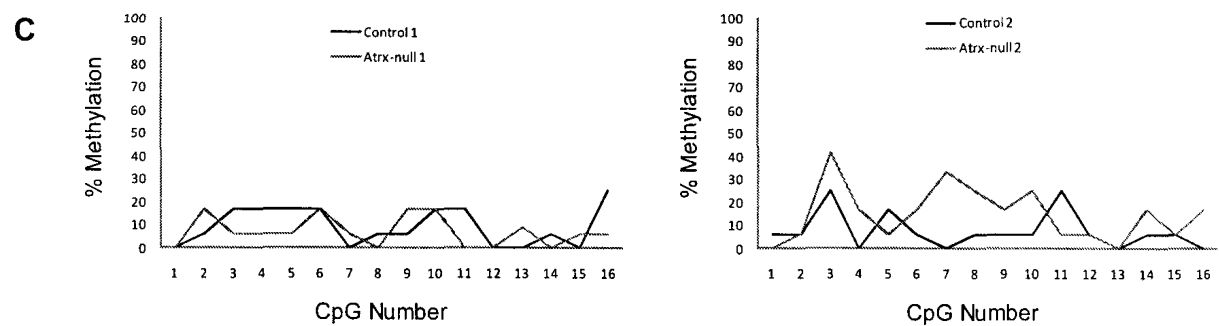
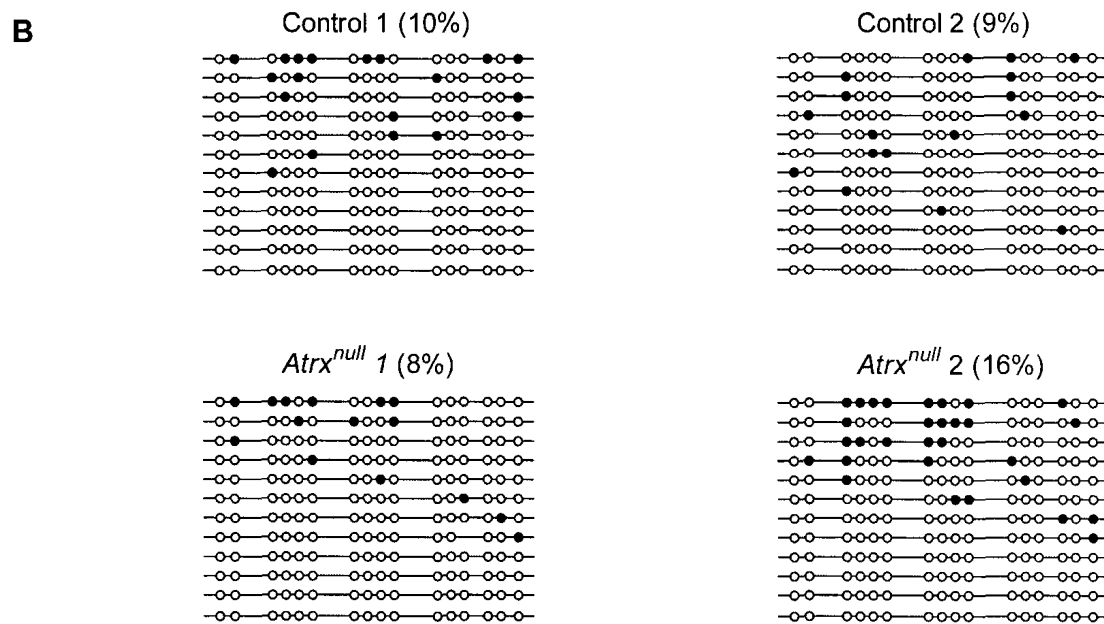
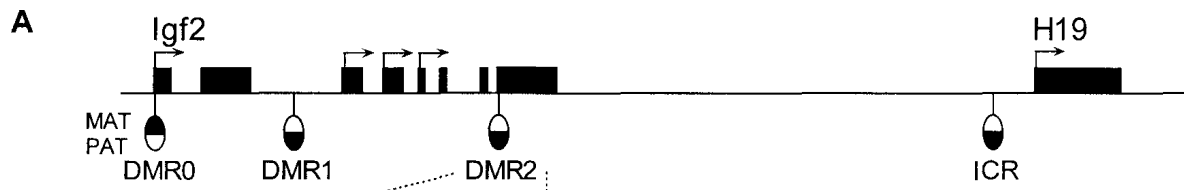


Figure 3.14 Bisulfite mutagenesis of the *Igf2* DMR2. (A) Schematic of the *H19 - Igf2* imprinted domain. Black squares represent exons. Black semi-ovals represent methylated DMRs and white semi-ovals represent unmethylated DMRs. The string with white circles represents the 16 CpG sites analyzed within the *Igf2* DMR2. (B) Twelve alleles from each sample were analysed and individual alleles are represented as a string with 16 CpG circles. Black circles are methylated and white circles are unmethylated. The total percent methylation for each sample is indicated beside the sample name. (C) Analysis of total methylation levels at individual CpG sites. Control samples are black and *Atrx*<sup>null</sup> samples are grey.



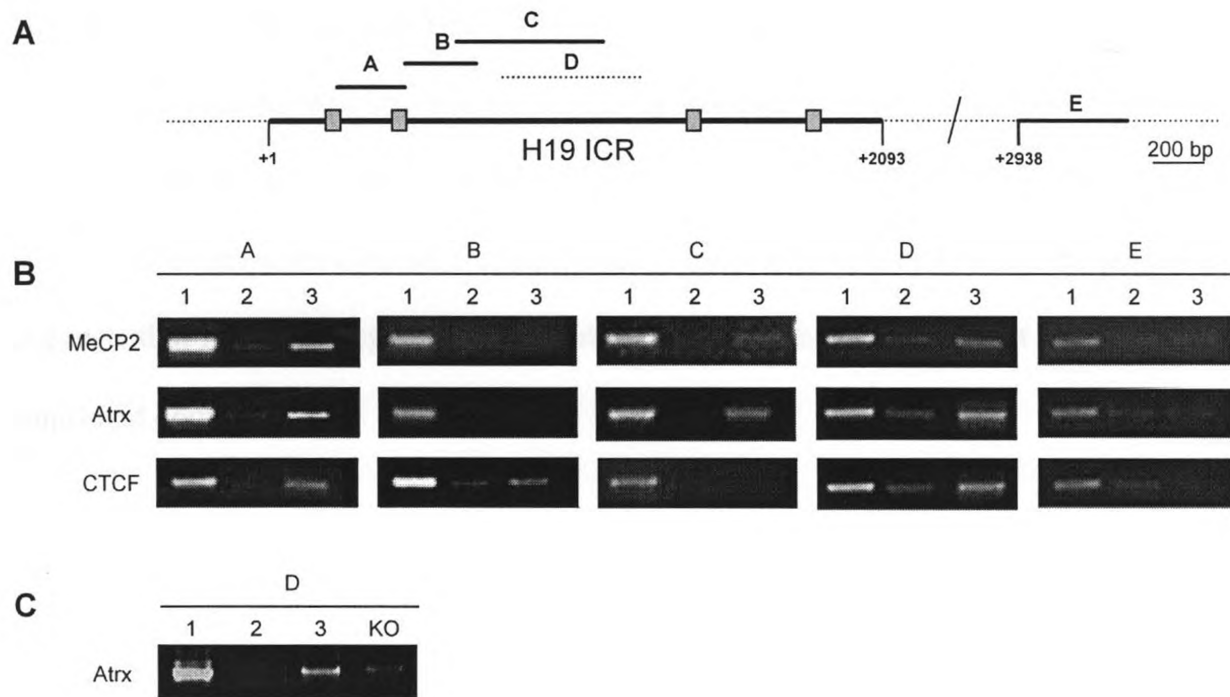
shows that these values are extreme outliers in comparison to all other samples. Taken together, DNA methylation patterns at the *H19-Igf2* DMRs are not changed in the *Atrx<sup>null</sup>* forebrain and do not correlate with upregulation of *H19* and *Igf2* expression.

### **3.6 Atrx and MeCP2 colocalize at the *H19* ICR**

Recent evidence has demonstrated that imprinting at the *H19 – Igf2* locus is regulated by a variety of epigenetic factors in addition to DNA methylation. Regulatory enzymes such as CTCF are known to be required both for the establishment and maintenance of imprinting at the *H19 – Igf2* domain (77, 128). Alternatively, enzymes such as MeCP2 have demonstrated allele-specific interactions but functional significance has not been fully established (78). Since deletion of *Atrx* in the mouse forebrain did not alter DNA methylation patterns at the *H19 – Igf2* domain, I reasoned that the regulatory effect *Atrx* has on *H19* and *Igf2* may be caused by interaction between *Atrx* and MeCP2 specifically at the paternally methylated *H19* ICR. Since MeCP2 is known to recruit histone modifying enzymes such as HDAC1 (69, 70), disruption of the putative *Atrx – MeCP2* interaction may affect acetylation of histone H3, rather than DNA methylation.

ChIP analysis was employed to determine if *Atrx* localizes to the *H19* ICR. Since no other gene-specific target sites have been identified for *Atrx*, known CTCF and MeCP2 binding sites in the *H19* ICR were used as a positive control to establish the ChIP protocol. As shown in Figure 3.15A, four CTCF binding sites are present within the *H19* ICR, while one MeCP2 interaction site has been mapped. Since no previous reports have shown successful ChIP analyses using *Atrx* antibodies, it was questioned whether the *Atrx* antibody would react with non-specific regions of chromatin. When

Figure 3.15 ChIP analysis of CTCF, MeCP2 and Atrx across the *H19* ICR. (A) Schematic of the *H19* ICR showing known binding sites for CTCF (grey boxes) and MeCP2 (dotted line D). Lettered lines indicate regions of PCR amplification. (B) Columns A – D show that antibodies for MeCP2 and Atrx strongly co-immunoprecipitate in the center of the *H19* ICR from wild type P18 mouse brain tissue (D region). CTCF binding is specific to previously mapped binding sites. Column E shows that antibodies for MeCP2, Atrx and CTCF do not immunoprecipitate the region upstream of the *H19* ICR from wild type P18 mouse brain tissue. Numbered lanes correspond to: (1) Input (2) Negative control antibodies for rabbit IgG, sheep IgG and goat IgG used alongside MeCP2, ATRX and CTCF antibodies, respectively (3) Wild type P18 mouse brain. (C) Control experiment showing that the Atrx antibody does not immunoprecipitate the *H19* ICR from *Atrx*<sup>null</sup> P18 mouse brain tissue. The KO lane corresponds to *Atrx*<sup>null</sup> P18 mouse forebrain.



comparing ChIP results in a control and *Atrx*<sup>null</sup> brain, the Atrx antibody only showed specificity for the control brain, proving that the Atrx antibody is specific (Figure 3.15C). To further address this issue, primer pairs spanning the *H19* ICR and a region approximately 8.5kb upstream of the *H19* ICR were designed (Figure 3.15A). As shown in Figure 3.15B panel E, the Atrx, MeCP2 and CTCF antibodies do not successfully immunoprecipitate DNA in the upstream region. Alternatively, Figure 3.15B panel D shows the novel finding that Atrx and MeCP2 co-localize in the center region of the *H19* ICR. CTCF binding was specific to previously mapped regions. This result outlines the first gene target site for Atrx and shows the novel finding that Atrx can co-localize with MeCP2 at target sites distinct from pericentric heterochromatin. Ultimately, this result suggests that Atrx is an epigenetic regulator of chromatin accessibility at the *H19 – Igf2* imprinted domain.

## CHAPTER FOUR – Discussion and Conclusions

### 4.1 Summary of Thesis Findings

In this thesis, I first presented the analysis of DNA methylation at repetitive sequences in the *Atrx*<sup>null</sup> forebrain demonstrating that 18S rDNA arrays are hypomethylated, while major satellite, minor satellite and IAP *gag* repeats are unchanged. Hypomethylation of 18S rDNA correlated with a 3.9-fold upregulation of 18S RNA expression in newborn *Atrx*<sup>null</sup> forebrain compared to controls. These results suggest that *Atrx* is targeted to rDNA arrays where it is involved in epigenetic silencing of transcription.

I then demonstrated that loss of *Atrx* in the forebrain results in upregulation of *H19*, *Igf2*, *Dlk1*, *Slc38a4*, *Dcn* and *Dlx5* in the neonatal and P17 forebrain. I found that aberrant imprinted gene regulation occurs sometime after E13.5 and before or at birth, suggesting that *Atrx* is required to maintain repressive epigenetic marks only at later stages of development. One exception was *Dlx5*, which showed downregulation at E13.5 and upregulation at P0.5 in the *Atrx*<sup>null</sup> forebrain. This finding indicates that *Atrx* may be involved in activation of *Dlx5* during embryonic development, and repression of *Dlx5* during postnatal development.

I have also demonstrated that deletion of *Atrx* in the mouse forebrain causes hypomethylation of the *Gtl2* DMR within the *Dlk1* – *Gtl2* imprinted domain. This change only occurred in one of two *Atrx*<sup>null</sup> forebrains and indicated that *Atrx* might be involved in the regulation of DNA methylation at the *Dlk1* – *Gtl2* imprinted domain, however allelic analysis will be required to definitively establish this link. Analysis of the *H19* –

*Igf2* domain revealed that transcriptional upregulation of these genes does not correlate with aberrant DNA methylation at the regulatory DMRs. Methylation analysis of control forebrain revealed that only half of the alleles are methylated at the *H19* ICR, suggesting that this genomic region is imprinted in the newborn forebrain. Conversely, minimal CpG methylation was observed at the *Igf2* DMR1 and DMR2, suggesting that chromatin conformation at the *H19 – Igf2* domain is likely to be different in the brain in comparison to other tissues such as the liver.

To determine whether Atrx acts directly or indirectly at the *H19 – Igf2* domain, we performed ChIP analysis of mouse brain tissue and showed that Atrx co-localizes with MeCP2 at the *H19* ICR, implicating Atrx as an epigenetic regulator of chromatin accessibility at the *H19 – Igf2* locus. Taken together, the results presented in this thesis demonstrate a novel role for Atrx in the regulation of imprinted gene expression and identify the *H19* ICR as the first genomic DNA target for the Atrx protein. This work sheds light on the functional significance of Atrx and can be used as a foundation for the future elucidation of the mechanism by which Atrx regulates gene expression.

#### **4.2 Developmental Implications of Aberrantly Expressed Imprinted Genes**

*H19*, *Igf2*, *Dlk1*, *Slc38a4*, *Dcn* and *Dlx5* all have complex tissue-specific imprinting and expression patterns, and each gene serves a unique function in the cell. The *H19* gene is transcribed into a non-coding RNA to which little functional significance has been established. It has recently been demonstrated that a 23-nucleotide primary microRNA is derived from the *H19* transcript, and it was proposed that this microRNA is involved in post-transcriptional downregulation of specific mRNAs during

embryonic development (131). Conversely, *Igf2* encodes a mitogenic hormone that is an autocrine regulator of cell proliferation and is involved in mediation of growth hormones, stimulation of insulin and embryonic growth (132). The *Dlk1* gene encodes a transmembrane protein that is a member of the Notch/Delta/Serrate family of signalling molecules (133, 134) and plays a role in the differentiation of several tissues (135-137). While the *Slc38a4* gene encodes a System A amino acid transporter that shuttles  $\alpha$ -(methylamino)-isobutyric acid between cells (138), *Dcn* encodes a member of the dermatan sulphate proteoglycan family that binds collagen and contributes to processes such as matrix assembly, cell adhesion, migration and proliferation in a variety of connective tissues (139). Finally, *Dlx5* encodes a distal-less homeobox protein that regulates the production of  $\gamma$ -aminobutyric acid (GABA) in GABAergic neurons (140).

Despite functional differences, there are two striking similarities between each of these genes. First, altered expression of some imprinted genes in the brain has been linked to different forms of autistic mental retardation and has led to the theory of the imprinted brain (141). Second, all of the identified genes except *Dlx5* have been implicated in the regulation of mouse placentation (142). As outlined below, these two observations may be significant as they relate first to the profound mental retardation observed in ATR-X patients and second to the placental defect observed in mice with tissue-wide deletion of *Atrx*.

#### **4.2.1 Conflict Theory and the Importance of Imprinted Genes in Placenta and Brain**

In mammals, imprinted genes have a high tendency to be implicated in the regulation of placental and foetal growth. The conflict theory of genomic imprinting is

the most widely recognized evolutionary explanation for this phenomenon, and states that imprinting is the result of conflict between the maternal and paternal genomes over the allocation of maternal resources to the offspring (143-146). Whereas paternally expressed genes are involved in extracting maternal resources for the benefit of individual offspring, maternally expressed genes act by allocating resources equally among all offspring (146). Ultimately, the battle of the parental genomes takes place between the placenta and foetus, at the levels of supply and demand for maternal resources (146, 147).

Outside the placenta, the other major tissue where imprinted genes are expressed is the brain (148). Conflict between the parental genomes can also be used to explain the theory of the imprinted brain and autistic mental retardation. Here, conflict is manifested by the transfer of resources via the behaviour of parents and offspring. Since the mammalian father's contribution to offspring comes from a single sperm and relies heavily on how his genes contribute to development of the brain, then these genes are expected to regulate self-interested behaviour at the expense of the mother and siblings (141). Alternatively, the mother provides resources before and after birth and is considerably more involved in rearing the offspring. Consequently, the mother has a strategic influential advantage as the main nurturer and her genetic contribution will favour development of brain structures that mediate cognitive activity related to the survival and fitness of the whole family (141).

To validate the theory of the imprinted brain, a role for genomic imprinting was clearly demonstrated in chimeric mouse brains, where it was found that cells expressing only paternal genes contribute to the development of 'systematic brain' structures such as the hypothalamus, amygdala and limbic system that mediate drives such as hunger, fear

and aggression (149, 150). Alternatively, cells expressing only maternal genes contribute to development of 'empathic brain' structures such as the neocortex and forebrain that mediate learning, planning, language, social interactions and empathic emotions (149, 150). Therefore, the paternal brain is recognized as expressing genes that differentially regulate growth, whereas the maternal brain expresses genes that differentially guide development (141). In relation to autistic mental retardation, extreme paternal brains are focused on systematic functions such as technical (eg. machines), natural (eg. biology) and abstract systems (eg. mathematics), whereas extreme maternal brains are centered on empathic functions such as social interactions, language skills and the ability to predict thoughts and feelings (141). Autistic mental retardation is therefore proposed to be caused by failure of the maternal brain that results in extreme favouring towards the impulsive and compulsive desires of the paternal brain (141).

#### **4.2.2 Expression and Role of Aberrantly Expressed Genes in the Brain**

In the mouse brain, expression analysis of the *Dcn* gene is limited to the embryo where it was shown that *Dcn* transcript is only present in the meninges and a region of the floor plate of the fourth ventricle (139). In contrast, there is detected *Dcn* expression in specific neuronal populations of the adult rat brain including Purkinje cells, stratum moleculare cells, and neurons in the olfactory cortex and pons (151). *DCN* is also expressed in the cerebral cortex and cerebellum of the human brain (152). Interestingly, it has been reported that imprinting of the mouse *Dcn* gene is specific to the placenta and all other tissues exhibit biallelic expression (110). Considering that imprinting was analyzed on whole brain, this study may not be accurate because other imprinted genes

show tissue-specific imprinting in localized regions of the brain (130). Regardless, *Dcn* has been implicated in inhibition of neurite outgrowth (153) and over-expression may result in cognitive abnormalities due to loss of axonal guidance and neuronal connections.

Expression and functional analyses of the imprinted gene *Slc38a4* has not been conducted in the brain and only limited analysis has been performed on *Dlk1*. In the adult brain, *Dlk1* is expressed in monoaminergic nuclei of the SNc (substantia nigra pars compacta) and the ventral tegmental area (VTA) (154). The role of *Dlk1* in these regions has only been explored with respect to the generation of dopaminergic neurons. It was found that during embryonic development, the onset of *Dlk1* expression in midbrain neurons correlates with the onset of the dopamine-synthesizing enzyme Tyrosine hydroxylase, which indicated that *Dlk1* is important for dopaminergic neuron maturation (155). According to the theory of the imprinted brain, increased expression of the maternally imprinted gene *Dlk1* should result in paternalization and hyperactivation of the systematic brain. *Dlk1* upregulation may therefore cause autistic abnormalities that manifest due to altered maturation of dopaminergic neurons.

More effort has been directed towards determining the expression and imprinting patterns of *H19* and *Igf2* in the brain. During embryonic brain development, *Igf2* is readily expressed throughout mesenchymal structures and the neural crest (119), however expression is restricted to the choroid plexus and leptomeninges in the postnatal brain, with transient expression in the granule cells of cerebellar parenchyma during the first week of postnatal development (120). Similarly, *H19* shows limited expression restricted to the choroid plexus stroma and leptomeninges. Interestingly, while *Igf2* is biallelically expressed in the epithelial layers of the choroid plexus, *H19* is not expressed at all (130).

The functional significance of this restricted expression pattern remains unclear, however it has been proposed that epigenetic mutations of *Igf2* will alter normal neurological or behavioural patterns by favouring the development of a paternal brain (156).

In the mouse and human brain, the *Dlx* genes play an important role in the development and transmission of GABAergic neurons. In particular, cortical expression of *Dlx5* regulates transcription of the glutamic acid decarboxylases that are responsible for the production of GABA (140). Past reports show that *Dlx5* is approximately 2-fold upregulated in the frontal cortex of *MeCP2<sup>null</sup>* mice and this result has been used to help explain the mechanism of Rett Syndrome (RTT) pathogenesis (106). RTT is an X-linked mental retardation syndrome that is caused by mutations in the *MECP2* gene and is characterized by autistic-like behaviour, impaired language, seizures, changes of head growth, loss of motor skills and repetitive hand wringing (157).

Since a cross-regulatory cascade has been shown for members of the *Dlx* family (140), it has been proposed that altered expression of *DLX5* would affect the GABA neurotransmission system by altering expression of other *DLX* genes (106). This proposal is supported by microarray analysis of the *Atrx<sup>null</sup>* P0.5 forebrain that identified the GABA-related genes Cerruloplasmin (*Cp*), Prostaglandin D2 synthase (*Ptgds*), Cadherin1 (*Cdh1*) and Transient receptor potential cation channel member 4 (*Trpc4*) as showing altered expression of at least 1.5-fold (Appendix I) (158-161). Therefore, loss of highly regulated expression of *Dlx5* in the *Atrx<sup>null</sup>* or *MeCP2<sup>null</sup>* mouse forebrain likely affects the development of GABAergic neurons and may be directly linked to the profound mental retardation observed in ATR-X and RTT patients. More specifically, the autistic-

like characteristics of ATR-X and RTT patients supports the theory of the imprinted brain in that over-expression of *DLX5* could disrupt maternal-brain development.

Problems with GABA neurotransmission have also been associated with the neurodevelopmental imprinting disorder Angelman Syndrome (AS) (162). AS is caused by chromosome 15 mutations in the maternally expressed ubiquitin protein ligase gene, *UBE3A* (163). Dysregulated *UBE3A* expression decreases paternally favoured *GABRB3* (GABA receptor beta-3) expression and alters GABA neurotransmission, ultimately causing dysfunction of cortical and thalamo-cortical systems (162). *UBE3A* mutation also disrupts Purkinje cell development in the cerebellum (164), which is a common abnormality found in autistic patients (165). Interestingly, Angelman syndrome shares phenotypic overlap with ATR-X syndrome in that patients show profound mental retardation with absent speech, walking seizures, happy disposition and emotional lability (20). This phenotypic overlap supports the presence of disrupted GABA neurotransmission in the ATR-X brain as well as further implicates ATR-X syndrome as an imprinted brain disorder.

#### **4.2.3 Expression and Role of Aberrantly Expressed Genes in the Placenta**

In comparison to the brain, significantly more research has been devoted to resolving the function and necessity of imprinted genes in the placenta. For example, it is known that human *DCN* negatively controls proliferation, migration and invasiveness of extravillous trophoblast (EVT) cells (166). In particular, *DCN* binds transforming growth factor (TGF)-beta (167), which is an inhibitor of EVTs (168-171). *DCN* and TGF-beta

co-localize in the decidual extracellular matrix in an inactive state and are proposed to be reactivated by proteolysis in order to prevent over-invasion of EVT cells (166).

It is important to note that in the human placenta the *DCN* gene is biallelically expressed and there are no regions with allele-specific chromatin modifications (172). It has been proposed that since most human pregnancies are singletons, there is no competition for maternal resources and this causes relaxation of *DCN* imprinting in the human placenta (172). Regardless, overexpression of *Dcn* in the mouse placenta could result in inhibition of migration, proliferation and invasiveness of EVT cells. In embryos where *Atrx* is globally deleted, lethality occurs at E9.5 due to failed formation and function of the invasive secondary trophoblast giant cell layer (8) and this may be linked to *Dcn* over-expression.

On a separate note, *Dlk1* is not ubiquitously expressed throughout embryonic development, but there are strong levels of expression in all layers of the placenta (173). Consequently, uniparental disomy of paternal chromosome 12 (pUPD12), which causes biallelic expression of *Dlk1*, results in placentomegaly, whereas uniparental disomy of maternal chromosome 12 (mUPD12) causes growth retardation (174). More specifically, pUPD12 conceptuses exhibit thickening of the middle trophoblast layer in the labyrinth, abnormal behaviour of glycogen cells in the junctional zone, and incomplete transformation of the central maternal artery in the placenta (175). These results indicate that the paternally expressed gene *Dlk1* is required for placental growth and upregulation of *Dlk1* may result in placentomegaly.

H19 RNA is present at high levels in extra-embryonic tissues as early as E5.5 (176) and in the embryo starting at E6.5, however strict monoallelic expression does not

occur until approximately E10.5 (177). *Igf2* is co-ordinately expressed in the same tissues as H19 at very high levels throughout embryonic development and both show a drastic expression decrease in all tissues after birth (178). Interestingly, the *Igf2* gene codes four promoters; P0 is a placenta-specific promoter located just upstream of the placenta-specific *Igf2* DMR0, whereas P1-P3 are ubiquitously active promoters located in each of the first three exons of the *Igf2* gene (175). In the placenta, *Igf2* is highly expressed in all cell layers from promoters P1-P3, with the exception of the labyrinthine trophoblast where *Igf2* is only expressed from the P0 promoter (175).

Although the *H19* regulatory elements are required for *Igf2* imprinting, H19 RNA is not essential and transgenic mice lacking the H19 transcript are viable (179). Alternatively, *Igf2* is essential for embryonic development and silencing of the gene results in embryonic lethality associated with placental stunting (180). Similar to the paternally expressed gene *Dlk1*, embryos over-expressing *Igf2* exhibit placentomegaly and foetal overgrowth (181). In addition, biallelic *IGF2* expression in humans caused by epimutations or microdeletions leads to foetal and placental overgrowth in utero and is diagnosed as the imprinting disorder Beckwith-Wiedemann syndrome (182). Taken together, these studies suggest that *Igf2* overexpression favours paternalization of the placenta in order to extract maternal nutrients and promote growth of the foetus.

Finally, *Slc38a4* shows tissue-specific imprinting that is monoallelic in all lineages except those of the liver and viscera (110). Interestingly, a link has been made between *Igf2* and *Slc38a4* in the regulation between placental nutrient supply and foetal demand. In placenta deficient of the *Igf2* P0 transcript, which is specific to the labyrinthine trophoblast cells, foetal demand signals are proposed to stimulate placental

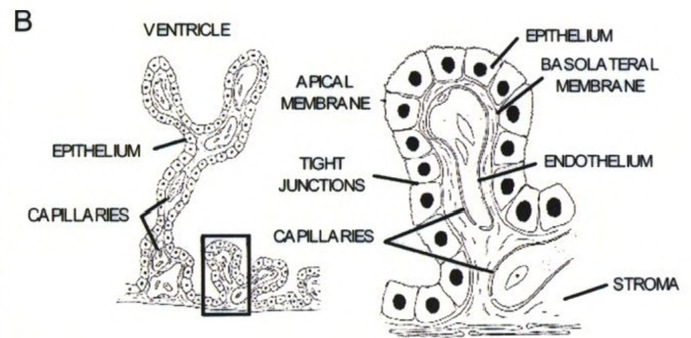
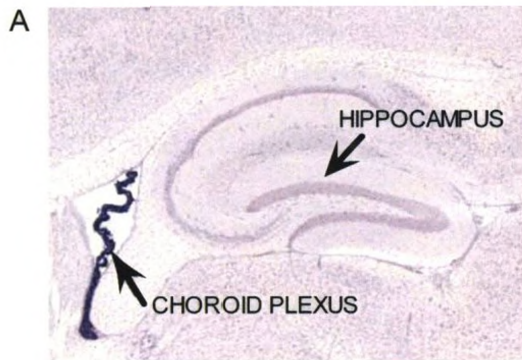
growth and upregulate placental expression of the nutrient supply gene *Slc38a4* (183). It was postulated that crosstalk between the paternally expressed demand gene *Igf2* in the foetus, and the paternally expressed supply gene *Slc38a4* in the placenta, support the conflict theory in that the paternally inherited genes act in concert to extract maternal resources and allocate maternal nutrients (183).

As mentioned previously, *Atrx<sup>null</sup>* embryos with global *Atrx* deletion die prior to E9.5 due to highly disorganized extra-embryonic tissue caused by defective formation of the secondary giant cell compartment in the developing trophoctoderm (8). According to the studies outlined above, it would be expected that upregulation of imprinted genes such as *Dlk1*, *Igf2* and *Slc38a4* should result in overgrowth of the placenta and foetus. Since placental overgrowth is not observed when murine *Atrx* is globally deleted, it is possible that ATRX either does not regulate imprinted genes in the placenta or that ATRX differentially regulates imprinted gene expression during prenatal and postnatal development.

#### **4.3 Proposed Mechanism of *H19 – Igf2* Regulation in the Mouse Forebrain**

In order to determine a possible mechanism of ATRX regulation at imprinted genes, research efforts were focused on the *H19 – Igf2* imprinted domain because this is the most widely studied locus throughout the imprinting literature. The main drawback to this approach is that the imprinting status of *H19* and *Igf2* has not been fully elucidated in the mouse brain. During postnatal stages of development, there is restricted expression of *H19* and *Igf2* in the choroid plexus stroma and leptomeninges (130), whereas in the choroid plexus epithelium *Igf2* is biallelically expressed and *H19* is not expressed (Figure

Figure 4.1 Choroid plexus structure. (A) The cortical choroid plexus is physically located beside the hippocampus in the cerebral cortex. (B) Schematic diagram of the choroid plexus ventricular outlining the location of epithelial and stromal tissue. The choroid plexus produces cerebral spinal fluid that is secreted through junctions in the epithelial layers of a highly vascular capillary bed.



4.1) (130). As mentioned previously, the significance of tissue-specific *H19 – Igf2* imprinting has not been resolved, and it is therefore possible that a variety of inter-related mechanisms could explain the regulation of *H19* and *Igf2* by *Atrx* in the mouse forebrain.

#### 4.3.1 Brain Specific Enhancers May Regulate *H19 – Igf2* Transcription

It was originally proposed that the *H19 – Igf2* imprinting variation between the choroid plexus epithelium and stroma is caused by differential epigenetic markings that are dependant on the embryonic lineage of the tissues (130); the epithelium is derived from neural tube ependyma whereas the stroma is derived from the same mesenchymal population that later forms the meninges (184). Interestingly, analysis of whole choroid plexus revealed biallelic methylation of the *Igf2* DMRs with concomitant monoallelic methylation of the *H19* promoter, supporting the presence of differential epigenetic markings (114).

It has also been shown that a centrally conserved domain (CCD) is involved in regulation of *Igf2* expression in both imprinted and non-imprinted brain tissues (130). It is proposed that a mesodermal or neural tube-derived enhancer lies within the CCD and drives expression of *Igf2* independant of the *H19* ICR (130). Considering that a specific CCD enhancer regulating biallelic *Igf2* expression exists in the choroid plexus (130), it is also possible that an additional unique enhancer regulates *Igf2*, but not *H19* expression in the forebrain. The concept of brain-specific enhancers is also supported by evidence from the *Gtl2 – Dlk1* imprinted domain. It was recently suggested that *Dlk1*-specific enhancers within the region 50 kb upstream from the *Dlk1* transcription start site show distinct activation of *Dlk1* in the brain (173). Alternatively, an unknown brain-specific enhancer

located between the regions 3.5 kb upstream of *Dlk1* and 69 kb downstream of *Gtl2* causes imprinted expression of *Gtl2* but not *Dlk1* (185). In the brain, *Dlk1* and *Gtl2* are therefore activated by separate gene-specific enhancers, which may also be the case for *H19* and *Igf2*.

#### 4.3.2 Transcriptional Regulation by Chromatin Looping and MARs

In the murine liver, the paternally methylated *H19* ICR interacts with the methylated *Igf2* DMR2 resulting in a chromatin loop where *Igf2* is actively transcribed but *H19* is silenced (77). The hypomethylated maternal *H19* ICR interacts with the MAR3 and the hypomethylated *Igf2* DMR1 via CTCF to silence *Igf2* and activate *H19* (77). Based on evidence from the liver it is likely that chromatin looping is also involved in *H19* – *Igf2* regulation in the forebrain, however, chromatin looping status has not been established thus far. In addition, the methylation status of the *H19* and *Igf2* DMRs has not been determined in brain structures exhibiting low levels of basal gene expression such as the cortex and hippocampus. I have shown for the first time that the *Igf2* DMRs have minimal levels of methylation in the mouse forebrain, which suggests that regulation of expression at the *H19* – *Igf2* domain is different than the liver and it is probable that a unique chromatin looping environment is present. Since the *H19* ICR showed a monoallelic methylation pattern, it is possible that the unmethylated maternal *H19* ICR is able to form a chromatin loop with the unmethylated maternal *Igf2* DMR1, resulting in *Igf2* silencing and *H19* activation. Alternatively, the methylated paternal *H19* ICR is unlikely capable of interacting with the unmethylated paternal *Igf2* DMR2, resulting in the formation of a unique chromatin loop or an open chromatin conformation.

Current reports demonstrate that methylation of the paternal *H19* ICR promotes DNMT access to the *Igf2* DMRs and should result in methylation (97), which is not observed in the forebrain. In order to prevent the spread of methylation to the paternal *Igf2* DMRs, then a paternal-specific barrier must be present. Since paternal-specific matrix attachment regions (MAR) are present in the liver (79), it is possible that these are also present in the brain, where they may act as boundary elements to prevent the spreading of chromatin modifications or to separate specific chromatin loops or domains. Conversely, loss of the *H19* ICR causes spread of methylation on both the maternal and paternal alleles (186). When the *H19* ICR is present, CTCF binding on the unmethylated maternal allele prevents the spread of methylation specifically at the *Igf2* DMRs on the maternal allele, whereas the paternal DMRs become methylated (97). Since it is proposed that the maternal loop is still present in the murine forebrain, then CTCF would prevent the spread of methylation to the maternal *Igf2* DMRs.

#### **4.3.3 Atrx and MeCP2 May Repress the Paternal Allele**

In addition to the requirement for unique boundary elements on the paternal allele, it is also possible that regulatory protein factors are required at the *H19* ICR to promote the formation of a heterochromatic state. Previous reports demonstrated that MeCP2 interacts with the methylated *H19* ICR in the mouse liver (78) as well as the *Gtl2* DMR in the mouse cerebellum (187). Examination of the functional significance of MeCP2 at the *H19* ICR has established that MeCP2 presence coincides with an increase in histone H3 lysine 9 (H3K9) methylation and reinforces a repressive chromatin state (188).

MeCP2 is also capable of recruiting the repressive enzyme HDAC1 to a variety of binding sites in the genome (69, 70), including the *H19 – Igf2* domain (71).

As outlined previously, a recent report showed that Atrx and MeCP2 directly interact at methylated pericentric heterochromatin of mature postnatal neurons through their C-terminal and methyl-binding domains, respectively (68). Interestingly, during embryonic development when MeCP2 is not expressed, Atrx is targeted to neuronal pericentric heterochromatin via the N-terminal ADD domain. However, in the post-natal brain, loss of MeCP2 results in a major decrease of ATRX at heterochromatin, despite both normal levels of ATRX protein and normal targeting to heterochromatin in non-brain tissues where MeCP2 is less abundant (68). In light of the developmental study of imprinted gene expression showing postnatal upregulation of target genes in the *Atrx*<sup>null</sup> forebrain, it is possible that Atrx and MeCP2 co-ordinately regulate *H19* and *Igf2* expression specifically during postnatal stages of forebrain development.

I have now established the novel finding that Atrx colocalizes with MeCP2 at the *H19* ICR in the P18 murine brain. Not only is this the first demonstration of a specific gene target site for Atrx, it is also the first evidence that Atrx and MeCP2 can interact at locations distinct from pericentric heterochromatin. Seeing as MeCP2 binding at the *H19* ICR is specific to the methylated allele, I propose that Atrx binding is specific to the paternally methylated allele. Since the paternal *Igf2* DMRs are unmethylated in the forebrain, it is unlikely that the *Igf2* DMR2 interacts with *H19* ICR, meaning that Atrx and MeCP2 likely promote a heterochromatic state that silences both *H19* and *Igf2* expression on the paternal allele. In support of this hypothesis, *H19* shows 2-fold

increased expression in *MeCP2<sup>null</sup>* mouse fibroblasts (188) and *IGF2* is upregulated in Rett syndrome lymphoblasts where MECP2 is mutated (189).

I further propose that Atrx and MeCP2 recruit repressive histone modifying enzymes to the *H19* ICR in an effort to restrict enhancer access to the *H19* and *Igf2* promoters. Since the DNMT3 enzymes have known interactions with HDAC1 via the ADD domain (54, 55), it is possible that the ATRX ADD domain also specifically recruits HDAC1 to the *H19* ICR. Furthermore, since DNMT3L is able to interact with unmethylated lysine 4 of histone H3 via the ADD domain (53), this suggests that lysine 4 of histone H3 may be a docking site for the ATRX ADD domain. Ultimately, I propose that deletion of Atrx or MeCP2 in the postnatal murine forebrain induces relaxation of the heterochromatic state and results in expression of *H19* and *Igf2* specifically from the paternal allele.

#### **4.3.4 Atrx May Regulate Chromatin Looping of $\alpha$ -globin and *Dlx5***

Several lines of evidence support a role for ATRX in the transcriptional control of genes that are regulated by higher order chromatin looping. First, the majority of ATR-X patients have a mild form of anemia known as  $\alpha$ -thalassaemia (20). This blood disorder is caused by downregulation of the  $\alpha$ -globin genes, resulting in aggregated  $\beta$ -globin exclusion bodies. In erythroid cells, chromatin looping partitions the  $\alpha$ -globin genes into an active transcription factory (66). Alternatively, in non-erythroid cells a different loop is formed in which the  $\alpha$ -globin genes are segregated from the transcriptional hub (66). Although a target binding site has not been identified for ATRX within the  $\alpha$ -globin

locus, the presence of  $\alpha$ -thalassaemia in patients suggests that ATRX may be involved in chromatin looping of  $\alpha$ -globin genes.

The second observation linking ATRX with chromatin looping is misregulation of the *Dlx5* gene in the *Atrx<sup>null</sup>* forebrain that I presented in this thesis. In the mouse, Hiroke *et al* demonstrated that *Dlx5* is upregulated in MeCP2-deficient brains resulting from loss of silent chromatin looping (106). They further showed that *Dlx5* exhibits preferential expression from the maternal allele, which suggested that *Dlx5* is partially imprinted in the murine brain. Using ChIP and chromosome conformation capture (3C) techniques, they demonstrated that MeCP2 mediates the formation of a repressive chromatin loop on both parental alleles, and that MeCP2 ablation causes loss of silent chromatin from both alleles that probably accounts for upregulation of *Dlx5*. Since *Dlx5* is misregulated in the *Atrx<sup>null</sup>* brain, and *Atrx* is a binding partner with MeCP2, it is possible that *Atrx* works with MeCP2 to promote repressive chromatin modifications at the *Dlx5* chromatin loop. However, a recent publication refutes the findings reported by Hiroke *et al*. This report suggests that *Dlx5* is biallelically expressed in the mouse brain and claims that MeCP2 is unable to regulate *Dlx5* looping based on inconsistencies with transcriptional profiling of the *MeCP2<sup>null</sup>* brain (107). While the argument was logical, no effort was made to experimentally reproduce the ChIP or 3C results, and the effect of MeCP2 on *Dlx5* needs to be revisited in order to resolve the conflicting data.

#### **4.3.5 Concise Model of *Atrx* Regulation of *H19* and *Igf2* in the Mouse Forebrain**

Taken together, I propose that ATRX is targeted to genes that are regulated by higher order chromatin looping. As outlined in Figure 4.2, methylation at regulatory

domains such as the *H19* ICR recruits MeCP2 localization, which in turn recruits ATRX via interaction between the MeCP2 methyl-binding domain and the ATRX C-terminal. Similar to CTCF, ATRX and/or MeCP2 then act as interaction sites for methylated boundary elements such as matrix attachment regions and result in the formation chromatin loops. ATRX also uses the ADD domain to dock onto unmethylated lysine 4 on histone H3. To establish the repressive heterochromatic state, ATRX and/or MeCP2 recruit histone modifying enzymes such as HDAC1 resulting in silencing of gene transcription. Deletion of either ATRX or MeCP2 would therefore result in aberrant activation of gene transcription due to relaxation of repressive epigenetic modifications.

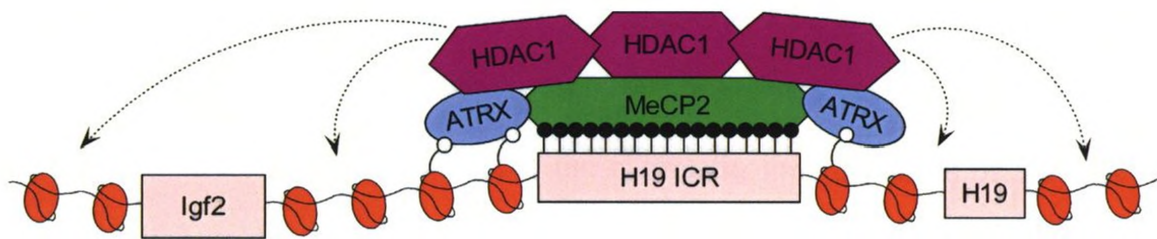
#### 4.4 Future Directions

Additional studies will be required in the future to fully elucidate the mechanism of ATRX regulation of imprinted genes. It will be imperative to establish whether the increased levels of imprinted transcripts originate from the maternal, paternal or both alleles in the *Atrx<sup>null</sup>* forebrain. It will also be interesting to determine if the identified imprinted genes are misregulated in the *Atrx<sup>null</sup>* placenta. To strengthen the proposed involvement of Atrx in chromatin looping, establishing the presence of Atrx at additional MeCP2 target sites such as the *Gtl2* DMR and the *Dlx5* locus will be required.

In order to fully elucidate a mechanism of action at the *H19 – Igf2* domain, it will be important to determine whether Atrx binding is specific to the paternal allele. Future research efforts should also be focused on determining if histone modifications or histone modifying enzymes are altered at the *H19* ICR in the *Atrx<sup>null</sup>* brain. Specifically, ChIP can be used to probe for loss of repressive histone modifications such as H3K9 methylation

Figure 4.2 Proposed mechanism of forebrain-specific Atrx-dependant regulation at the paternal *H19 – Igf2* imprinted domain. *H19* ICR methylation (black circles) recruits MeCP2, which in turn recruits Atrx. Docking of Atrx is facilitated by unmethylated lysine 4 (white circles) on histone H3 (orange ovals). Atrx and/or MeCP2 recruit histone modifying enzymes such as HDAC1 resulting in repression of gene transcription across the *H19 – Igf2* imprinted domain (dotted arrows).

PATERAL ALLELE



or gain of activating histone modifications such as H3 and H4 lysine acetylation. In light of the preferential binding of the DNMT3L ADD domain to unmethylated lysine 4 of histone H3, this would also be a good modification to examine. Alternatively, ChIP can be used to probe for the presence or absence of repressive histone modifying enzymes such as the histone deacetylase HDAC1 or the histone methyltransferase Suv39h1. This experiment will determine whether the presence of Atrx induces a repressive heterochromatic state by recruiting histone modifying enzymes to the *H19* ICR.

Perhaps the most important future experiment will be to determine the chromatin looping status of the *H19 – Igf2* locus in the mouse forebrain, which requires establishment of the technically demanding 3C protocol (190). This technique is used to detect physical interactions in both *cis* and *trans* between genes and regulatory elements. It will first be necessary to determine the chromatin looping status of the *H19 – Igf2* domain in the wild type forebrain, which would help to establish whether *H19* and *Igf2* are imprinted in the mouse forebrain. Determining the effect of Atrx deletion on chromatin looping is the ultimate goal for the future of this project and will hopefully elucidate a mechanism for the regulation of *H19* and *Igf2* by Atrx. This experiment may also establish chromatin looping domains as sites of interest for identification of new genes that are transcriptionally regulated by Atrx.

#### **4.5 Conclusions**

In summary, I have shown that rDNA repeats are hypomethylated upon Atrx deficiency in the mouse forebrain. Atrx deletion also results in upregulation of *H19*, *Igf2*, *Dlk1*, *Slc38a4*, *Dcn* and *Dlx5* expression in the newborn forebrain. To elucidate the

mechanisms underlying changes in imprinted gene expression at the *H19 – Igf2* domain, I examined the status of DNA methylation at regulatory DMRs, but found no correlation between methylation and gene expression. However, I discovered that Atrx co-localizes with MeCP2 at the *H19* ICR, therefore identifying the first direct gene target site for Atrx. My findings suggest that Atrx acts in concert with MeCP2 to promote the formation of a silent brain-specific chromatin loop. I propose that Atrx loss-of-function in the mouse forebrain causes relaxation of the heterochromatic state and activation of *H19* and *Igf2* transcription. Overall, examining the effect of Atrx deletion on imprinted genes has identified a novel link between the neuronal developmental processes associated with chromatin remodelling, imprinted gene expression and epigenetic modifications.

**CHAPTER 5 - References**

1. Gibbons, R., Picketts, D., Villard, L. and Higgs, D. (1995) Mutations in a putative global transcriptional regulator cause X-linked mental retardation with alpha-thalassaemia (ATR-X syndrome). *Cell*, **80**, 837-845.
2. Villard, L., Gecz, J., Mattei, J., Fontes, M., Saugier-veber, P., Munnich, A. and Lyonnet, S. (1996) XNP mutation in a large family with Juberg-Marsidi syndrom. *Nature Genetics*, **12**, 359-360.
3. Lossi, A., Millan, J., Villard, L., Orellana, C., Cardoso, C., Prieto, F., Fontes, M. and Martinez, F. (1999) Mutation of the XNP/ATR-X gene in a family with severe mental retardation, spastic paraplegia and skewed pattern of X-inactivation: demonstration that the mutation is involved in the inactivation process. *American Journal of Medical Genetics*, **65**, 558-562.
4. Stevenson, R., Abidi, F., Schwartz, C., Lubs, H. and Holmes, L. (2000) Holmes-Gang syndrome is allelic with XLMR-hypotonic face syndrome. *American Journal of Medical Genetics*, **94**, 383-385.
5. Abidi, F., Schwartz, C., Carpenter, N., Villard, L., Fontes, M. and Curtis, M. (1999) Carpenter-Waziri syndrome results from mutations in XNP. *American Journal of Medical Genetics*, **85**, 249-251.
6. Abidi, F., Cardoso, C., Lossi, A., Lowry, R., Depetris, D., Mattei, M., Lubs, H., Stevenson, R., Fontes, M., Chudley, A. *et al.* (2005) Mutations in the 5' alternatively spliced region of the XNP/ATR-X gene causes Chudley-Lowry syndrome. *European Journal of Human Genetics*, **13**, 176-183.
7. Villard, L., Fontes, M., Ades, L. and Gecz, J. (2000) Identification of a mutation in the XNP/ATR-X gene in a family reported as Smith-Fineman-Myers syndrome. *American Journal of Medical Genetics*, **91**, 83-85.
8. Garrick, D., Sharpe, J.A., Arkell, R., Dobbie, L., Smith, A.J.H., Wood, W.G., Higgs, D.R. and Gibbons, R.J. (2006) Loss of Atrx affects trophoblast development and the pattern of X-inactivation in extraembryonic tissues. *PLoS Genetics*, **2**, 438-450.
9. Berube, N.G., Mangelsdorf, M., Jagla, M., Vanderluit, J., Garrick, D., Gibbons, R.J., Higgs, D.R., Slack, R.S. and Picketts, D.J. (2005) The chromatin-remodelling protein ATRX is critical for neuronal survival during corticogenesis. *The Journal of Clinical Investigation*, **115**, 258-267.

10. Weatherall, D., Higgs, D., Bunch, C., Old, J., Hunt, D., Pressley, L., Clegg, J., Bethenfalvay, N., Sjolín, S., Koler, R. *et al.* (1981) Hemoglobin H disease and mental retardation: a new syndrome or a remarkable coincidence? *New England Journal of Medicine*, **305**, 607-612.
11. Bowcock, A., van Tonder, S. and Jenkins, T. (1984) The haemoglobin H disease mental retardation syndrome: molecular studies on the South African case. *Br J Haematol*, **56**, 69-78.
12. Buckle, V., Higgs, D., Wilkie, A., Super, M. and Weatherall, D. (1988) Localization of human alpha-globin to 16p13.3-pter. *Journal of Medical Genetics*, **25**, 847-849.
13. Wilkie, A., Zeitlin, H., Lindenbaum, R., Buckle, V., Fischel-Ghodsian, N., Chui, D., Gardner-Medwin, D., MacGillivray, M., Weatherall, D. and Higgs, D. (1990) Clinical features and molecular analysis of the alpha thalassemia/mental retardation syndromes. II. Cases without detectable abnormality of the alpha globin complex. *American Journal of Human Genetics*, **46**, 1127-1140.
14. Wilkie, A., Buckle, V., Harris, P., Lamb, J., Barton, N., Reeders, S., Lindenbaum, R., Nicholls, R., Barrow, M., Bethenfalvay, N. *et al.* (1990) Clinical features and molecular analysis of the alpha thalassemia/mental retardation syndromes. I. Cases due to deletions involving chromosome band 16p13.3. *American Journal of Human Genetics*, **46**, 1112-1126.
15. Cole, T., May, A. and Hughes, H. (1991) Alpha thalassemia/mental retardation syndrome (non-deletional type): report of a family supporting X linked inheritance. *Journal of Medical Genetics*, **28**, 734-737.
16. Wilkie, A., Pembrey, M., Gibbons, R., Higgs, D., Porteous, M., Burn, J. and Winter, R. (1991) The non-deletion type of alpha thalassemia/mental retardation: a recognizable dysmorphic syndrome with X linked inheritance. *Journal of Medical Genetics*, **28**, 724.
17. Donnai, D., Clayton-Smith, J., Gibbons, R. and Higgs, D. (1991) The non-deletion alpha thalassemia/mental retardation syndrome: further support for X linkage. *Journal of Medical Genetics*, **28**, 742-745.
18. Chudley, A. and Lowry, R. (1992) X linked alpha thalassemia/mental retardation (ATR-X) syndrome. *Journal of Medical Genetics*, **29**, 357.
19. Gibbons, R., Suthers, G., Wilkie, A., Buckle, V. and Higgs, D. (1992) X-linked alpha-thalassaemia/mental retardation (ATR-X) syndrome: localization to Xq12-q21.31 by X-inactivation and linkage analysis. *American Journal of Human Genetics*, **51**, 1136-1149.

20. Gibbons, R. (2006) Alpha thalassaemia-mental retardation, X linked. *Orphanet Journal of Rare Diseases*, **1**, 1-15.
21. Gibbons, R.J. and Higgs, D.R. (2000) Molecular-clinical spectrum of the ATR-X syndrome. *American Journal of Medical Genetics*, **97**, 204-212.
22. Gibbons, R.J., McDowell, T.L., Raman, S., O'Rourke, D.M., Garrick, D., Ayyub, H. and Higgs, D.R. (2000) Mutations in *ATRX*, encoding a SWI/SNF-like protein, cause diverse changes in the pattern of DNA methylation. *Nature Genetics*, **24**, 368-371.
23. Villard, L., Lacombe, D. and Fontes, M. (1996) A point mutation in the XNP gene, associated with an ATR-X phenotype without alpha-thalassaemia. *European Journal of Human Genetics*, **4**, 316-320.
24. Villard, L., Toutain, A., Lossi, A., Gecz, J., Houdayer, C., Moraine, C. and Fontes, M. (1996) Splicing mutation in the ATR-X gene can lead to a dysmorphic mental retardation phenotype without alpha-thalassaemia. *American Journal of Human Genetics*, **58**, 499-505.
25. Higgs, D., Vickers, M., Wilkie, A., Pretorius, I., Jarman, A. and Weatherall, D. (1989) A review of the molecular genetics of the alpha-globin gene cluster. *Blood*, **73**, 1081-1104.
26. Wada, T., Sugie, H., Fukushima, Y. and Saitoh, S. (2005) Non-skewed X-inactivation may cause mental retardation in a female carrier of X-linked alpha-thalassaemia/mental retardation syndrome (ATR-X): X-inactivation study of nine female carriers of ATR-X. *American Journal of Human Genetics*, **138**, 18-20.
27. Plenge, R., Stevenson, R., Lubs, H., Schwartz, C. and Willard, H. (2002) Skewed X-chromosome inactivation is a common feature of X-linked mental retardation disorders. *American Journal of Human Genetics*, **71**, 168-173.
28. Muers, M., Sharpe, J.A., Garrick, D., Sloane-Stanley, J., Nolan, P., Hacker, T., Wood, W., Higgs, D. and Gibbons, R. (2007) Defining the cause of skewed X-chromosome inactivation in X-linked mental retardation by use of a mouse model. *American Journal of Human Genetics*, **80**, 1138-1149.
29. Badens, C., Martini, N., Courrier, S., DesPortes, V., Touraine, R., Levy, N. and Edery, P. (2006) *ATRX* syndrome in a girl with a heterozygous mutation in the *ATRX* Zn finger domain and a totally skewed X-inactivation pattern. *American Journal of Human Genetics*, **140A**, 2212-2215.

30. Cox, G., Burger, J., Lip, V., Mau, U., Sperling, K., Wu, B. and Horsthemke, B. (2002) Intracytoplasmic sperm injection may increase the risk of imprinting defects. *American Journal of Human Genetics*, **71**, 162-164.
31. DeBaun, M., Niemitz, E. and Feinberg, A. (2003) Association of in vitro fertilization with Beckwith-Wiedemann syndrome and epigenetic alterations of LIT1 and H19. *American Journal of Human Genetics*, **72**, 156-160.
32. Orstavik, K., Eiklid, K., van der Hagen, C., Spetalen, S., Kierulf, K., Skjeldal, O. and Buiting, K. (2003) Another case of imprinting defect in a girl with Angelman syndrome who was conceived by intracytoplasmic sperm injection. *American Journal of Human Genetics*, **72**, 218-219.
33. Mao, X., Fujiwara, Y. and Orkin, S. (1999) Improved reporter strain for monitoring Cre recombinase-mediated DNA excision in mice. *PNAS*, **96**, 5037-5042.
34. Hebert, J.M. and McConnell, S.K. (2000) Targeting of *cre* to the *Foxg1* (*BF-1*) locus mediates *loxP* recombination in the telencephalon and other developing head structures. *Developmental Biology*, **222**, 296-306.
35. Houdayer, C., Toutain, A., Ronce, N., Lefort, G., Sarda, P., Taib, J., Briault, S., Lambert, J. and Moraine, C. (1993) X-linked alpha-thalassaemia mental retardation syndrome. Linkage analysis in a new family further supports localization in proximal Xq. *Ann Genet.*, **36**, 194-199.
36. Gecz, J., Pollard, H., Conzalez, G., Villard, L., Stayton, C., Millasseau, P., Khrestchatisky, M. and Fontes, M. (1994) Cloning and expression of the murine homolog of a putative human X-linked nuclear protein gene closely linked to *PGK1* in Xq13.3. *Human Molecular Genetics*, **3**, 39-44.
37. Stayton, C., Dabovic, B., Gulisano, M., Gecz, J., Broccoli, V., Giovanazzi, S., Bossolasco, M., Monaco, L., Rastan, S., Boncinelli, E. *et al.* (1994) Cloning and characterization of a new human Xq13 gene, encoding a putative helicase. *Human Molecular Genetics*, **3**, 1957-1964.
38. Picketts, D.J., Higgs, D.R., Bachoo, S., Blake, D.J., Quarrell, O.W.J. and Gibbons, R.J. (1996) *ATRX* encodes a novel member of the SNF2 family of proteins: mutations point to a common mechanism underlying ATR-X syndrome. *Human Molecular Genetics*, **5**, 1899-1907.
39. Villard, L., Lossi, A., Cardoso, C., Proud, V., Chiaroni, P., Colleaux, L., Schwartz, C. and Fontes, M. (1997) Determination of the genomic structure of the XNP/ATRX gene encoding a potential zinc finger helicase. *Genomics*, **43**, 149-155.

40. Picketts, D., Tastan, A., Higgs, D. and Gibbons, R. (1998) Comparison of the human and murine ATRX gene identifies highly conserved, functionally important domains. *Mammalian Genome*, **9**, 400-403.
41. Eisen, J.A., Sweder, K.S. and Hanawalt, P.C. (1995) Evolution of the SNF2 family of proteins: subfamilies with distinct sequences and functions. *Nucleic Acids Research*, **23**, 2715-2723.
42. Aapola, U., Shibuya, K., Scott, H.S., Ollila, J., Vihinen, M., Heino, M., Shintani, A., Kawasaki, K., Minoshima, S., Krohn, K. *et al.* (2000) Isolation and initial characterization of a novel zinc finger gene, *DNMT3L*, on 21q22.3, related to the cytosine-5-methyltransferase 3 gene family. *Genomics*, **65**, 293-298.
43. Gibbons, R.J., Bachoo, S., Picketts, D.J., Aftimos, S., Asenbauer, B., Bergoffen, J., Berry, S.A., Dahl, N., Fryer, A., Keppler, K. *et al.* (1997) Mutations in transcriptional regulator ATRX establish the functional significance of a PHD-like domain, **17**, 146-148.
44. Eisen, J.A., Sweder, K.S. and Hanawalt, P.C. (1995) Evolution of the SNF2 family of proteins: subfamilies with distinct sequences and functions. *Nucleic Acids Research*, **23**, 2715-2723.
45. Berube, N.G., Smeenk, C.A. and Picketts, D.J. (2000) Cell cycle-dependant phosphorylation of the ATRX protein correlates with changes in nuclear matrix and chromatin association. *Human Molecular Genetics*, **9**, 539-547.
46. McDowell, T.L., Gibbons, R.J., Sutherland, H., O'Rourke, D.M., Bickmore, W.A., Pombo, A., Turley, H., Gatter, K., Picketts, D.J., Buckle, V.J. *et al.* (1999) Localization of a putative transcriptional regulator (ATRX) at pericentric heterochromatin and the short arms of acrocentric chromosomes. *PNAS*, **96**, 13983-13988.
47. Garrick, D., Samara, V., McDowell, T., Smith, A., Dobbie, L., Higgs, D. and Gibbons, R. (2004) A conserved truncated isoform of the ATR-X syndrome protein lacking the SWI/SNF-homology domain *Gene*, **326**, 23-34.
48. Gibbons, R., Bachoo, S., Picketts, D., Aftimos, S., Asenbauer, B., Bergoffen, J., Berry, S., Dahl, N., Fryer, A., Keppler, K. *et al.* (1998) Mutations in transcriptional regulator ATRX establish the functional significance of a PHD-like domain. *Nature Genetics*, **17**, 146-148.
49. Mellor, J. (2006) It takes a PHD to read the histone code. *Cell*, **126**, 22-24.
50. Gibbons, R., Bachoo, S., Picketts, D., Aftimos, S., Asenbauer, B., Bergoffen, J., Berry, S., Dahl, N., Fryer, A., Keppler, K. *et al.* (1997) Mutations in

- transcriptional regulator ATRX establish the functional significance of a PHD-like domain. *Nature Genetics*, **17**, 146-148.
51. Argentaro, A., Yang, J., Chapman, L., Kowalczyk, M., Gibbons, R., Higgs, D., Neuhaus, D. and Rhodes, D. (2007) Structural consequences of disease-causing mutations in the ATRX-DNMT3-DNMT3L (ADD) domain of the chromatin-associated protein ATRX. *PNAS*, **104**, 11939-11944.
  52. Xie, S., Wang, Z., Okano, M., Nogami, M., Li, Y., He, W., Okumura, K. and Li, E. (1999) Cloning, expression and chromosome locations of the human DNMT3 gene family. *Gene*, **236**, 87-95.
  53. Ooi, S., Qiu, C., Bernstein, E., Li, K., Jia, D., Yang, Z., Erdjument-Bromage, H., Tempst, P., Lin, S., Allis, C. *et al.* (2007) DNMT3L connects unmethylated lysine 4 of histone H3 to de novo methylation of DNA. *Nature*, **448**, 714-717.
  54. Deplus, R., Brenner, C., Burgers, W., Putmans, P., Kouzarides, T., de Launoit, Y. and Fuks, F. (2002) Dnmt3L is a transcriptional repressor that recruits histone deacetylase. *Nucleic Acids Research*, **30**, 3831-3838.
  55. Fuks, F., Burgers, W., Godin, N., Kasai, M. and Kouzarides, T. (2001) Dnmt3a binds deacetylases and is recruited by a sequence-specific repressor to silence transcription. *EMBO J*, **20**, 2536-2544.
  56. Lee, N., Hong, Y., Yu, S., Han, S., Geum, D. and Cho, K. (2001) dXNP, a *Drosophila* homolog of XNP/ATRX, induces apoptosis via Jun-N-terminal kinase activation. *FEBS letters*, **581**, 2625-2632.
  57. Mohrmann, L. and Verrijzer, C. (2005) Composition and functional specificity of SWI2/SNF2 class chromatin remodelling proteins. *Biochim. Biophys. Acta*, **1681**, 59-73.
  58. Klein, H. (1997) RDH54, a RAD54 homolog in *Saccharomyces cerevisiae*, is required for mitotic diploid-specific recombination and repair and for meiosis. *Genetics*, **147**, 1533-1543.
  59. Ritchie, K., Seah, C., Moulin, J., Isaac, C., Dick, F. and Berube, N. (2007) Loss of ATRX leads to chromosome cohesion and congression defects. *Under revision*.
  60. De La Fuente, R., Viveiros, M.M., Wigglesworth, K. and Eppig, J.J. (2004) ATRX, a member of the SNF2 family of helicase/ATPases, is required for chromosome alignment and meiotic spindle organization in metaphase II stage mouse oocytes. *Developmental Biology*, **272**, 1-14.

61. Ishov, A.M., Vladimirova, O.V. and Maul, G.G. (2004) Heterochromatin and ND10 are cell-cycle regulated and phosphorylation-dependant alternate nuclear sites of the transcription repressor Daxx and SWI/SNF protein ATRX. *Journal of Cell Science*, **117**, 3807-3820.
62. Xue, Y., Gibbons, R.J., Yan, Z., Yang, D., McDowell, T.L., Sechi, S., Qin, J., Zhou, S., Higgs, D.R. and Wang, W. (2003) The ATRX syndrome protein forms a chromatin-remodelling complex with Daxx and localizes in promyelocytic leukemia nuclear bodies. *PNAS*, **100**, 10635-10640.
63. Jaskelioff, M., Van Komen, S., Krebs, J., Sung, P. and Peterson, C. (2003) Rad54p is a chromatin remodeling enzyme required for heteroduplex joint formation with chromatin. *Journal of Biological Chemistry*, **278**, 9212-9218.
64. Luciani, J.J., Depetris, D., Usson, Y., Metzler-Guillemain, C., Mignon-Ravix, C., Mitchell, M.J., Megarbane, A., Sarda, P., Sirma, H., Moncla, A. *et al.* (2006) PML nuclear bodies are highly organised DNA-protein structures with a function in heterochromatin remodelling at the G2 phase. *Journal of Cell Science*, **119**, 2518-2531.
65. Kumar, P., Bischof, O., Purbey, P., Notani, D., Urlaub, H., Dejean, A. and Galande, S. (2007) Functional interaction between PML and SATB1 regulates chromatin loop architecture and transcription of the MHC class I locus. *Nature Cell Biology*, **9**, 45-56.
66. Zhou, G., Xin, L., Song, W., Di, L., Liu, G., Wu, X., Liu, D. and Liang, C. (2006) Active chromatin hub of the mouse alpha-globin locus forms in a transcription factory of clustered housekeeping genes. *Molecular and Cellular Biology*, **26**, 5096-5105.
67. Cardoso, C., Timsit, H., Villard, L., Khrestchatisky, M., Fontes, M. and Colleaux, L. (1998) Specific interaction between the XNP/ATR-X gene product and the SET domain of the human EZH2 protein. *Human Molecular Genetics*, **7**, 679-684.
68. Nan, X., Hou, J., Maclean, A., Nasir, J., Lafuente, M., Shu, X., Kriaucionis, S. and Bird, A. (2007) Interaction between chromatin proteins MECP2 and ATRX is disrupted by mutations that cause inherited mental retardation. *PNAS*, **104**, 2709-2714.
69. Jones, P., Veenstra, G., Wade, P., Vermaak, D., Kass, U., Landsberger, N., Strouboulis, J. and Wolffe, A. (1998) Methylated DNA and MeCP2 recruit histone deacetylase to repress transcription. *Nature Genetics*, **19**, 187-191.

70. Nan, X., Ng, H., Johnson, C., Laherty, C., Turner, B., Eisenman, R. and Bird, A. (1998) Transcriptional repression by the methyl-CpG binding protein MeCP2 involves a histone deacetylase complex. *Letters to Nature*, **393**, 386-389.
71. Zupkovitz, G., Tischler, J., Posch, M., Sadzak, I., Ramsauer, K., Egger, G., Grausenburger, R., Schweifer, N., Chiocca, S., Decker, T. *et al.* (2006) Negative and positive regulation of gene expression by mouse histone deacetylase 1. *Molecular and Cellular Biology*, **26**, 7913-7928.
72. Amir, R., Van den Veyver, I., Wan, M., Tran, C., Francke, U. and Zoghbi, H. (1999) Rett syndrome is caused by mutations in X-linked MECP2, encoding methyl CpG binding protein 2. *Nature Genetics*, **23**, 185-188.
73. McGrath, J. and Solter, D. (1984) Completion of mouse embryogenesis requires both the maternal and paternal genomes. *Cell*, **37**, 179-183.
74. Surani, M., Barton, S. and Norris, M. (1984) Development of reconstituted mouse eggs suggest imprinting of the genome during gametogenesis. *Nature*, **308**, 548-550.
75. Cattanaach, B. and Kirk, M. (1985) Differential activity of maternally and paternally derived chromosome regions in mice. *Nature*, **315**, 496-498.
76. Bartolomei, M.S., Webber, A.L., Brunkow, M.E. and Tilghman, S.M. (1993) Epigenetic mechanisms underlying the imprinting of the mouse H19 gene. *Genes Dev.*, **7**, 1663-1673.
77. Kurukuti, S., Tiwari, V.K., Tavoosidana, G., Pugacheva, E., Murrell, A., Zhao, Z., Lobanenkov, V., Reik, W. and Ohlsson, R. (2006) CTCF binding at the *H19* imprinting control region mediates maternally inherited higher-order chromatin conformation to restrict enhancer access to *Igf2*. *PNAS*, **103**, 10684-10689.
78. Drewell, R., Goddard, C., Thomas, J. and Surani, M. (2002) Methylation-dependant silencing at the H19 imprinting control region by MeCP2. *Nucleic Acids Research*, **30**, 1139-1144.
79. Weber, M., Hagege, H., Murrell, A., Brunel, C., Reik, W., Cathala, G. and Forne, T. (2003) Genomic imprinting controls matrix attachment regions in the *Igf2* gene. *Molecular and Cellular Biology*, **23**, 8953-8959.
80. Engemann, S., Stroedicke, M., Paulsen, M., Franck, O., Reinhardt, R., Lane, N., Reik, W. and Walter, J. (2000) Sequence and functional comparison in the Beckwith-Wiedeman region: implications for a novel imprinting centre and extended imprinting. *Human Molecular Genetics*, **9**, 2691-2706.

81. Paulsen, M., El-Maarri, O., Engemann, S., Stroedicke, M., Franck, O., Davies, K., Reinhardt, R., Reik, W. and Walter, J. (2000) Sequence conservation and variability of imprinting in the Beckwith-Wiedemann syndrome gene cluster in human and mouse. *Human Molecular Genetics*, **9**, 1829-1841.
82. Fitzpatrick, G., Soloway, P. and Higgins, M. (2002) Regional loss of imprinting and growth deficiency in mice with a targeted deletion of KvDMR1. *Nature Genetics*, **32**, 426-431.
83. Mancini-DiNardo, D., Steele, S., Levorse, J., Ingram, R. and Tilghman, S.M. (2006) Elongation of the *Kcnqlot1* transcript is required for genomic imprinting of neighboring genes. *Genes and Development*, **20**, 2096-2106.
84. Vongs, A., Kakutani, T., Martienssen, R. and Richards, E. (1993) *Arabidopsis thaliana* DNA methylation mutants. *Science*, **260**, 1926-1928.
85. Jeddloh, J., Stokes, T. and Richards, E. (1999) Maintenance of genomic methylation requires a SWI2/SNF2-like protein. *Nature Genetics*, **22**, 94-97.
86. Kakutani, T., Munakata, K., Richards, E. and Hirochika, H. (1999) Meiotically and mitotically stable inheritance of DNA hypomethylation induced by *ddm1* mutation of *Arabidopsis thaliana*. *Genetics*, **151**, 831-838.
87. Vielle-Calzada, J., Thomas, J., Spillane, C., Coluccio, A., Hoepfner, M. and Grossniklaus, U. (1999) Maintenance of genomic imprinting at the *Arabidopsis medea* locus requires zygotic DDM1 activity. *Genes and Development*, **13**, 2971-2982.
88. Sun, L., Lee, D., Zhang, Q., Xiao, W., Raabe, E., Meeker, A., Miao, D., Huso, D. and Arceci, R. (2004) Growth retardation and premature aging phenotypes in mice with disruption of the SNF2-like gene, PASG. *Genes and Development*, **18**, 1035-1046.
89. Dennis, K., Fan, T., Geiman, T., Yan, Q. and Muegge, K. (2001) Lsh, a member of the SNF2 family, is required for genome-wide methylation. *Genes and Development*, **15**, 2940-2944.
90. Huang, J., Fan, T., Yan, Q., Zhu, H., Fox, S., Issaq, H., Best, L., Gangi, L., Munroe, D. and Muegge, K. (2004) Lsh, an epigenetic guardian of repetitive elements. *Nucleic Acids Research*, **32**, 5019-5028.
91. Fan, T., Hagan, J.P., Kozlov, S.V., Stewart, C.L. and Muegge, K. (2005) Lsh controls silencing of the imprinted *Cdkn1c* gene. *Development*, **132**, 635-644.

92. Ishihara, K., Oshimura, M. and Nakao, M. (2006) CTCF-dependant chromatin insulator is linked to epigenetic remodeling. *Molecular Cell*, **23**, 733-742.
93. Diaz-Meyer, N., Yang, Y., Sait, S., Maher, E. and Higgins, M. (2005) Alternative mechanisms associated with silencing of CDKN1C in Beckwith-Wiedemann syndrome. *Journal of Medical Genetics*, **42**, 648-655.
94. Kainz, B., Shehata, M., Bilban, M., Kienle, D., Heintel, D., Kromer-Holzinger, E., Le, T., Krober, A., Heller, G., Schwarzer, I. *et al.* (2007) Overexpression of the paternally expressed gene 10 (PEG10) from the imprinted locus on chromosome 7q21 in high-risk B-cell chronic lymphocytic leukemia. *International Journal of Cancer*, **Epub ahead of print**.
95. Martens, J.H.A., O'Sullivan, R.J., Braunschweig, U., Opravil, S., Radolf, M., Steinlein, P. and Jenuwein, T. (2005) The profile of repeat-associated histone lysine methylation states in the mouse epigenome. *The EMBO Journal*, **24**, 800-812.
96. Takada, S., Paulsen, M., Tevendale, M., Tsai, C.-E., Kelsey, G., Cattanch, B.M. and Ferguson-Smith, A.C. (2002) Epigenetic analysis of the *Dlk1-Gtl2* imprinted domain on mouse chromosome 12: implications for imprinting control from comparison with *Igf2-H19*. *Human Molecular Genetics*, **11**, 77-86.
97. Lopes, S., Lewis, A., Hajkova, P., Dean, W., Oswald, J., Forne, T., Murrell, A., Constancia, M., Bartolomei, M., Walter, J. *et al.* (2003) Epigenetic modifications in an imprinting cluster are controlled by a hierarchy of DMRs suggesting long-range chromatin interactions. *Human Molecular Genetics*, **12**, 295-305.
98. Olek, A., Oswald, J. and Walter, J. (1996) A modified and improved method for bisulphite based cytosine methylation analysis. *Nucleic Acids Research*, **24**, 5064-5066.
99. Lucifero, D., Mertineit, C., Clarke, H.J., Bestor, T.H. and Trasler, J.M. (2002) Methylation dynamics of imprinted genes in mouse germ cells. *Genomics*, **79**, 530-538.
100. Lippman, Z., Gendrel, A.V., Black, M., Vaughn, M.W., Dedhia, N., McCombie, W.R., Lavine, K., Mittal, V., May, B.P., Kasschau, K.D. *et al.* (2004) Transposable elements in heterochromatin and epigenetic control. *Nature*, **430**, 471-476.
101. Rabinowicz, P.D., Palmer, L.E., May, B.P., Hemann, M.T., Lowe, S.W., McCombie, W.R. and Martienssen, R.A. (2003) Genes and transposons are differentially methylated in plants, but not in mammals. *Genome Research*, **13**, 2658-2664.

102. Gibbons, R.J. (2006) Alpha thalassaemia-mental retardation, X linked. *Orphanet Journal of Rare Diseases*, **1**, 15.
103. Kobayashi, S., Wagatsuma, H., Ono, R., Ichikawa, H., Yamazaki, M., Tashiro, H., Aisaka, K., Miyoshi, N., Kohda, T., Ogura, A. *et al.* (2000) Mouse *Peg9/Dlk1* and human *PEG9/DLK1* are paternally expressed imprinted genes closely located to the maternally expressed imprinted genes: mouse *Meg3/Gtl2* and human *MEG3*. *Genes to Cells*, **5**, 1029-1037.
104. Schmidt, J.V., Matteson, P.G., Jones, B.K., Guan, X.-J. and Tilghman, S.M. (2000) The *Dlk1* and *Gtl2* genes are linked and reciprocally imprinted. *Genes and Development*, **14**, 1997-2002.
105. Takada, S., Tevendale, M., Baker, J., Georgiades, P., Campbell, E., Freeman, T., Johnson, M.H., Paulsen, M. and Ferguson-Smith, A.C. (2000) *Delta-like* and *Gtl2* are reciprocally expressed, differentially methylated linked imprinted genes on mouse chromosome 12. *Current Biology*, **10**, 1135-1138.
106. Horike, S., Cai, S., Miyano, M., Cheng, J. and Kohwi-Shigematsu, T. (2005) Loss of silent chromatin looping and impaired imprinting of *DLX5* in Rett Syndrome. *Nature Genetics*, **37**, 31-40.
107. Schule, B., Li, H., Fisch-Kohl, C., Purmann, C. and Francke, U. (2007) *DLX5* and *DLX6* expression is biallelic and not modulated by *MECP2* deficiency. *American Journal of Human Genetics*, **81**, 492-506.
108. Reik, W., Dean, W. and Walter, J. (2001) Epigenetic reprogramming in mammalian development. *Science*, **293**, 1089-1093.
109. Smith, R., Dean, W., Konfortova, G. and Kelsey, G. (2003) Identification of novel imprinted genes in a genome-wide scale for maternal methylation. *Genome Research*, **13**, 558-569.
110. Mizuno, Y., Sotomaru, Y., Katsuzawa, Y., Kono, T., Meguro, M., Oshimura, M., Kawai, J., Tomaru, Y., Kiyosawa, H., Nikaido, I. *et al.* (2002) *Asb4*, *Ata3* and *Dcn* are novel imprinted genes identified by high-throughput screening using RIKEN cDNA microarray. *Biochem. Biophys. Res. Commun.*, **290**, 1499-1505.
111. Schuster-Glosser, K., Bilinski, P., Sado, T., Ferguson-Smith, A. and Gossler, A. (1998) The mouse *Gtl2* gene is differentially expressed during embryonic development, encodes multiple alternatively spliced transcripts, and may act as an RNA. *Dev Dyn*, **212**, 214-228.

112. Lin, S.-P., Youngson, N., Takada, S., Seitz, H., Reik, W., Paulsen, M., Cavaille, J. and Ferguson-Smith, A.C. (2003) Asymmetric regulation of imprinting on the maternal and paternal chromosomes at the *Dlk1-Gtl2* imprinted cluster on mouse chromosome 12. *Nature Genetics*, **35**, 97-102.
113. Steshina, E., Carr, M., Glick, E., Yevtodiyenko, A., Appelbe, O. and Schmidt, J. (2006) Loss of imprinting at the *Dlk1-Gtl2* locus caused by insertional mutagenesis in the *Gtl2* 5'-region. *BMC Genetics*, **7**, 44-65.
114. Feil, R., Walter, J., Allen, N.D. and Reik, W. (1994) Developmental control of allelic methylation in the imprinted mouse *Igf2* and *H19* genes. *Development*, **120**, 2933-2943.
115. Ferguson-Smith, A.C., Sasaki, H., Cattanach, B.M. and Surani, M.A. (1993) Parental-origin-specific epigenetic modification of the mouse *H19* gene. *Letters to Nature*, **362**, 751-755.
116. Moore, T., Constancia, M., Zubair, M., Bailleul, B., Feil, R., Sasaki, H. and Reik, W. (1997) Multiple imprinted sense and antisense transcripts, differential methylation and tandem repeats in a putative imprinting control region upstream of mouse *Igf2*. *PNAS*, **94**, 12509-12514.
117. Murrell, A., Heeson, S. and Reik, W. (2004) Interaction between differentially methylated regions partitions the imprinted genes *Igf2* and *H19* into parent-specific chromatin loops. *Nature Genetics*, **36**, 889-893.
118. Ling, J.Q., Li, T., Hu, J.F., Vu, T.H., Chen, H.L., Qiu, X.W., Cherry, A.M. and Hoffman, A.R. (2006) CTCF mediates interchromosomal colocalization between *Igf2/H19* and *Wsb1/Nf1*. *Science*, **312**, 269-312.
119. Lee, J.E., Pintar, J. and Efstratiadis, A. (1990) Pattern of the insulin-like growth factor II gene during early mouse embryogenesis. *Development*, **110**, 151-159.
120. Hetts, S.W., Rosen, K.M., Dikkes, P., Villa-Komaroff, L. and Mozell, R.L. (1997) Expression and imprinting of the insulin-like growth factor II gene in neonatal mouse cerebellum. *Journal of Neuroscience Research*, **50**, 958-966.
121. DeChiara, T.M., Robertson, E.J. and Efstratiadis, A. (1991) Parental imprinting of the mouse insulin-like growth factor II gene. *Cell*, **64**, 849-859.
122. Charalambous, M., Menhenniott, T.R., Bennett, W.R., Kelly, S.M., Dell, G., Dandolo, L. and Ward, A. (2004) An enhancer element at the *H19/Igf2* locus drives gene expression in both imprinted and non-imprinted tissues. *Developmental Biology*, **271**, 488-497.

123. Jones, B., Levorse, J. and Tilghman, S.M. (2001) Deletion of a nuclease-sensitive region between the *Igf2* and *H19* genes leads to *Igf2* misregulation and increased adiposity. *Human Molecular Genetics*, **10**, 807-814.
124. Kaffer, C., Srivastava, M., Park, K., Ives, E., Hsieh, S., Battle, J., Grinberg, A., Huang, S. and Pfeifer, K. (2000) A transcriptional insulator at the imprinted *H19/Igf2* locus. *Genes and Development*, **14**, 1908-1919.
125. Ishihara, K., Hatano, N., Furuumi, H., Kato, R., Iwaki, K., Miura, K., Jinno, Y. and Sasaki, H. (2000) Comparative genomic sequencing identifies novel tissue-specific enhancers and sequence elements for methylation-sensitive factors implicated in *Igf2/H19* imprinting. *Genome Research*, **10**, 664-671.
126. Leighton, P., Saam, J., Ingram, R., Stewart, C. and Tilghman, S.M. (1995) An enhancer deletion affects both *H19* and *Igf2* expression. *Genes and Development*, **9**, 2079-2089.
127. Svensson, K., Walsh, C.P., Fundele, R. and Ohlsson, R. (1995) *H19* is imprinted in the choroid plexus and leptomeninges of the mouse foetus. *Mechanisms of Development*, **51**, 31-37.
128. Pant, V., Kurukuti, S., Pugacheva, E., Shamsuddin, S., Mariano, P., Renkawitz, R., Klenova, E., Lobanenkova, V. and Ohlsson, R. (2004) Mutation of a single CTCF target site within the *H19* imprinting control region leads to loss of *Igf2* imprinting and complex patterns of de novo methylation upon maternal inheritance. *Molecular and Cellular Biology*, **24**, 3497-3504.
129. Drewell, R., Brenton, J., Ainscough, J., Barton, S., Hilton, K., Arney, K., Dandolo, L. and Surani, M. (2000) Deletion of a silencer element disrupts *H19* imprinting independently of a DNA methylation epigenetic switch. *Development*, **127**, 3419-3428.
130. Charalambous, M., Menhenniott, T., Bennett, W., Kelly, S., Dell, G., Dandolo, L. and Ward, A. (2004) An enhancer element at the *Igf2/H19* locus drives gene expression in both imprinted and non-imprinted tissue. *Developmental Biology*, **271**, 488-497.
131. Cai, X. and Cullen, B. (2007) The imprinted *H19* noncoding RNA is a primary microRNA precursor. *RNA*, **13**, 313-317.
132. Jones, J. and Clemmons, D. (1995) Insulin-like growth factors and their binding proteins: biological actions. *Endocrine Reviews*, **16**, 3-34.
133. Jenson, C., Krogh, T., Hojrup, P., Clausen, P.S., K, Larsson, L., Enghild, J. and Teisner, B. (1994) Protein structure of fetal antigen 1 (FA1). A novel circulating

- human epidermal-growth-factor-like protein expressed in neuroendocrine tumors and its relation to the gene products of dlk and pG2. *European Journal of Biochemistry*, **225**, 83-92.
134. Laborda, J., Sausville, E., Hoffman, T. and Notario, V. (1993) Dlk, a putative mammalian homeotic gene differentially expressed in small cell lung carcinoma and neuroendocrine tumor cell line. *Journal of Biological Chemistry*, **268**, 3817-3820.
  135. Laborda, J. (2000) The role of the epidermal growth factor-like protein Dlk1 in cell differentiation. *Histology and Histopathology*, **15**, 119-129.
  136. Moon, Y., Smas, C., Lee, K., Villena, J., Kim, K., Yun, E. and Sul, H. (2002) Mice lacking paternally expressed Pref-1/Dlk1 display growth retardation and accelerated adiposity. *Molecular and Cellular Biology*, **22**, 5585-5592.
  137. Smas, C. and Sul, H. (1993) Pref-1, a protein containing EGF-like repeats, inhibits adipocyte differentiation. *Cell*, **73**, 725-734.
  138. Sugawara, M., Nakanishi, T., Fei, Y., Martinadle, R., Ganapathy, N., Leibach, F. and Ganapathy, V. (2000) Structure and function of ATA3, a new subtype of amino acid transport system A, primarily expressed in the liver and skeletal muscle. *Biochem. Biophys. Acta.*, **1509**, 7-13.
  139. Scholzen, T., Solursh, M., Suzuki, S., Reiter, R., Morgan, J., Buchberg, A., Siracusa, L. and Iozzo, R. (1994) The murine decorin: Complete cDNA cloning, genomic organization, chromosomal alignment and expression during organogenesis and tissue differentiation. *Journal of Biological Chemistry*, **269**, 28270-28281.
  140. Stuhmer, T., Anderson, S., Ekker, M. and Rubenstein, J. (2002) Ectopic expression of the Dlx genes induces glutamic acid decarboxylase and Dlx expression. *Development*, **129**, 245-252.
  141. Badcock, C. and Crespi, B. (2006) Imbalanced genomic imprinting in brain development: an evolutionary basis for the aetiology of autism. *J. Evol. Biol.*, **19**, 1007-1032.
  142. Wagschal, A. and Feil, R. (2006) Genomic imprinting in the placenta. *Cytogenetic and Genome Research*, **113**, 90-98.
  143. Moore, T. and Haig, D. (1991) Genomic imprinting in mammalian development: a parental tug-of-war. *TRENDS in Genetics*, **7**, 45-49.

144. Wilkins, J. and Haig, D. (2003) What good is genomic imprinting: the function of parent-specific gene expression. *Nature Reviews Genetics*, **4**, 359-368.
145. Haig, D. (2004) Genomic imprinting and kinship: How good is the evidence? *Annu Rev Genet*, **38**, 553-585.
146. Constancia, M., Kelsey, G. and Reik, W. (2004) Resourceful imprinting. *Nature*, **432**, 53-57.
147. Reik, W., Constancia, M., Fowden, A., Anderson, N., Dean, W., Ferguson-Smith, A., Tycko, B. and Sibley, C. (2003) Regulation of supply and demand for maternal nutrients in mammals by imprinted genes. *J. Physiol.*, **547**, 35-44.
148. Keverne, E. (1997) Genomic imprinting in the brain. *Current Opinion in Neurobiology*, **7**, 463-468.
149. Allen, N., Logan, K., Lally, G., Drage, D., Norris, M. and Keverne, E. (1995) Disruption of parthenogenetic cells in the mouse brain and their influence on brain development and behaviour. *PNAS*, **92**, 10782-10786.
150. Keverne, E., Fundele, R., Narasimha, M., Barton, S. and Surani, A. (1996) Genomic imprinting and the differential roles of parental genomes in brain development. *Dev. Brain Res.*, **92**, 91-100.
151. Hanemann, C., Kuhn, G., Lie, A., Gillen, C., Bosse, F., Spreyer, P. and Muller, H. (1993) Expression of decorin mRNA in the nervous system of rat *J. Histochem. Cytochem.*, **41**, 1383-1391.
152. Voss, B., Glossi, J., Cully, Z. and Kresse, H. (1986) Immunocytochemical investigation on the distribution of small chondroitin sulfate-dermatan sulfate proteoglycan in the human. *J. Histochem. Cytochem.*, **34**, 1013-1019.
153. Bovolenta, P. and Feraud-Espinosa, I. (2000) Nervous system proteoglycans as modulators of neurite outgrowth. *Progress in Neurobiology*, **61**, 113-132.
154. Jensen, C., Meyer, M., Schroder, H., Kliem, A., Zimmer, J. and Teisner, B. (2001) Neurons in the monoaminergic nuclei of the rat and human central nervous system express FA1/dlk1. *NeuroReport*, **12**, 3959-3963.
155. Christopherson, N., Gronborg, M., Peterson, T., Fjord-Larson, L., Jorgenson, J., Juluisson, B., Blom, J., Rosenblad, C. and Brundin, P. (2007) Midbrain expression of Delta-like 1 homolog is regulated by GDNF and is associated with dopaminergic differentiation. *Experimental Neurology*, **204**, 791-801.

156. Davies, W., Isles, A.R. and Wilkinson, L.S. (2005) Imprinted gene expression in the brain. *Neuroscience and Biobehavioral Reviews*, **29**, 421-430.
157. LaSalle, J. (2007) The odyssey of MeCP2 and parental imprinting. *Epigenetics*, **2**, 5-10.
158. Ohkuma, S., Narihara, H., Katsura, M., Hasegawa, T. and Kuriyama, K. (1995) Nitric oxide-induced [3H] GABA release from cerebral cortical neurons is mediated by peroxynitrite. *J. Neurochem.*, **65**, 1109-1114.
159. Eguchi, N., Minami, T., Shirafuji, N., Kanaoka, Y., Tanaka, T., Nagata, A., Yoshida, N., Urade, Y., Ito, S. and Hayaishi, O. (1999) Lack of tactile pain (allodynia) in lipocalin-type prostaglandin D synthase-deficient mice. *PNAS*, **96**, 726-730.
160. Munsch, T., Freichel, M., Flockerzi, V. and Pape, H. (2003) Contribution of transient receptor potential channels to the control of GABA release from dendrites. *PNAS*, **100**, 16065-16070.
161. Benson, D. and Tanaka, H. (1998) N-cadherin redistribution during synaptogenesis in hippocampal neurons. *J. Neurosci.*, **18**, 6892-6904.
162. Dan, B. and Boyd, S. (2003) Angelman syndrome reviewed from a neurophysiological perspective. *Neuropediatrics*, **34**, 169-176.
163. Vu, T. and Hoffman, A. (1997) Imprinting of the Angelman syndrome gene, UBE3A, is restricted to brain. *Nature Genetics*, **17**, 12-13.
164. Jiang, Y., Armstrong, D., Albrecht, U., Atkins, C., Noebels, J., Eichele, G., Sweatt, J. and Beaudet, A. (1998) Mutation of the Angelman ubiquitin ligase in mice causes increased cytoplasmic p53 and deficits of contextual learning and long-term potentiation. *Neuron*, **21**, 799-811.
165. Bauman, M. and Kemper, T. (2005) Neuroanatomic observations of the brain in autism: a review and future directions. *International Journal of Developmental Neuroscience*, **23**, 183-187.
166. Xu, G., Guimond, M., Chakraborty, C. and Lala, P. (2002) Control of proliferation, migration and invasiveness of human extravillous trophoblast by decorin, a decidual product. *Biology of Reproduction*, **67**, 681-689.
167. Yamaguchi, Y., Mann, D. and Ruoslahti, E. (1990) Negative regulation of transforming growth factor-beta by the proteoglycan decorin. *Nature*, **346**, 281-284.

168. Graham, C. and Lala, P. (1991) Mechanism of control of trophoblast invasion in situ. *J. Cell Physiol.*, **148**, 228-234.
169. Graham, C., Lysiak, J., McCrae, K. and Lala, P. (1992) Localization of transforming growth factor-beta at the human fetal-maternal interface: role in trophoblast growth and differentiation. *Biol. Reprod.*, **46**, 561-572.
170. Irving, J. and Lala, P. (1995) Functional role of cell surface integrins on human trophoblast cell migration: regulation by TGF-beta, IGF-II and IFGBP. *J. Exp. Cell Res.*, **217**, 419-427.
171. Graham, C., McCrae, K. and Lala, P. (1993) Molecular mechanisms controlling trophoblast invasion of the uterus. *Trophoblast Research*, **7**, 237-250.
172. Monk, D., Arnaud, P., Apostolidou, S., Hills, F., Kelsey, G., Stainer, P., Feil, R. and Moore, G. (2006) Limited evolutionary conservation of imprinting in the human placenta. *PNAS*, **103**, 6623-6628.
173. da Rocha, S., Tevendale, M., Knowles, E., Takada, S., Watkins, M. and Ferguson-Smith, A. (2007) Restricted co-expression of Dlk1 and the reciprocally imprinted non-coding RNA, Gtl2: implications for cis-acting control. *Developmental Biology*, **306**, 810-823.
174. Georgiades, P., Watkins, M., Surani, M. and Ferguson-Smith, A. (2000) Parental origin-specific developmental defects in mice with uniparental disomy for chromosome 12. *Development*, **127**, 4719-4728.
175. Georgiades, P., Watkins, M., Burton, G. and Ferguson-Smith, A. (2001) Roles for genomic imprinting and the zygotic genome in placental development. *PNAS*, **98**, 4522-4527.
176. Poirier, F., Chan, C., Timmons, P., Robertson, E., Evans, M. and Rigby, P. (1991) The murine H19 gene is activated during embryonic stem cell differentiation in vitro and at the time of implantation in the developing embryo. *Development*, **113**, 1105-1114.
177. Szabo, P. and Mann, J. (1995) Allele-specific expression and total expression levels of imprinted genes during early mouse development: Implications for imprinting mechanisms. *Genes and Development*, **9**, 3097-3108.
178. Lee, J., Pintar, J. and Efstratiadis, A. (1990) Pattern of the insulin-like growth factor II gene during early mouse embryogenesis. *Development*, **110**, 151-159.
179. Jones, B., Levorse, J. and Tilghman, S.M. (1998) Igf2 imprinting does not require its own DNA methylation or H19 RNA. *Genes and Development*, **12**, 2200-2207.

180. Baker, J., Liu, J., Robertson, E. and Efstratiadis, A. (1993) Role of insulin-like growth factors in embryonic and postnatal growth. *Cell*, **75**, 73-82.
181. Eggenschwiler, J., Ludwig, T., Fisher, P., Leighton, P. and Tilghman, S.M. (1997) Mouse mutant embryos overexpressing IGF-II exhibit phenotypic features of the Beckwith-Wiedeman and Simpson-Golabi-Behmel syndromes. *Genes and Development*, **11**, 3128-3142.
182. Smith, A., Choufani, S., Ferreira, J. and Weksberg, R. (2007) Growth regulation, imprinted genes and chromosome 11p15.5. *Pediatric Research*, **61**, 43R-47R.
183. Constancia, M., Angiolini, E., Sandovici, L., Smith, P., Smith, R., Kelsey, G., Dean, W., Ferguson-Smith, A., Sibley, C., Reik, W. *et al.* (2005) Adaptation of nutrient supply to fetal demand in the mouse involves interaction between the *Igf2* gene and placental transporter systems. *PNAS*, **102**, 19219-19224.
184. Catala, M. (1998) Embryonic and fetal development of structures associated with the cerebro-spinal fluid in man and other species. Part I: The ventricular system, meninges and choroid plexuses. *Arch. Anat. Cytol. Pathol.*, **46**, 153-169.
185. Yevtodiyenko, A., Steshina, E.Y., Farner, S.C., Levorse, J.M. and Schmidt, J.V. (2004) A 178-kb BAC transgene imprints the mouse *Gtl2* gene and localizes tissue-specific regulatory elements. *Genomics*, **84**, 277-287.
186. Forne, T., Oswald, J., Dean, W., Saam, J.R., Bailleul, B., Dandolo, L., Tilghman, S.M., Walter, J. and Reik, W. (1997) Loss of the maternal *H19* gene induces changes in *Igf2* methylation in both cis and trans. *PNAS USA*, **94**, 10243-10248.
187. Jordan, C., Li, H. and Kwan, H.F., U (2007) Cerebellar gene expression profiles of mouse models for Rett syndrome reveal novel MeCP2 targets. *BMC Med Genet*, **8**, 36-52.
188. Fuks, F., Hurd, P., Wolf, D., Nan, X., Bird, A. and Kouzarides, T. (2003) The Methyl-CpG-Binding protein MeCP2 links DNA methylation to histone methylation. *Journal of Biological Chemistry*, **278**, 4035-4040.
189. Ballestar, E., Ropero, S., Alaminos, M., Armstrong, J., Setien, F., Agrelo, R., Fraga, M.H., M, Avila, S., Pineda, M., Monros, E. *et al.* (2005) The impact of MECP2 mutations in the expression patterns of Rett syndrome patients. *Human Genetics*, **116**, 91-104.
190. Dekker, J., Rippe, K., Dekker, M. and Kleckner, N. (2002) Capturing Chromosome Conformation. *Science*, **295**, 1306-1311.

## APPENDIX I

<b>Fold Change</b>	<b>Common Name</b>	<b>Full Name</b>	<b>Broad Functional Category</b>
4.334	Tcf15	Transcription factor-like 5	Testes-specific transcription factor
3.914	Pigt	18S RNA	Ribosome
3.015	Fmod	Fibromodulin	Bone development
2.922	Colec12	Collectin sub-family member 12	Immune response
2.733	Clic6	Chloride intracellular channel 6	Ion transport in brain (chloride)
2.712	1500015O10Rik	RIKEN clone	Clone from cerebellar tissue
2.705	Lepr	Leptin receptor	Glucose metabolism
2.575	Calml4	Calmodulin-like 4	Ion transport (calcium)
2.539	Ogn	Osteoglycin	Bone development
2.484	Cldn11	Claudin 11	Brain development (myelination)
2.451	Cfh	Complement component factor H	Kidney development
2.433	Otx2	Orthodentical homolog 2	Early patterning
2.42	Tdo2	Tryptophan 2,3-dioxygenase	Tryptophan metabolism
2.391	Gjb6	Gap junction membrane channel protein beta 6	Ion transport
2.316	1500031B24Rik	RIKEN clone	Clone from cerebellar tissue
2.307	Ankrd3	Ankyrin repeat domain 3	Serine-Threonine Kinase
2.305	Postn	Periostin, osteoblast specific factor	Bone development
2.295	Aqp1	Aquaporin 1	Water transport
2.274	1500015O10Rik	RIKEN clone	Clone from hippocampal tissue
2.253	H19	H19	Non-coding RNA
2.209	Col1a1	Procollagen type 1 alpha 1	Bone development
2.198	5730453H04Rik	RIKEN clone	Clone from whole E8 embryo
2.191	Col3a1	Procollagen type 3 alpha 1	Bone development
2.187	Cp	Cerruloplasmin	Ion transport in brain (Cu & Fe)
2.185	UIMBH3atah050UI	NIH clone	Clone from mouse brain
2.165	Xtrp3s1	X transporter protein 3 similar 1 gene	Neurotransmitter
2.156	Trpm3	Transient receptor potential cation channel 3	Ion transport
2.095	Ptgds	Prostaglandin D2 synthase (brain)	Fatty acid biosynthesis in brain
2.087	Tbx18	T-box18	Early patterning
2.078	Col1a2	Procollagen type 1 alpha 2	Bone development
2.051	Folr1	Folate receptor 1	Folic acid metabolism
2.043	Apod	Apolipoprotein D	Transport
2.04	Dcn	Decorin	Proteoglycan in connective tissue
2.034	F13a	Coagulation factor XI11 subunit a	Coagulation
2.031	Cdh1	Cadherin 1	Epithelial cell adhesion
2.012	Foxc1	Corkhead box c1	Transcription factor
0.495	1810009N02Rik	Hypothetical Maf-like protein containing protein	Clone from pancreatic tissue
0.482	Trpc4	Transient receptor potential cation channel 4	Ion transport in brain
0.481	2510022D24Rik	RIKEN clone	Clone from E13 embryonic liver
0.478	Cbln4	Cerebellin 4 precursor protein	Brain development
0.475	Spon1	Spondin 1, (f-spondin) extracellular matrix protein	cell adhesion
0.459	3010033P07Rik	Hypothetical pyruvate kinase M3	Pyruvate kinase
0.455	Mbp	Myelin basic protein	Brain development
0.453	Dsc3	Desmocollin 3	cell adhesion
0.446	2410026K10Rik	Glycine-rich containing protein homolog	Clone from whole E18 embryo
0.359	AI838057	IMAGE clone	Clone from kidney tissue
0.353	5656844	IMAGE clone	Clone from pancreas tissue
0.34	4833408C14Rik	RIKEN clone	Clone from mammary tumour
0.3	354942	IMAGE clone	Clone from embryonic tissue
0.253	Nr4a2	Nuclear receptor subfamily 4, group A, member 2	Brain development
0.14	Csf2ra	Colony stimulating factor 2 receptor, alpha	Interferon